DEVELOPMENT OF A BIOREACTOR FOR IN-VITRO ENGINEERING OF SOFT TISSUES

KYAW MOE

NATIONAL UNIVERSITY OF SINGAPORE

2005

DEVELOPMENT OF A BIOREACTOR FOR IN-VITRO ENGINEERING OF SOFT TISSUES

KYAW MOE

(B.Eng. (Hons.), YTU, Yangon)

A THESIS SUBMITTED

FOR THE DEGREE OF MASTER OF ENGINEERING

DEPARTMENT OF MECHANICAL ENGINEERING

NATIONAL UNIVERSITY OF SINGAPORE

2005

ACKNOWLEDGEMENT

SUMMARY

The injuries of the ligament and tendon are very common. Surgical reconstruction is often recommended because of poor intrinsic healing. The current methods of surgical treatment, including allografts, autografts and synthetic graft replacement exhibit limited success. Some limitations for these methods are donor site morbidity, rejection, infection, and fatigue failure. Tissue engineering offers the possibility of replacing damaged human tissue with functional neotissue (engineered tissue) with similar mechanical and functional characteristics. One approach of tissue engineering for replacing damaged tissue is to culture the cell–scaffold composite in a bioreactor *in-vitro* for a period of time before transplantation.

The aim of this research is to design a bioreactor and to investigate the effect of cyclic strain on cell growth and effect of strain frequency on cellular morphology. A bioreactor was designed and fabricated using polycarbonate. Human dermal Fibroblast cells (HDFs) seeded on knitted PLGA scaffolds were strained with 1.8% strain and 0.1 Hz frequency. After two weeks straining at 4 hours per day, cell seeded scaffolds were harvested and analyzed for cell morphology, cell proliferation rate and RT-PCR analysis.

When compared with unstrained samples, the shapes of cells are more elongated in strained sample and show alignment due to cyclic straining. The mean nuclei lengths of cells from strained and unstrained samples are 8.05 ± 2.39 µm and 7.46 ± 2.35 µm respectively. The cell proliferations in strained samples are also higher than in unstrained samples. The mRNA level of Collagen type I, collagen type III and Tenascin-C are also higher in strained sample. These show that cyclic mechanical straining has positive effects on cell growth.

TABLE OF CONTENTS

Publication 112

NOMENCLATURE

ACL,   Anterior Cruciate Ligament

CMFDA/CFDA,   5-Chloromethyl Fluorescein Diacetate

DMEM,   Dulbecco's Modified Eagle's Medium

DNA   deoxy-ribonucleic acid

dNTP,   deoxynucleotides

ECM,   Extracellular Matrix

FBS,   Foetal Bovine Serum

GAPDH,   Glyceraldehyde Phosphate Dehydrogenase

ILM,   Inverted Light Microscopy

LAD   Ligament-Augmentation Device

LSCM,   Laser Scanning Confocal Microscopy

mRNA   messenger ribonucleic acid

PBS,   Phosphate Buffered Saline

PCR,   Polymerase Chain Reaction

PGA,   Poly (glycolic acid)

PLA,   Poly (lactic acid)

PLGA,   Poly (lactide-co-glycolide)

PLLA,   Poly (l-lactic acid)

RT-PCR,   Reverse-Transcriptase-mediated PCR

SD,   Standard Deviation

SEM,   Scanning Electron Microscopy

UTS,   Ultimate Tensile Strength

List of Figures

List of Tables

Chapter 1. Introduction

Ligaments and tendons are connective tissues in the body, joining bone to bone and bone to skeletal muscles, respectively and transmitting tensile forces between them. Injuries to ligaments and tendons are among the most common injuries in the body. Surgical reconstruction is often recommended because of poor intrinsic healing. The current methods of surgical treatments are allografts, autografts and synthetic graft replacement. Despite many improvements in these techniques, there remains significant limitation in our management of these conditions and substitutes are far from ideal and each technique has their specific problems and limitations. Some limitations for these methods are donor site morbidity, rejection, infection, and fatigue failure.

Advances in tissue engineering now allow for new approaches to treat these ligament and tendon injuries. Tissue engineering offers the possibility of replacing damaged human tissue with functional neotissue (engineered tissue) with similar mechanical and functional characteristics. Currently there are two approaches to tissue engineering: one is to implant a cell–scaffold composite directly into the injured site, as such, the body acts like a "bioreactor"; the other is to culture the cell–scaffold composite in a bioreactor *in-vitro* for a period of time before transplantation. The *in vitro* bioreactor allows controlled introduction of biochemical and physical regulatory signals to guide cell differentiation, proliferation, and tissue development. As such, engineering of tissue ex vivo in a bioreactor offers several exciting prospects, such as better understanding of tissue development and the mechanisms of disease, off-the-shelf provision of essential transplantable tissue, and possible scale-up for commercial production of engineered tissues.

Mechanical stress plays a significant role in tissue formation and repair *in vivo*. Recently, more focus has been given to the utilization of mechanical signals *in vitro* either in the form of shear stress generated by fluid flow, hydrodynamic pressure or as direct mechanical stress applied to the cell seeded scaffold.

Most of the previous studies are done on the investigation of the effect of mechanical stress on cell seeded collagen matrices. Only a few researchers [Altman et al, 2002 and Kwan, 2003] study the effect of cyclic mechanical strain on the cell seeded biodegradable polymer scaffolds. Therefore in this research, knitted PLGA scaffold was chosen to study the effect of cyclic mechanical strain on that cell seeded scaffolds.

1.1 Objectives of this Study

In this study, an attempt is made in designing a bioreactor for the study of the effect of mechanical straining parameters on cellular morphology, to provide a better understanding of condition for the *in-vitro* growth of engineering tissue by using knitted PLGA scaffold. The objectives are:

(1) to design and fabricate a bioreactor for *in-vitro* engineering tissue and

(2) to investigate the effect of cyclic mechanical strain on fibroblast cell growth *in-vitro* condition

1.2 Thesis Organization

The present chapter describes the background and objectives of this study. A brief summary of relevant literature survey on ligament and tendon tissues and existing bioreactor are discussed in chapter 2. The preliminary studies on the effect of cyclic

mechanical strain on different scaffold forms are described in chapter 3. Chapter 4 describes the design and fabrication of the new bioreactor. Next, description of experimental work is given in chapter 5. In chapter 6, the results of the experiments and discussion are presented. Finally the conclusions and recommendation for future study are provided in chapter 7.

Chapter 2. Literature Survey

2.1 Ligament and Tendon

Ligaments and tendons are soft collagenous tissues. Ligaments connect bone to bone and tendons connect skeletal muscles to bone. The function of ligament is to maintain the stability of the joints in the musculoskeletal system and tendons serve to transmit tensile loads between muscles (Figure 2.1). Contraction of a muscle results in transmission of the load from muscle, via its tendon, to a bone across a joint, resulting in movement of the bone around the joints. This subjects the ligaments between the bones to strain. Thus, tendons operate to bring around movements of the joints, and ligaments prevent excessive movement of the joints and thereby provide stability.

| (a) | (b) |
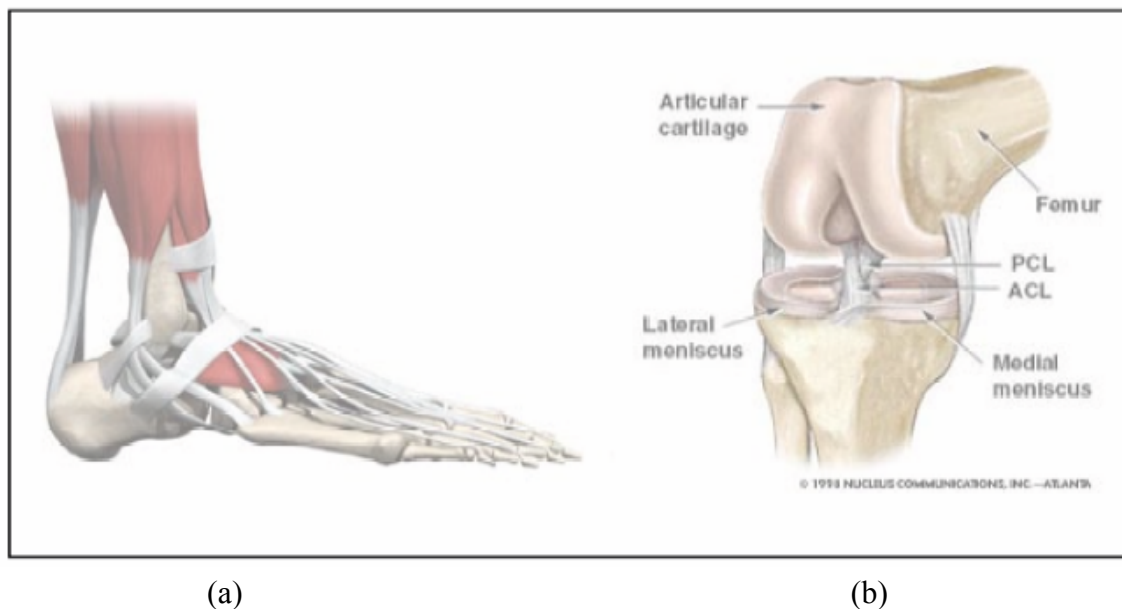
Figure 2.1: (a) Tendons of the foot (b) Ligaments of the knee joints.

Ligaments and tendons are collagenous tissues with their primary building unit being the tropocollagen molecule [Viidik, 1973]. Tropocollagen molecules are organized into long cross-striated fibrils that are arranged into bundles to form fibers. Fibers are further grouped into bundles called fascicles which group then together to form the ligament (Figure 2.2). Collagen fiber bundles are arranged in the direction of functional need and act in conjunction with elastic and reticular fibers along with ground substance, which is a composition of glycosaminoglycans (GAG) and tissue fluid, to give ligaments their mechanical characteristics. In unstressed ligaments, collagen fibers take on a sinusoidal pattern. This pattern is referred to as a "crimp" pattern and is believed to be created by the cross-linking or binding of collagen fibers with elastic and reticular fibers.
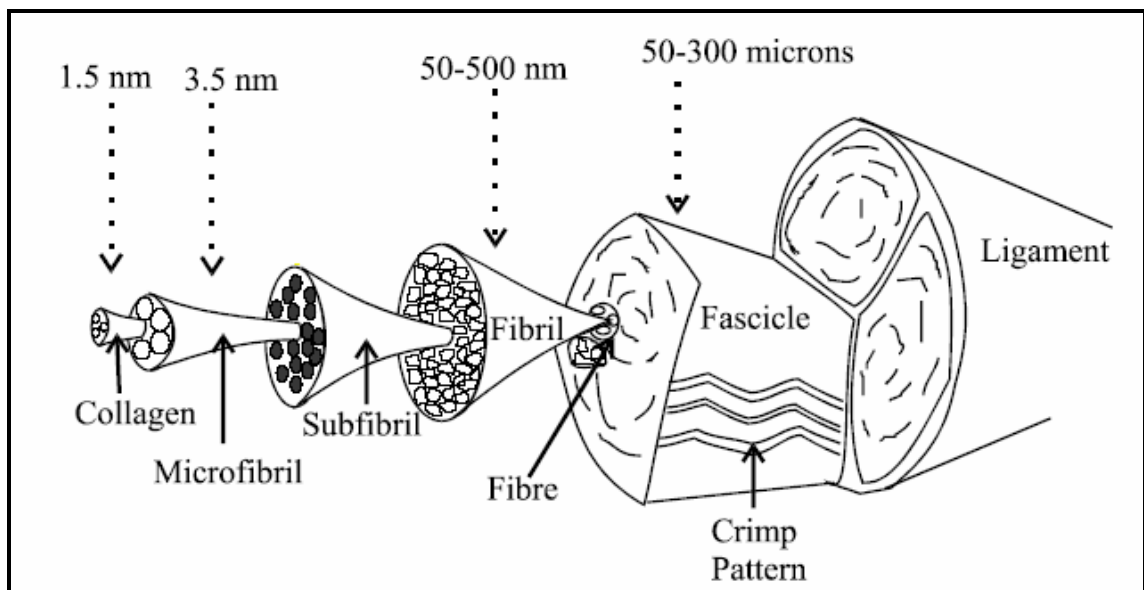
Figure 2.2: Schematic diagram of the structural hierarchy of ligament.

2.2 Biochemical Constituents

The major constituents of ligaments and tendon are collagen, elastin, glycoproteins, protein polysaccharides, glycolipids, water and cells [Akeson et al, 1984]. Water makes up about 55% of wet weight of tendons and 60-80 % of wet weight of ligaments. Collagen is arranged in the form of fibers within a matrix of GAGs, thus imparting "fiber reinforced composite" like properties to the tissues [Ker et al, 1999]. The approximate compositions are given in Table 2.1.

Table 2.1: Extra cellular matrix composition of tendons and ligaments (modified from Harrison's Principle of Internal Medicine [Fauci et al, 2001])

Major constituents	Approximate amount, % dry weight	Characteristics or functions
Type I collagen	80	Bundles of fibrils
Type III collagen	5-15	Thin fibrils
Type IV collagen, laminin, nidogen	<5	In basal laminae under epithelium and endothelium
Types V, VI, and VII collagens	<5	VII forms anchoring fibrils; others unknown
Elastin, fibrillin	<5	Provides elasticity
Fibronectin	<5	Associated with collagen fibers and cell surfaces
Proteoglycans, hyaluronate	0.5	Provide resiliency

2.3 Biomechanics

The main function of ligaments and tendons is to transmit tensile loads across joints, largely in a uniaxial direction. Consistent with this function, their structure of aligned collagen fibers provides for load bearing primarily in one direction and contributes to highly anisotropic material properties. Their properties are usually described in the axial direction, and can be classified into two sub categories (1) structural properties and (2) viscoelastic properties.

2.3.1 Structural Properties

Structural properties of tendons/ligaments are extrinsic measures of the tensile performance of the overall structure. As a result, they depend on the size and shape of the tendons/ligaments, in addition to the variations of the unique properties from tissue to the insertion into bone. These properties are obtained by loading a tendon/ligament to the failure limit and are represented in the resulting load-elongation curve and stress- strain curve as shown in Figure 2.3.

<center>(a)   (b)</center>
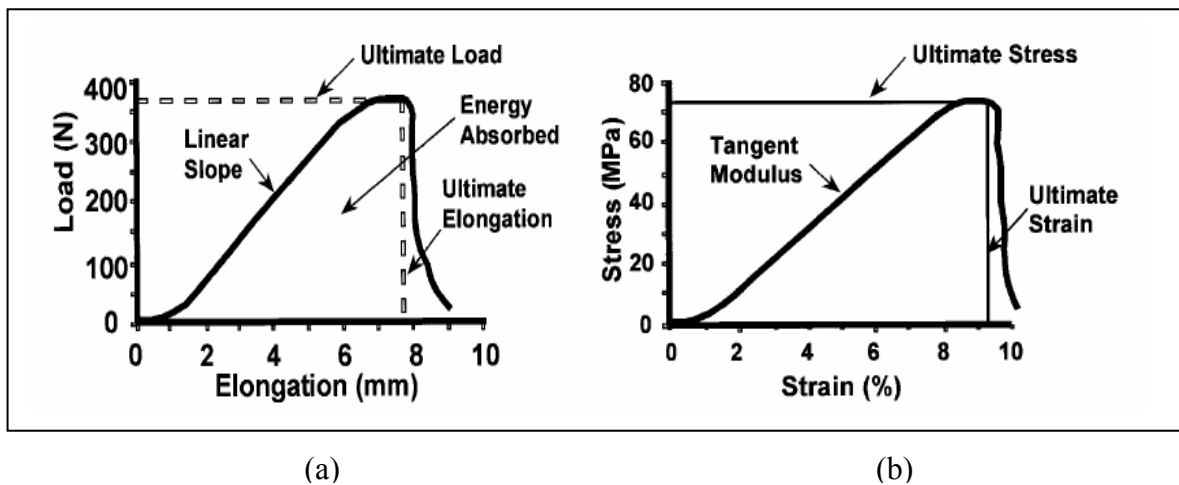
Figure 2.3: A typical (a) load-elongation curve and (b) stress- strain curve for tendon/ligament. [Woo et al, 1998]

From the load-elongation curve (Figure 2.3(a)) the **ultimate load P_0** (N) is the highest load placed on the complex before failure; the **ultimate elongation** (mm) is the maximum elongation of the complex at failure; the **stiffness** (N/mm) is the slope of the load-elongation curve between two defined limits of elongation; and **energy absorbed at failure** (N-mm) is the area under the entire curve which represents the maximum energy stored by the complex. At forces above 50% of ultimate load, tissue stiffness was nearly constant, and a pronounced "toe region" was observed only at forces below ~25% of ultimate load. Stiffness increased as the muscle–tendon unit was lengthened.

The cross-sectional areas of tissues are measured with laser micrometry method, which was employed for accurate measurement of the tissues without deforming the cross section of tissues [Lee et al, 1988]. Figure 2.3(b) represents a typical stress-strain curve for tendons/ligaments. The **ultimate tensile strength** (**UTS**; N/mm^2) is the maximum stress achieved; the **ultimate strain** is the strain at failure; the **Young's modulus** (*E*; N/mm^2 or MPa) is the tangent modulus in the linear region of the stress–strain curve; the **strain energy density** (MPa) is the area under the stress-strain curve. The peak stress to which a tendon is subjected varies according to its anatomical site and the species. Values obtained vary with the testing protocol and conditions, and are enumerated in Table 2.2 for some tendons and ligaments.

Among adult mammalian limb tendons, the stress-in-life ranges from 10 to 70 MPa, with the most common stress value being approximately 13 MPa. Higher values of stress-in-life are found in few tendons such as the human Achilles tendon (67 MPa) [Ker et al, 2000]. The data for ultimate tensile strength in a ramp test to rupture are mostly in the range 50–

100 MPa, ultimate strain has been reported to be in the range of 2–5% [Monti et al, 2003].

Human ACL has been shown to possess values of Young's Modulus of 345.0 ± 22.4 MPa,

UTS of 36.4 ± 2.5 MPa and ultimate strain of 15.0 ± 0.8 %[Weiss et al,2001].

Table 2.2: Structural properties of human tendons and ligaments (UTS: Ultimate Tensile Strength; *E*: Young's modulus) [Woo et al, 1998]

Tissue	UTS (*MPa*)	Ultimate Strain (%)	*E* (*MPa*)
Anterior cruciate ligament (Knee)	13-46	9-44	65-541
Patellar tendon (Knee)	24-69	14-27	143-660
Achilles tendon (Ankle)	14-61	24-59	65
Inferior glenohumeral ligament (Shoulder)	5-6	8-15	30-42
Anterior Longitudinal ligament (Spine)	8-37	10-57	286-724

2.3.2 Viscoelastic Properties

Biological materials, like ligaments and tendons, possess viscoelastic properties [Weiss et al, 2001]. Thus, the loading and unloading of a specimen yields different paths of the load-elongation curve for each testing cycle, forming a hysteresis loop that represents the energy lost as a result of a non-conservative or dissipative process, as shown in Figure 2.4. This viscoelastic behavior is assumed to be due to complex interactions of the constituents

of the tissues, i.e. collagen, water, surrounding protein, and ground substance (composition of GAG).
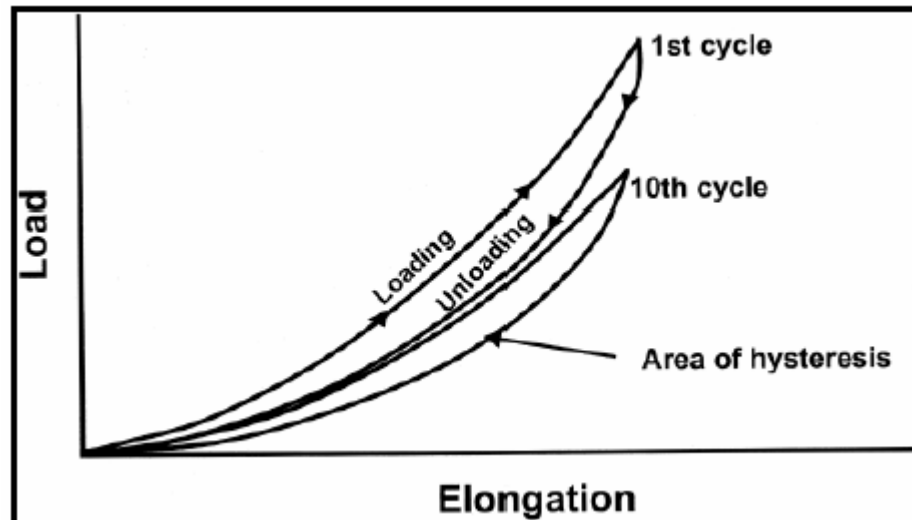
Figure 2.4: Cyclic load-elongation behavior shows that during cyclic loading, the loading and unloading curves do not follow the same path and create hysteresis loops indicating the absorption of energy; [Weiss et al, 2001].

Viscoelastic behavior is illustrated by two classic experimental tests: stress relaxation and creep tests. A stress relaxation test involves stretching the specimen to a constant length and allowing the stress to relax with time. A creep test involves subjecting a specimen to a constant force while the length gradually increases with time. Many researchers [Dehoff,1978 and Fung,1972] have modeled the results of these tests mathematically in order to better understand the time-dependent and nonlinear behaviors of ligaments and tendons.

Stress relaxation properties are important characteristics of the dimensional stability of a given material. Observing mechanical properties is important in tissue engineering since engineered scaffold should mimic function of natural tendons/ligaments. It is expected

that after tissue regeneration, the scaffolds would simulate the viscoelastic behavior of natural tissues.

2.4 Tendon/Ligament Injury

2.4.1 Prevalence

Tendons, such as the patellar tendon of the knee, the Achilles tendon of the foot, flexor digitorum profundus tendons of the hand, and ligaments, such as the collateral and cruciate ligaments of the knee, are frequently injured. Specifically, the anterior cruciate ligament (ACL) and the medial collateral ligament (MCL) of the knee (Figure 2.1(b)) account for as much as 90% of all ligament injuries at the knee in young and active individuals, primarily during sports activities. In the United States, more than 100,000 patients per year undergo surgery to repair tendon or ligament injuries [Goulet et al, 1997]. Tendon injuries can consist of tendinitis, which is an inflammation of the tendon, tendon laceration, or tendon rupture.

2.4.2 Mechanism of injury

Tendons and ligaments are injured primarily by two mechanisms:

1). Single impact macro-trauma: Rupture of a tendon like the Achilles tendon generally occurs due to a sudden overload strain (more than about 8%, as shown in Figure 2.5) in the occasional athlete during an explosive push-off maneuver. Most frequently, these athletes are middle-aged males who are involved in only intermittent athletic activities. However, this injury has also been seen in young, high performance athletes. Another possible etiologic factor is a direct blow to the tendon during contraction.
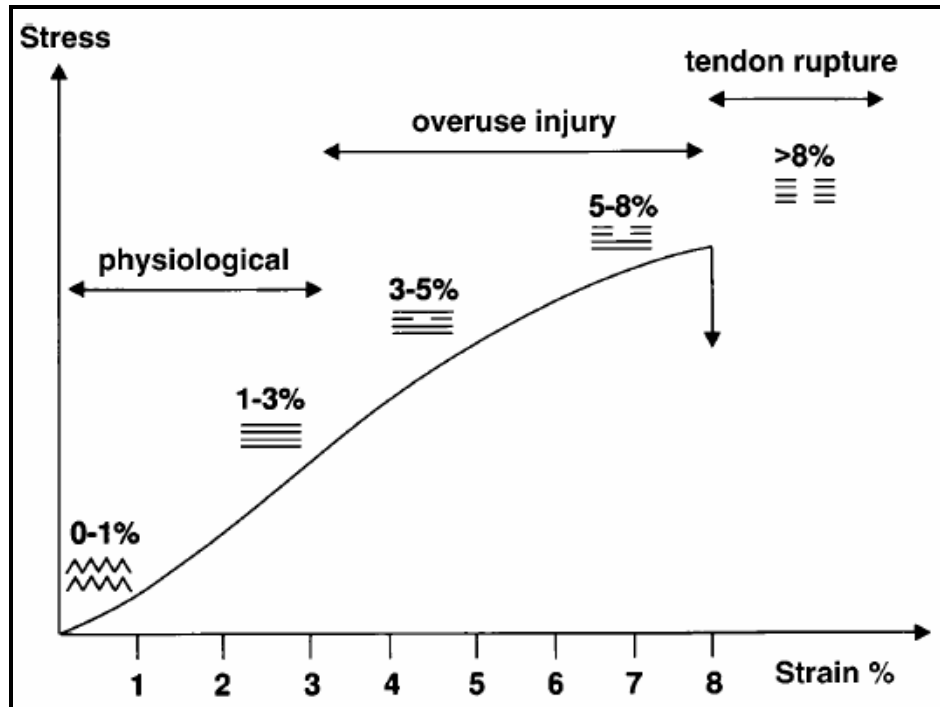
Figure 2.5: Graph showing the stress-strain curve for tendon. Wavy lines indicate the wavy configuration of the tendon at rest, straight unbroken lines indicate the effect of tensile stresses, one or two broken lines indicate that the collagen fibers are starting to slide past one another as the intermolecular cross-links fail, and the set of completely broken lines indicate macroscopic rupture due to the tensile failure of the fibers and the interfibrillar shear failure. [Maffullin, 1999]

2). Repetitive exposure to low magnitude force: Normal healthy individuals are estimated to walk approximately 1million–1.5 million strides per year. During locomotion, the in vivo repetitive loading of tendons in the lower limbs may induce damage. Extensive physical activity will incur damage which may exceed the regenerative ability of tendons and, therefore result in overuse injuries [Schechtman et al, 2002].

Tendinitis is one of the most common problems both in occupational and athletic settings. It has been estimated that overuse injuries are responsible for 30% to 50% of all sports injuries. Although the majority of patients respond well to conservative treatment following weeks or months of rest and therapeutic exercises, a percentage of patients do

not recover satisfactorily with this protocol and require surgery to restore function. The etiology of tendinitis is unknown but is thought to be related to repetitive overloads or overuse demands placed on tendons, leading to microscopic failure of collagen fibrils or bundles, and an inflammatory process usually ensues in symptomatic tissues [Woo et al, 2000].

2.4.3 Healing and Re-injury

Healing has been found to be a long and complex process that is subjected to local and external influences. Generally, the process involves several overlapping but discrete phases: the acute inflammatory or reactive response phase, the regenerative or repair phase, and the tissue remodeling phase. In the acute inflammatory response, the cellular and tissue responses to injury occur within approximately the first 72 hours following a given insult. The formation of healing matrix consisting of randomly aligned collagen, and amorphous ground substance can be seen during this early stage of the body's response to injury. The repair and regeneration phase occurs from 48 to 72 hours until roughly 6 weeks post injury. The healed matrix becomes progressively more organized with time, although electron microscopy has confirmed that the collagen fibrils laid down by the fibroblasts remain relatively disorganized within an amorphous ground substance. Subsequently, the remodeling phase is marked by tissue remodeling, lasting up to one year or longer after the time of the initial injury while never regaining the properties of the normal tendon/ligament, thus demonstrating the need for tissue engineering approaches. During the course of healing, the level of pain decreases gradually below a threshold when the patient feels comfortable again. During this period, which is usually around 3 to 5

weeks post-injury, the mechanical properties are still quite subnormal and exercising leads

to re-injury (Figure 2.6).
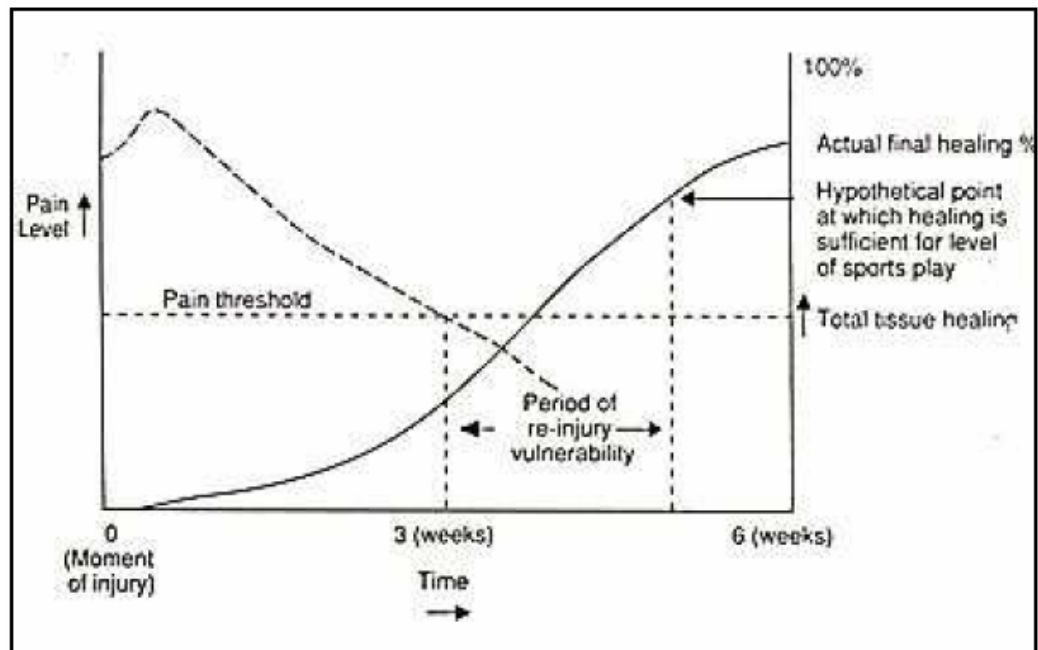
Figure 2.6: Re-injury in tendon and ligaments may occur when the pain-level is lower than pain threshold and healing is not complete. [Woo et al, 1988]

2.5 Current Therapy for Ligament

Currently the therapeutic options to treat ligament injuries are autograft, allograft and synthetic material replacement. Autografts (tissue taken from the patient) of patellar tendons or hamstring tendons harvested from the patient at the time of surgery have produced the most satisfactory long-term results and are referred to as the "gold standard" [Fu et al, 1999]. The autografts have many advantages, such as avoidance of immunological and infectious problems of grafts rejection or disease transmission, quick incorporation, and good remodeling. Donor site morbidity remains the limiting factor of patellar tendon grafts, because it is often associated with pain, muscle atrophy, and tendonitis, resulting in prolonged rehabilitation periods [Weitzel et al, 2002].

Allografts (tissue taken from donor) is accompanied by immunological rejection, disease transmission and limited availability. Frozen allografts of ligaments with bony attachments frequently result in an immunological foreign-body response [Jackson et al, 1993] that hinders tissue remodeling [Noyes et al, 1984 and Woo et al, 1988]. The risks of disease transmission and a lack of donors are significant problems of allografts.

A variety of synthetic materials have been used for ligament replacement (e.g., Dacron, Gore-Tex, polypropylene-based Kennedy Ligament-Augmentation Device), but with limited success [Richmond et al, 1992, Moyen et al, 1992 and Amiel et al, 1990]. The Gore-Tex® ACL is made of a single strand of expanded polytetrafluorethylene that is wound into multiple loops. This prosthesis was designed to give immediate fixation with early load-bearing capabilities, thus promising early mobilization and return to activity.

Gore-Tex® graft ultimately failed from material fatigue owing to the lack of tissue ingrowth, likely the result of both the graft design and material properties; fraying at the bone tunnels and chronic effusions were observed [Markolf et al, 1989 and McCarthy et al, 1993].

The Dacron® ligament was designed as a hybrid prosthesis to solve the problems of stiffness (i.e., stress shielding) that led to high failure rates in previous devices[Richmond et al, 1992]. Although tissue ingrowth was significant, the graft did not provide knee stability because organized collagenous ingrowth was not observed, likely owing to stress shielding and the nondirectionality of the sheath covering. The Kennedy Ligament-Augmentation Device® (LAD) was designed to provide protection to a weak portion of the quadriceps patellar tendon autograft using an over-the-top reconstruction as well as to the primary repair of the (e.g., partially torn) ACL. LADs had high rate of complications in primary ACL reconstructions (up to 63%) and experienced a delay in maturation because of stress shielding [Kumar et al, 1999].

2.6 Tissue Engineering

Tissue engineering has been defined as "an interdisciplinary field that applies the principles of engineering and the life sciences toward the development of biological substitutes that restore, maintain or improve tissue function" [Langer et al, 1993]. There are two approaches in tissue engineering: (i) repair of small-scale injuries, such as damage to blood vessels or to walls of intestines, can be made by injecting individual patients or

donor cells, or small aggregates of these cells, together with a degradable scaffold directly into damaged tissue such that host cells are stimulated to promote local tissue repair; (ii) repair or replacement of more complex organs depends on growing tissues or organs *in vitro* by seeding synthetic scaffolds with patient or donor cells. Thus, there are three basic components in tissue engineering: (1) Cells; (2) Scaffold; (3) Bioreactors.

2.6.1 Cells

A key factor in the tissue-engineering approach to tissue repair and regeneration is the availability of appropriate cells. The presence of cells is crucial; this is because of their proliferation potential, cell-to-cell signaling, biomolecule production, and formation of extracellular matrix. The number of cells initially seeded strongly influence the nature of cell-mediated processes involved in tissue formation and the rate at which these developmental and physiological processes occur. It seems clear that some minimum threshold of the quantity of cells may be required at the repair site for normal neotissue formation. The cells can be autogeneic, allogeneic or xenogeneic; they can be differentiated cells, stem or progenitor cells, or cells that have been genetically modified to make specific molecules [Laurencin et al, 1999]. Cells used for ligament regeneration include skin fibroblasts, ACL fibroblasts, bone marrow stromal cells (BMSCs) [Van Eijk et al,2004].

2.6.2 Scaffolds

Paramount to an engineered tissue is the biomaterial from which the scaffold is created, its biological inertness, as well as its overall three-dimensional (3-D) architecture. As a result of the inherent difficulties associated with tissue grafts, several biodegradable polymeric systems have been used as materials for the engineering of load-bearing biological tissues. These include polyesters, polyanhydrides, poly(orthoesters), polyurethanes and polycarbonates among others.

An ideal scaffold should possess the following characteristics:

1. Biocompatibility and biodegradability;

2. Porosity;

3. Sufficient surface area for cell attachment, growth and proliferation; and

4. Geometry that imparts the required mechanical properties; as new tissues generate, the cell-scaffold construct should closely simulate the mechanical properties of the natural tissue.

In short, it has to mimic the natural extra-cellular matrix.

Typically, scaffolds created from biodegradable polymers are fabricated using particulate leaching, textile technologies, or three-dimensional (3D) printing techniques. In the traditional particulate leaching method, a matrix is created by casting a polymer solution over water-soluble particles such as NaCl salt, evaporating the solvent, and leaching out the salt afterwards to yield a porous scaffold. However, the interconnectivity between the pores is low and difficult to control, and the pore walls often have uncontrollable morphologies [Yang et al, 2001]. Textile technologies can be used to fabricate woven or

non-woven fabrics as scaffolds [Karamuk et al, 1999]. Knitted PLGA scaffolds [Ouyang et al, 2003] have high porosity and internal connective spaces compared with a braided structure, especially when it is under tension. These spaces allow enough cells to be seeded initially and permit ECM to form and deposit therein during the repair process; this helps in functional integration of the engineered tissue into the surrounding tissues.

2.6.3 Bioreactor

Currently there are two approaches to tissue engineering: one is to implant a cell–scaffold composite directly into the injured site, as such the body acts like a "bioreactor"; the other is to culture the cell–scaffold composite in a bioreactor *ex vivo* for a period of time before transplantation. The *ex vivo* bioreactor allows controlled introduction of biochemical and physical regulatory signals to guide cell differentiation, proliferation, and tissue development. Engineered tissue, cultured in a bioreactor can provide a basis for quantitative in vitro studies of tissue development. It is also possible to produce engineered tissues commercially by using appropriate bioreactor.

2.7 Existing Straining Bioreactors

2.7.1 Cell Stretcher

The dual-stretch device as shown in figure 2.7 was designed by Yost et al (2000). This device applied a linear strain by displacing a 3-cm x 6-cm rectangular membrane that was clamped along the short sides (3cm) with the long sides (6cm) left free. Two versions of the device had been built: a single and dual unit. Each device used standard 150-mm

culture dishes as the cell culture vessel. The dual-stretch unit consisted of a poly amide-imide base plate that fits inside a standard laboratory 150-mm culture dishes. The fixed end of the clamping mechanism was a press-fit poly-ether-etherk-etone (PEEK, DSM) rod assembly. The silicone rubber stretch membrane (0.01 in. thick, gloss finish) was attached using polytetrafluorethylene (PTFE) snap-on clamps. The displacement end of the clamping mechanism was a PEEK dual-rod slider mechanism. The membrane was clamped to one rod on the slider. A Tin -coated stainless steel yoke assembly [C] was attached to the other rod on the dual-rod slider. Motion was applied to the slider through the yoke assembly by a 0.1-in. per turn lead screw cartridge assembly. A hybrid stepping motor (1.8° step) [A] was attached to the lead screw [B] to supply the force to rotate the screw. The motor was controlled by a hybrid stepping motor indexer and programmable controller. The indexer was set to micro-step at 1/125 step per pulse. The indexer used a proximity switch to identify the mechanical home position. The culture dish and lead screw were attached to an aluminum base plate with a polycarbonate dust cover and could be installed in an incubator. The motion profile was programmed into the controller with a laptop. Two motion profiles were programmed: static and cyclic. For constant or static stretch, the user provided the required displacement. The stretcher operated to that displacement and held it there until the user ended the test, at which time the stretcher returned to the zero position. For cyclical stretch, the user provided the stretch displacement, frequency, and duration. After the set duration, the stretcher returned to the zero displacement position. The cardiac fibroblasts were allowed to attach for 24 h and then loaded in the stretcher apparatus to begin stretching. Stretch conditions were 3%, 6%, and 12% stretch at frequencies of 0 (static), 5 and 10 cycles/min. Cells were stretched for 12 h and then harvested at the end of the 12-h period. All stretch frequencies were

continuous throughout the 12-h period. The experimental controls were cells plated on the aligned collagen-coated membranes but not stretched. The fibroblasts responded with an increase in β1- integrin at 3% stretch and a decrease at 6% and 12% stretch.

The limitation of this system is that only two samples could be strained in this system and thus poses a limited number of test samples available for analysis after each testing.
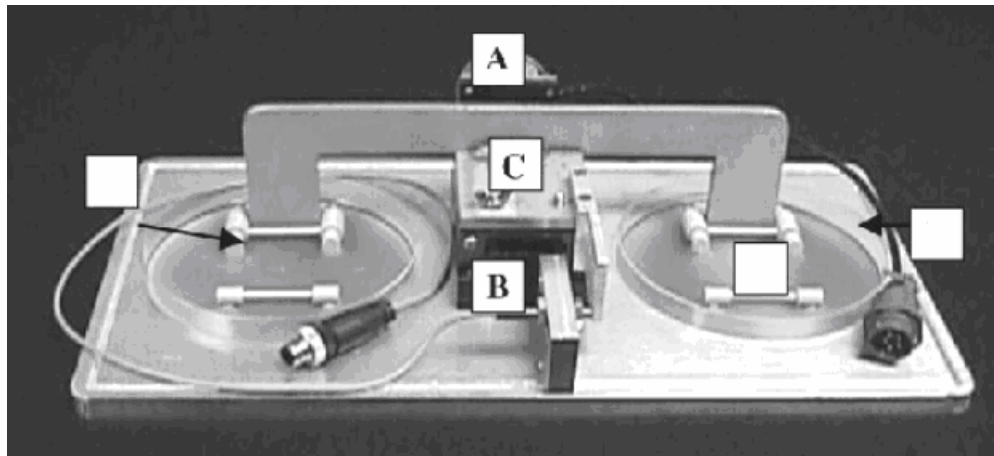
Figure 2.7: Schematic of the cell stretcher. The cell stretch membrane is placed in between the PEEK slider components and clamped with PTFE clamps. [Yost et al, 2000]

2.7.2 Cell Straining system driven by Linear Actuators

Figure 2.8 shows the schematic diagram of the cell straining system designed by Cacou et al (2000) from University College London medical school. There are two main components: a controlled loading system and culture chambers within a tissue culture incubator, creating six loading stations. The tissue culture incubator contained two level platforms, each supporting three Perspex culture chambers. Each of the chambers was

held between two restraining bars, and was linked by parallel shafts to two linear motors. The two linear motors with limit switches were placed one above the other on two platforms outside the incubator. Displacements of each linear motor, controlled by appropriate software, were transmitted via a single shaft through the incubator to each of the stations. Latex bellows were attached to each shaft and the incubator. Six identical dermal fibroblasts-seeded collagen gels were tested simultaneously in tension, each gripped within a chamber. The gripping mechanism comprised two 3mm-diameter stainless steel posts mounted vertically to loop through the specimen. Six 5N load cells were conditioned and amplified by a multi-channel transducer conditioner and amplifier, digitised by a 12 bit analogue to digital converter and stored on the hard disk of a PC. A program, written in C++, was used for data acquisition and processing. The specimens were subjected to strain regimes for 24 hours at a frequency of 1Hz. These gels were subjected to a cyclic strain of 10% superimposed on two separate tare loads of 2 and 10mN, while being maintained in cell culture conditions. The computer controlled apparatus was shown to be capable of monitoring the individual loads on six specimens simultaneously, to an accuracy of 0.02mN. Following cyclic loading, the cell seeded collagen gels exhibited an increase in structural stiffness compared with the unloaded controls.

In this system the shafts were used to join the motors (outside the incubator) and cell chambers (inside the incubator) and thus modification of incubator was needed. Moreover proper sealing of the holes, where the shafts passed through, is very crucial in maintaining the sterility of the cell culture environment.
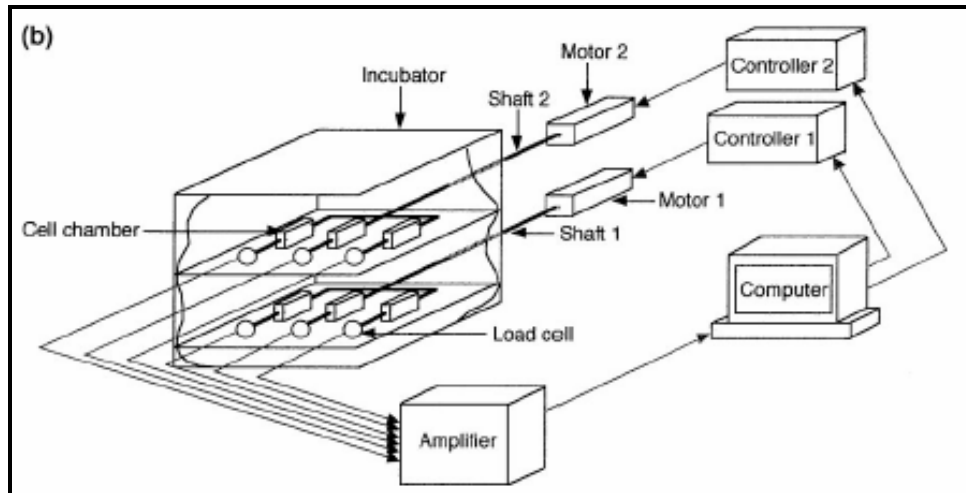
Figure 2.8 Schematic diagram of the cell straining system, showing the arrangement for data acquisition and control [Cacou et al, 2000]
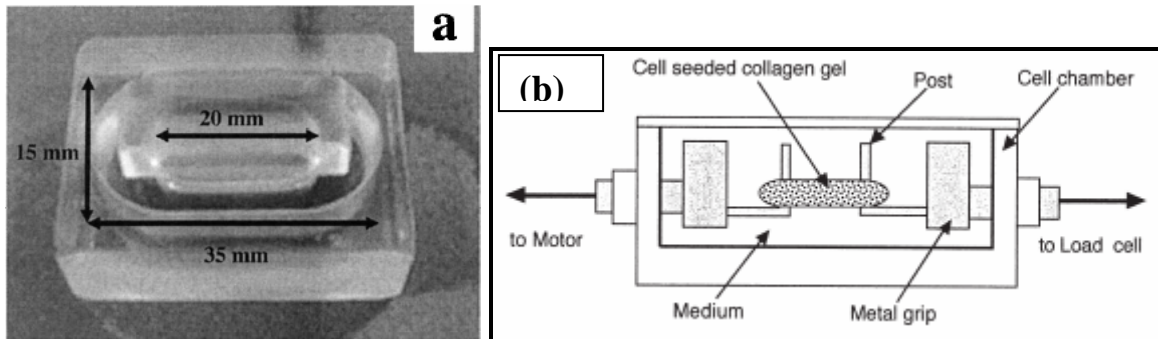
Figure 2.9 (a) Perspex mold, containing a 20 × 5 mm removable central island, used to cast cell-seeded collagen gel constructs (b) Schematic indicating the position of the cell seeded gel construct within the culture chamber [Cacou et al, 2000 and Catherine et al, 2003]

2.7.3 Straining system driven by a Crank Mechanism

Kim et al (2000) from University of Michigan designed an apparatus to subject smooth muscle cell (SMC)-seeded scaffolds to cyclic strain (Figure 2.10). Scaffolds were immersed in PBS or medium and clamped in the tissue culture chamber. The scaffolds were subjected to cyclic strain by periodical movement of a crank back and forth as an

eccentric disk that was driven by a motor and connected to the crank rotated. The frequency and amplitude of cyclic strain were regulated by controlling the speed of motor rotation with a controller and the position of the crank connection to the eccentric disk, respectively. SMCs were subjected to cyclic strain in vitro using custom-made strain units. The seeded PGA fibre-based scaffolds were clamped in the tissue culture chamber and subjected to cyclic strain by movement of the crank back and forth as the eccentric disk connected to the crank rotates. The strain units were placed in a humidified incubator with 5 percent CO_2 at 37°C. The seeded scaffolds were subjected to cyclic strain at a frequency of 1 Hz (1 cycle per second) and amplitude of 7 percent of initial length, which are similar to those of SM tissues in vivo for up to 20 weeks. As a control, seeded scaffolds were fixed at only one end of the clamps and moved back and forth at the same frequency and amplitude as the mechanical strain conditions. Smooth muscle tissues engineered with type I collagen sponges subjected to cyclic strain were found to contain more elastin than control tissues, and the SMCs in these tissues exhibited a contractile phenotype. In contrast, SMCs in control tissues exhibited a structure more consistent with the non-differentiated, synthetic phenotype.

The actuating mechanism of this system is based on crank system, so the system limits the range of extension that can be applied to the scaffold according to the size of eccentric disk. In addition, the design and fabrication of the crank and eccentric disk require precise accuracy for a smooth straining movement.
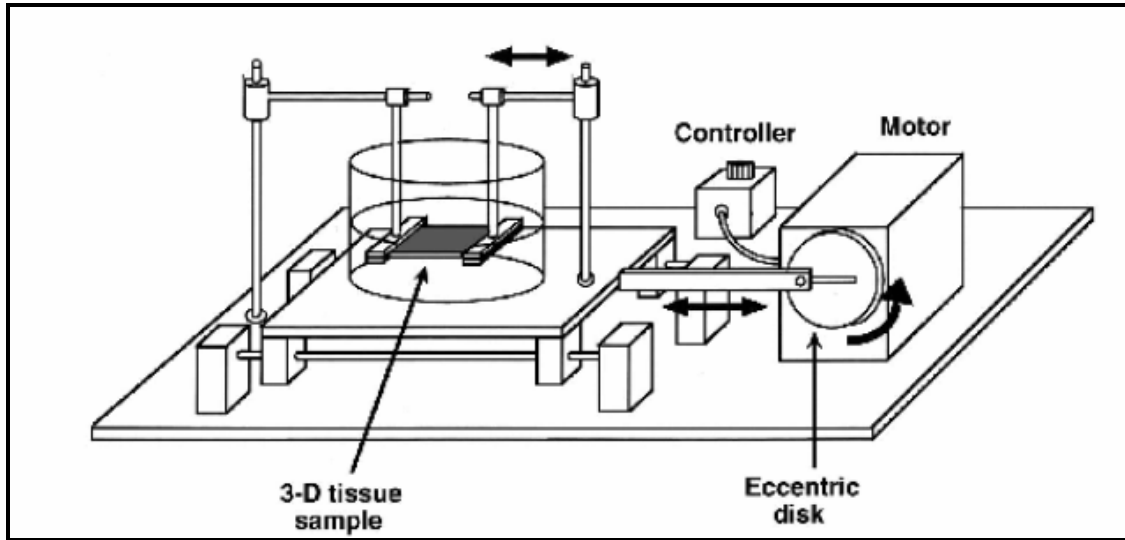
Figure 2.10: Apparatus utilized to subject scaffolds to cyclic strain. The scaffolds were subjected to cyclic strain by periodical movement of a crank back and forth as an eccentric disk that was driven by a motor and connected to the crank rotated. [Kim et al, 2000]

2.7.4 Spool design Bioreactor
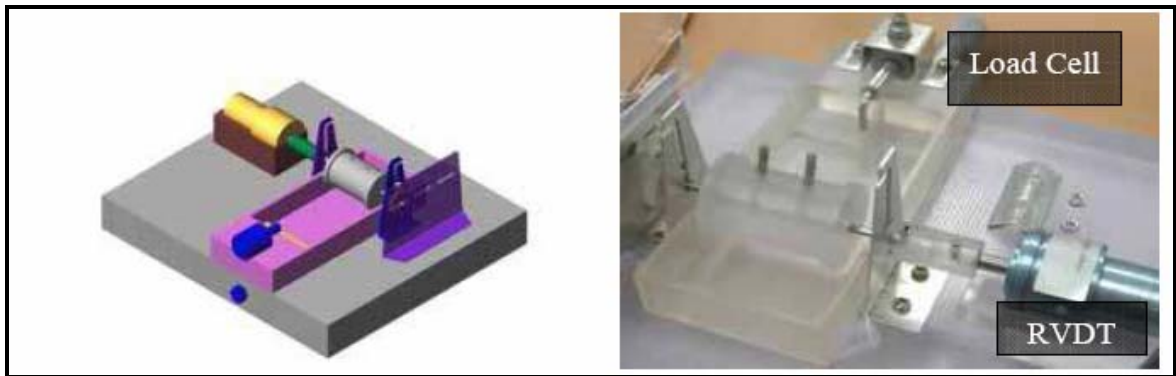
Figure 2.11: Spool design bioreactor

Kwan, (2003) from National University of Singapore designed a bioreactor with spool. The actuating unit from that design is made up of a stepper motor (PM 35S-024, Minebea Hamamatsu) actuating via a pair of spur gear with the gear ratio of 0.33. The motor is controlled by standalone microprocessor where the control program can be stored. The

knitted PLGA scaffolds seeded with Human dermal fibroblast cells (HDFs) were attached to spool. Another end of cell seeded scaffold is fixed in Petri dish and scaffolds were strained by rotating of spool in a 1.8% strain amount and 1 Hz frequency. A force and displacement monitoring system is integrated in this system. Cell seeded scaffolds were strained 4 hour per day for two week period. The bioreactor can strained three tubular form scaffolds together. Another set of cell seeded scaffolds are clamp on the clamp fixture for control (without strain). After two week straining, the results show that cell in strained sample have more elongated morphology and better alignment as compared to control sample.

The design of this bioreactor is very simple and easy to fabricate. The limitation of this system is that the straining frequency of the bioreactor could not be set to lower than 1 Hz frequency.

2.7.5 Advanced Bioreactor
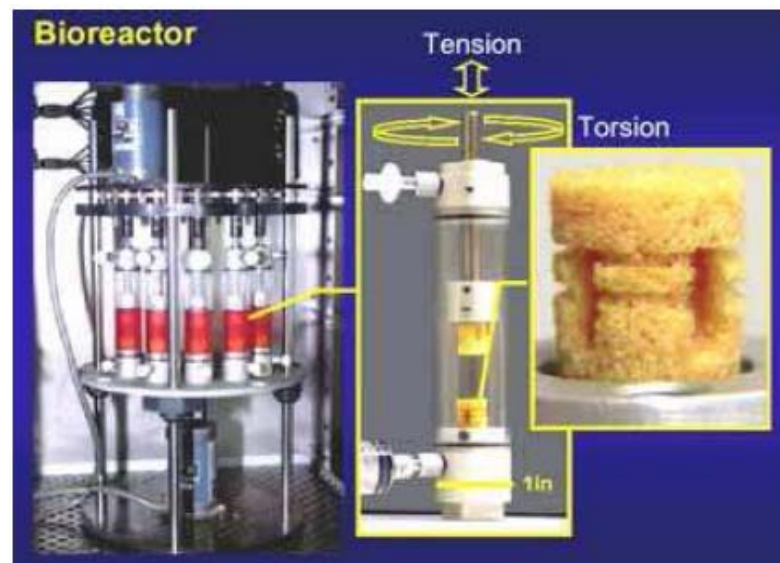
Figure 2.12: An overview of the bioreactor (left), the cylindrical testing compartment (middle) and the collagen gel scaffold (right).[Altman et al, 2001]

Altman et al (2001) from Tufts University had designed a bioreactor (Figure 2.12) that can accommodate up to 12 individual tubes (2.5 cm in diameter × 4 cm long), each providing an environment for the growth of one vertically oriented ligament attached between two anchors positioned 2 cm apart. Tube dimensions and anchor placement were selected based on culture volumes previously used to grow ligaments (20 ml per ligament), and the dimensions of anterior cruciate ligaments in goats (approximately 16 mm long). This novel bioreactor was capable to provide a combined tensile-compressive and torsional loading to mimic the unique combination of forces to which a ligament is exposed during physiological function and repair *in vivo*. Translational strain (10%, 2 mm) and rotational strain (25%, 90º) were applied concurrently at a frequency of 0.0167 Hz (one full cycle of stress and relaxation per minute) to collagen gels seeded with bone marrow-derived cells. The complete bioreactor system was placed in an incubator (37˚C, humidified, 5% CO_2) and operated by using an external computer. Software used to control the device was written by using C programming language and Borland C++ Compiler Version 5.0. For both bovine and human cell studies, mechanical stimulation was applied after an initial period of 2 days allowed for gel hardening. Coral and cancellous bone anchors were used in the reactor tubes to mimic ligament-bone attachment *in vivo* and to support tissue in growth *in vitr*o. Collagen gels of 2-cm long between anchors were seeded in a 2.54 cm tube with human bovine bone marrow-derived cells and were cultured up to 21 days, with or without mechanical loading.

The application of mechanical stress over a period of 21 days up-regulated ligament fibroblast markers, including collagen types I and III and Tenascin-C, fostered statistically significant cell alignment and density and resulted in the formation of oriented collagen

fibers, all features characteristic of ligament cells. Mechanical stimulation of ligaments based on bone marrow-derived cells induced elongated, ligament-like cell morphology, and cell alignment in the direction of loading, in contrast to the round and randomly distributed cells in static controls. Cell alignment in the direction of mechanical loading was 2.5-fold higher as compared to that found in the control. Helically organized collagen fibres formed in the direction of the applied load at the periphery of the mechanically stimulated ligaments, a feature absent in the controls.

Another version of the same bioreactor is shown in Figure 2.14 (Altman et al, 2002). Twenty-four silk fiber matrices seeded with human bone marrow stromal cells (hBMSCs) housed within reactor vessels were maintained at constant temperature (37°C), pH (7.4), and pO_2 (20 %) over 14 days in culture. The system supported cell spreading and growth on the silk fiber matrices based on SEM characterization, as well as the differentiation of the cells into ligament-like cells and tissue.

In this modified version, a multi-component environmental chamber (Figure 2.13b) was built to provide precise pH and pO_2 control to all 24 reactor vessels via silicone tubing gas exchangers. Environmental chamber components included 12 individual chamber sections designed to house two coils per section, an additional chamber to house two thermocouples to measure chamber wall and internal temperature, a gas mixing plenum with 3 gas inlets, a gas distribution manifold and a chamber outlet port. Each chamber section provided, on opposite faces, an inlet and outlet port for recirculating vessel medium. The chamber sections were designed as independent components to provide flexibility to the system. Chamber sections were stackable and removable for quick turn-around, sterilization without entire system shutdown, and easy clean up in the case of leaks. The entire chamber or individual sections, including inlet and outlet ports, could be

steam sterilized. Hose dimensions and length were chosen to achieve vessel medium equilibrium with the gas environment of the environmental chamber over the range of possible medium flow rates provided by the pump system. Vessel medium was recirculated via a multi-drive micro bore peristaltic pump (12 channels per pump). Chamber atmosphere was maintained equilibrium through the silicone gas permeable hose at 1.7 ml/min; therefore, control over inlet gas flow rates could be used to adjust the dissolved gas concentrations of the reactor vessels. Independent mass flow controllers individually controlled the flow rates of the three gasses into the mixing plenum. The ratiometrically correct mixture was then distributed into the chamber by the orifices of the gas inlet distribution manifold that had been sized for even distribution of the gas into the chamber taking into account the mass flow rate and the associated drag of the gas mixture. The gas permeable platinum-cured silicone hose of the coils allowed diffusion of the gases into the medium. Thus, pH and dissolved pO_2 were maintained at the same levels in all reactor vessels. The chamber gas outlet tube remains opened to allow gas flow through the chamber maintaining steady state. Low inlet gas flow rates were maintained such that inexpensive commercially available CO_2, O_2, and N_2 tanks would last for approximately 3 weeks.

In this system, there is a possibility for serum proteins to deposit on the interior wall of tubes. Any proteins deposition will affect the flow of the medium and thus compromise the proper functioning of the nutrient and gaseous exchange system.
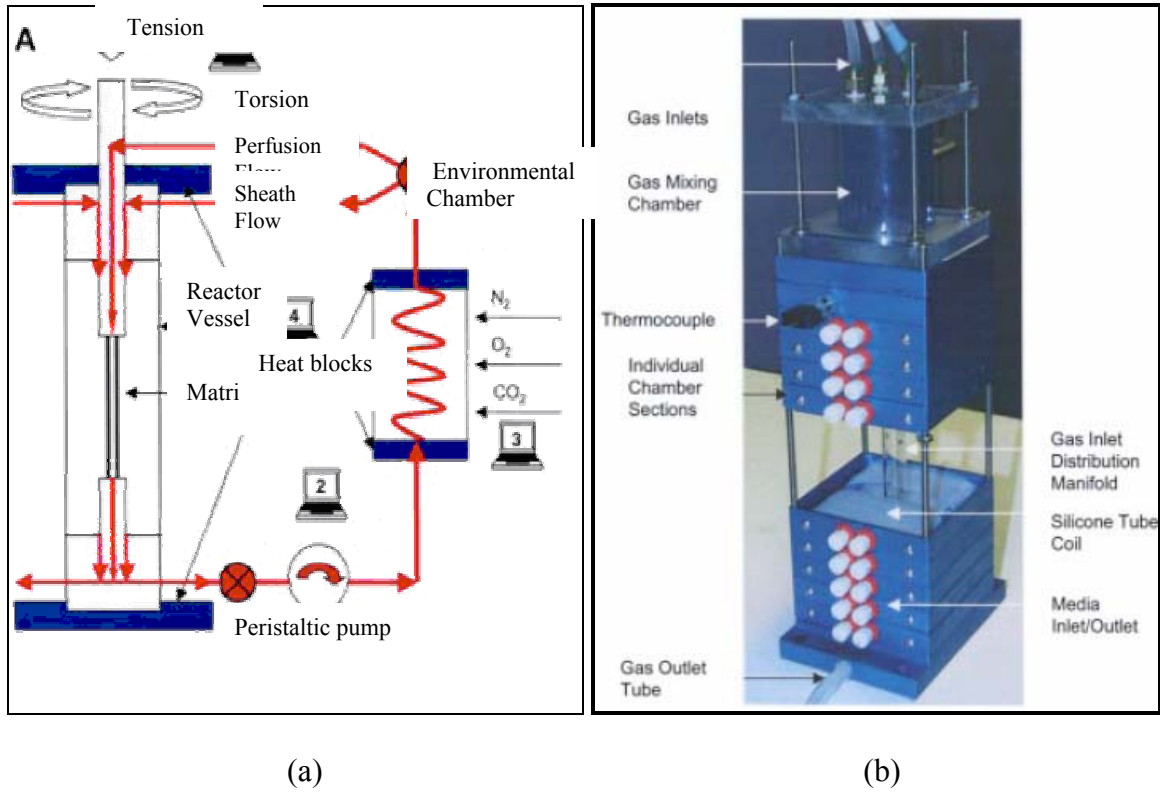
Figure 2.13: (a) Schematic illustration of the bioreactor system, (b) Environmental chamber prior to closure to show the internal silicone hose coils and gas inlet distribution manifold [Altman et al, 2002]
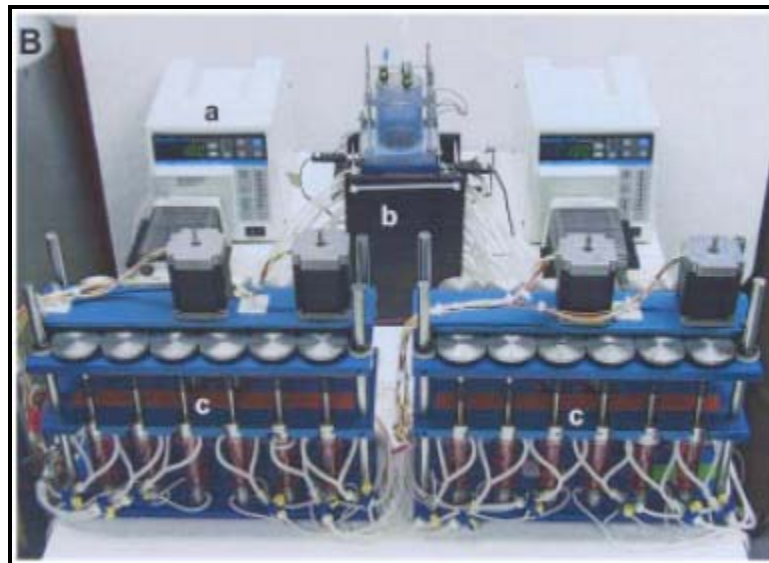
Figure 2.14: Functioning bioreactor system includes: (a) peristaltic pump,(b) environmental gas chamber and, (c) the two bioreactors containing 24 vessels. [Altman et al, 2002]

Chapter 3. Preliminary Study

Before designing and fabricating the new bioreactor, a preliminary study was done by using existing bioreactors [Darrel, L.C.L., 2002/2003 and Kwan, M. S.,2003].The objective of this study is to investigate the effect of cyclic mechanical strain on different forms of scaffolds (Tubular form and sheet form scaffolds). Histology examination was done after two weeks straining on the cell seeded scaffolds. The cell morphology was investigated and results of strained samples were compared with unstrained samples in both forms of scaffolds.

3.1 Scaffold preparation and Cell Culture

One sheet form scaffold for each strained and unstrained group was used and two tubular form scaffolds were used for both groups. All the scaffolds were knitted from 3-yarns PLGA fibres. (Refer to section 5.2 for more details). For tubular form scaffold, 12 needles from knitting machine were used to knit the scaffold. The width of scaffold was around 2cm before rolling it up into the tubular form. When rolled up, the diameter of scaffold is about 5 mm. For sheet form scaffold, 24 needles from knitted machine were used. The width of sheet form scaffold was approximately 35 mm (Figure 3.1).

 Human dermal fibroblasts (HDFs) cells were used in this experiment. Cells were cultured and sub cultured until it reached the required amount. (Refer to section 5.1 for more detail). Approximately 12 millions cells were seeded on the 50mm length of tubular form

scaffold in both strained and unstrained group. In sheet form scaffolds, approximately 20 millions cells were seeded to cover larger area (50mm × 20mm).
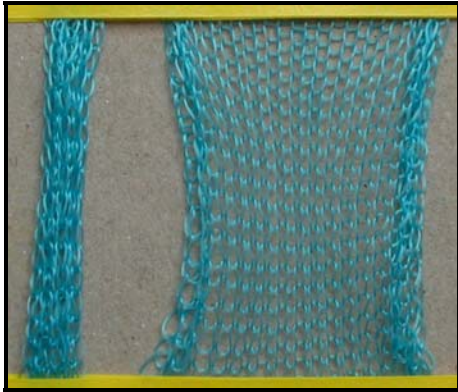
Figure 3.1: Tubular form and Sheet form scaffold used in preliminary study.

3.2 Bioreactor setup and Cell seeding

All parts of bioreactors were sterilised under ultraviolet radiation for 30 minutes and followed by the swabbing of 70% ethanol. The scaffolds were sterilised with 70% ethanol for 1 hour. After that, all bioreactors parts are assembled inside a biological safety cabinet. The basic straining mechanism of bioreactors for tubular form scaffolds and sheet form scaffolds are the same. One end of the scaffolds was fixed in spools and another end of scaffolds was fixed to the load cells which were then placed in a Petri dish. The spool is directly connected to the stepper motor in the bioreactor for sheet form scaffolds. In the bioreactor for tubular form scaffold, the spool is connected to the motor by a pair of spur gears. By turning on the motor, the cyclic strain was applied on the scaffolds.

For unstrained samples, the clamping fixtures as shown in figure 3.2(a) were used for both tubular form and sheet form scaffolds. This was to ensure that both strained and unstrained samples had the similar stretched profile during the whole experiment.

Fibrin Glue, 1 ml kit, (Tisseel[TM] Co. Hyland Immuno, Baxter) was used as a temporary, biodegradable adhesive for the cells onto the scaffolds. (Figure 3.2)

| (a) | (b) | (c) |
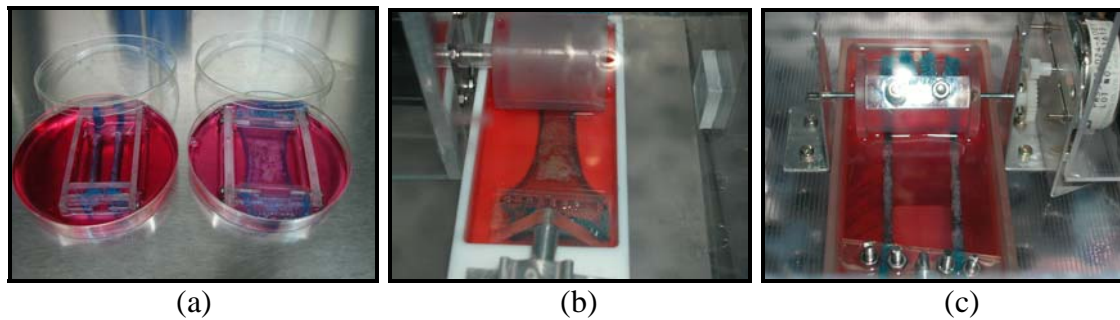
Figure 3.2: Cell seeded scaffolds; (a) unstrained samples, (b) bioreactor for sheet form scaffold, (c) bioreactor for tubular form scaffold

3.3 Cyclic Straining and Histology examination

All the samples were placed in humidified incubator (5% CO_2, 37˚C, and 95% humidity). After cells seeding, no cyclic straining was applied to the scaffolds within the first 3 days to allow a good cell adherence to be established before any straining was conducted. The system was programmed to apply a cyclic strain of 1.8% with a frequency of 1 Hz. Three days after cell seeding, cyclic mechanical strain was then applied to the scaffolds. The cyclic straining was set up constantly for 4 hours per day for a 2 week period. The culture medium was changed every three days to maintain a balanced level of nutritional contents of the medium.

Upon completion of two weeks of cyclic straining, scaffolds from strained and unstrained groups were washed with PBS and then fixed in 4% Formalin for one day. The samples were then stained with Haematoxylin & Eosin (H & E) stain using paraffin sectioning.

Histology examination was conducted on both transverse and longitudinal sections. Quantitative measurements (cell nuclei length and orientation angle) were conducted from longitudinal section in both tubular form and sheet form scaffolds.

For the measurement of length, the longest dimension of the selected cell nuclei was considered as the length of the cell. The average length of a normal cell nucleus without elongation falls in the range between 5μm and 10μm. For a more realistic analysis, cells with their lengths that fall between 5μm and 15μm were chosen for all quantitative measurements.

In the case of the orientation of the cell nuclei, the direction of the straining axis (as in strained group) or longitudinal axis (as in unstrained group) was needed to be defined. The orientation angle was defined as the angle between the major axis of each cell nucleus and straining axis or longitudinal axis in strained group and unstrained group respectively. The clockwise angle from straining axis and longitudinal axis was measured as positive orientation angle and anticlockwise angle from these axes was measured as negative orientation angle (Figure 5.11). The orientation angle was then expressed as ±0-90°. The number of cells whose orientation angles fall in the range of ±5°, ±10° and ±30° was counted and compare to each group. (Refer to section 5.5.3 for details on procedure)
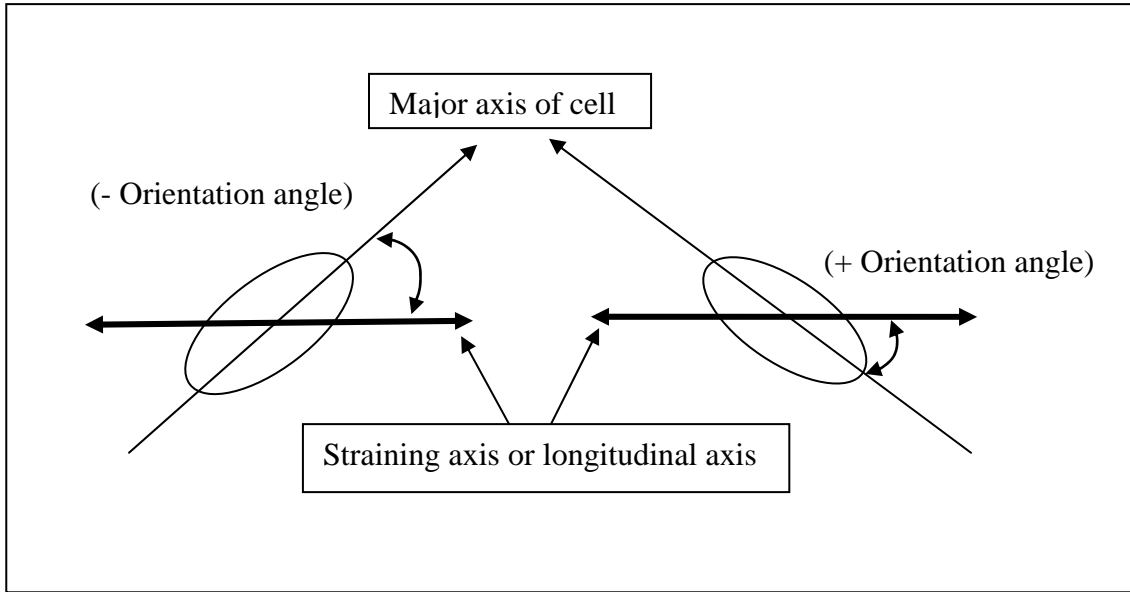
Figure 3.3: Explanation of cell orientation angle

3.4 Results and discussion

3.4.1 Transverse section

(a)   (b)
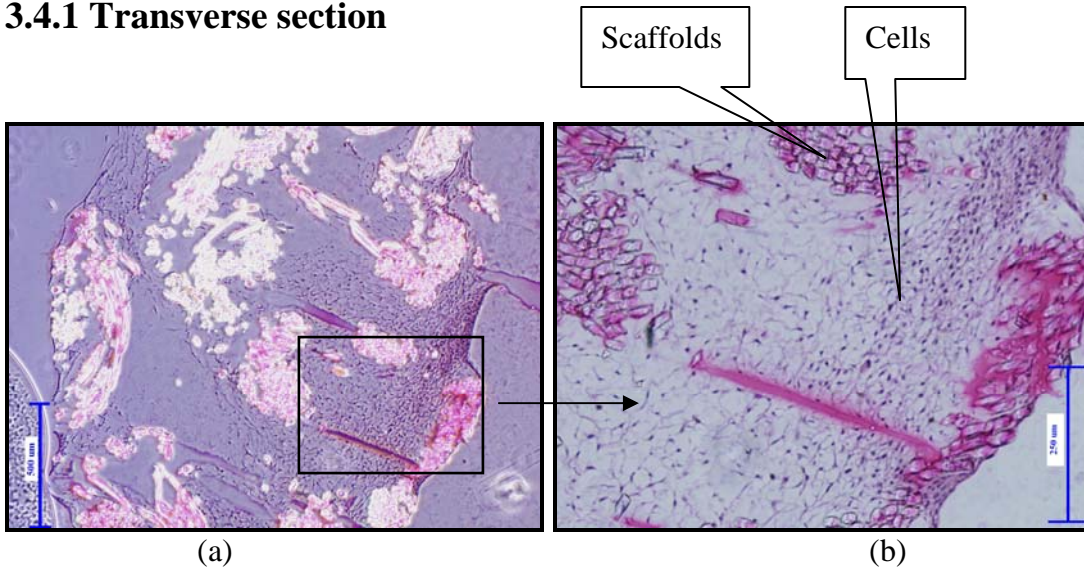
Figure 3.4: Transverse section of tubular form scaffolds from strained group after two weeks of straining shows cell growth was mainly found at the periphery;(a) 40X magnification ,scale bar = 500 µm, (b) 100X magnification, scale bar = 250 µm
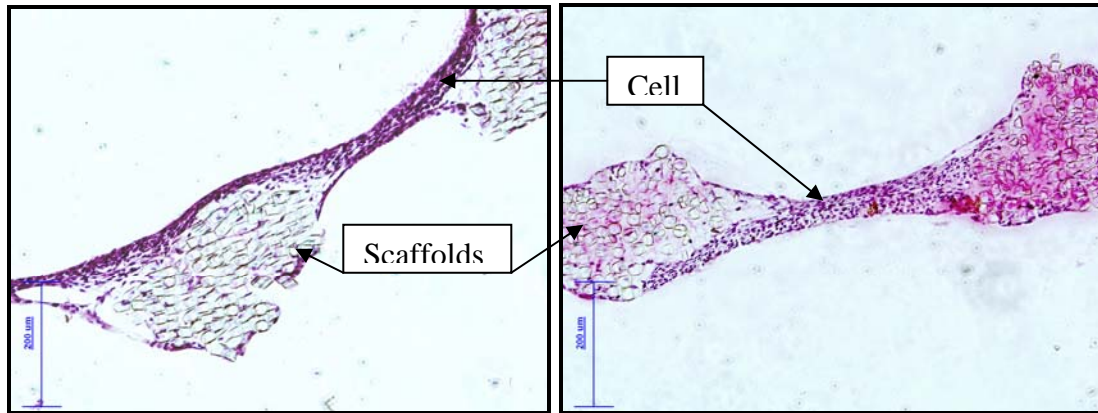
Figure 3.5: Transverse section of sheet form scaffolds from strained group after two weeks of cyclic straining (Magnification 100X, scale bar = 200 µm)

Transverse sections of tubular form scaffold show that the cell growth was mainly found at the periphery (Figure 3.3(a)). One possible reason for this observation is that the nutrients (CO_2, O_2) available for the cells from the interior part of the scaffold may not be enough. In this condition, nutrients diffusion into the construct resulted in a gradient of nutrients from exterior to interior. Cells in the interior of the matrices were likely to grow slower than those on the surfaces of the matrix, and this enhanced the lower cellularity and less even cell distribution. [Kim et al, 1997]. In sheet form scaffolds, similar problem did not occur because nutrients could reach to every part of the scaffolds. This kind of nutrient gradient problem may be solved by using perfusion system which allows the nutrients to pass through to the core of the scaffolds.

3.3.2 Longitudinal Section

Figure 3.5 shows the longitudinal sections of histology staining for all groups of scaffolds. The cells of strained samples from both tubular form and sheet form scaffolds show more elongated morphology and better alignments than cells from unstrained samples.

According to the quantitative measurements, the length of cell nuclei in strained and unstrained samples of tubular form scaffolds are 7.95 ± 2.93 μm (Mean ± Standard Deviation) (n=1855) and 7.19 ± 2.33 μm (n=1933) respectively. That is the cell from strained samples is 10.8% longer than that of unstrained sample.

In sheet form scaffold, the cell nuclei length of strained samples is about 8.87 ± 2.91 μm (n=1825) while cells from unstrained sample have length of 7.46 ± 2.35 μm (n=1935). This finding shows that the cells from strained samples are 18.9 % longer than that of unstrained sample in sheet form scaffolds.

These observations suggested that the cyclic mechanical strain affects cell morphology as it causes a more elongated cell. In the sheet form scaffolds, the mean cell nuclei length of strained samples is 18.9% longer than that of unstrained sample. In the tubular form scaffolds, the mean cell nuclei length of strained samples is only 10.8% longer than that of unstrained sample. These findings suggested that the better effect of cyclic mechanical strain occurred for sheet form scaffolds. Actually, there is more space for cell growth inside the tubular form scaffolds as compare to sheet form scaffold. The cells from tubular form scaffolds also can growth to the perpendicular direction of the straining direction while the cells from sheet form scaffold can growth only on the scaffold surface. So the cell from tubular form scaffold processes more chance to growth to the other directions rather than strained direction as compare to sheet form scaffolds. This fact may be the reason of why the better effect of cyclic mechanical strain occurred for sheet form scaffolds.
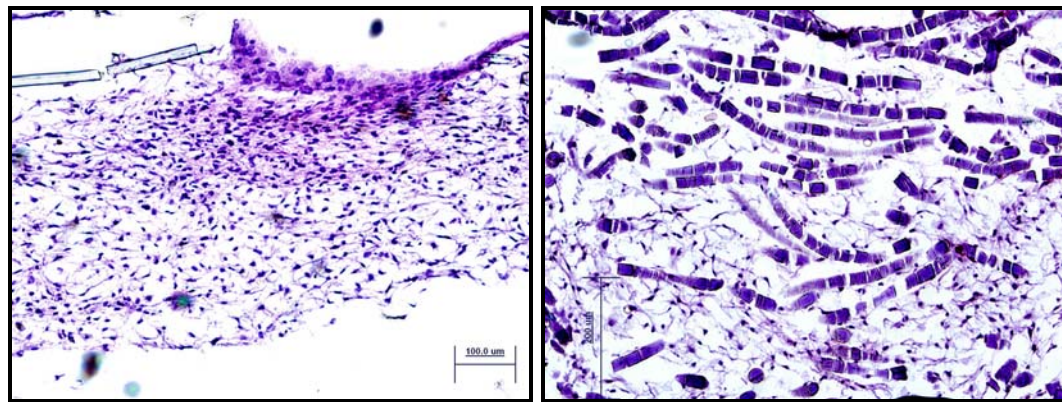
(a: scale bar=100μm)   (b: scale bar = 200 µm)
(Longitudinal section of Tubular form scaffolds, 100X)
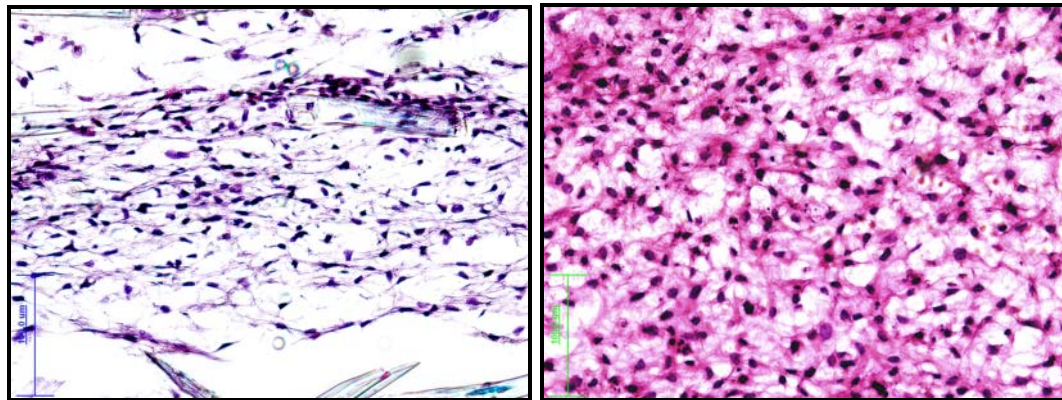
(c: scale bar=100μm)   (d: scale bar=100μm)
(Longitudinal section of Sheet form scaffolds, 200X)

Figure 3.6: Longitudinal section of tubular form scaffolds and sheet form scaffolds after two weeks of cyclic straining; (a & c) Strained samples, (b& d) Unstrained sample.

In the case of cell alignment, the orientation angles of cells were measured and the number of cells where orientation angle fall in the specific ranges was counted and compared in each group. Table 3.1 shows percentage of cells from each group which fall in the specific orientation angle range. More cell populations from strained samples fall in the specific orientation angle compared with unstrained samples in both tubular form and sheet form scaffolds. It shows that the cells from strained sample are more aligned than unstrained sample in both forms of scaffolds due to applied cyclic strain. The difference of cell

population in each orientation angle between strained and unstrained samples of sheet form scaffold is larger than that in tubular form scaffolds. This seems that cyclic mechanical strain is more effective on sheet form scaffolds.

Table 3.1: Percentage of cells in each orientation angle for all sample groups

		Orientation angle		
		$\pm 30^{\bullet}$	$\pm 10^{\bullet}$	$\pm 5^{\bullet}$
Tubular-form Scaffold	Strained sample	65.2%	28.7%	14.1%
	Unstrained sample	63.7%	25.8%	13.4%
	% difference	**1.5%**	**2.9%**	**0.7%**
Sheet-form Scaffold	Strained sample	50.3 %	19.8 %	9.5 %
	Unstrained sample	38.1 %	13.2 %	5.9 %
	% difference	**12.2 %**	**6.6 %**	**3.6 %**

According to the results of this preliminary study, it is clear that application of cyclic mechanical strain cause more elongated cells and better alignment as compared with unstrained samples. Moreover the effect of cyclic mechanical strain is more significant for sheet form scaffolds.

Chapter 4. Design and Fabrication of Bioreactor

One of the objectives of this research is to develop a bioreactor for the in-vitro engineering of soft tissues. The existing bioreactor have some limitations; (i) the bioreactor could strain only one sheet form scaffold, (ii) the minimum straining frequency is limited at 1-Hz. To fulfill the objective of this research and to solve the limitation of existing bioreactor, a new bioreactor was designed and fabricated. This design will assist in the study of the effect of varying straining parameters on the cellular response. By studying the effect of straining parameter on cellular response, we will know the optimum condition for the cell growth under in-vitro conditions.

4.1 Design Criteria

According to the preliminary study, the results show that cyclic mechanical strains have a better effect on sheet form scaffolds as compared to tubular form scaffold. The cell from sheet form scaffolds show more elongated cells and better alignment. In this study, sheet form PLGA scaffolds were chosen for the whole experiment.

Ideally, a tissue engineering bioreactor must provide;

1- an appropriate environment (temperature, humidity), the maintenance of biochemical condition (pH, pO_2, concentration of nutrients);

2- sufficient metabolic transport to and from the developing tissue;

3- Structurally defined support for cell attachment and tissue formation; [Altman et al, 2002]

In this research, all the cell cultures were done inside an incubator (Sanyo) which can maintain the appropriate environment for cell culture (5% CO_2, 37°C and 95% humidity). To get sufficient metabolic transport for the growing tissue, sheet form scaffolds are used and the culture medium is changed (100%) every 3 days. The designed bioreactor can support various straining parameters. The straining frequency and straining value are adjustable.

The following criteria are used in the design of the bioreactor;

1- The bioreactor must be able to stimulate at least three scaffolds at the same time.

2- It must be possible to operate for at least a two-week time period without the need for any maintenance in a humid incubator environment.

3- All material used in this design must be biocompatible and resistant to corrosion.

4- The straining parameters (frequency and amount of strain) must be adjustable.

5- The design must be simple and easy to assemble.

4.2 Material selection

The material used in the bioreactor must withstand the highly humid environment in the bioreactor as well as high temperature and pressure in the steam autoclave machine. Moreover, the selection for the parts that come into direct contact with the culture medium and scaffolds is also crucial. The incubator environment is constantly maintained at 5% CO_2, 37°C and 95% humidity. In such a highly humid environment, most of the metals will corrode. The steam autoclave operates at a temperature range of 110-120°C and 0.1

MPa. Hence, materials used in the design must be able to withstand such a high temperature and pressure level without any distortion. The dimensional stability of the bioreactor parts is also important as the input strain is directly portion to the size of the spool.

The material selection is done based on following requirements:

1. Materials must be biocompatible

2. Must possesses good machinability

3. Must be able to autoclave

4. Must be corrosion resistant

5. Must have low water absorption and be able to withstand high temperature

6. Must be compatible with alcohol used in sterilization

After some consideration, plastics are preferred to metals due to its better machinability and biocompatibility. Table 3.1 shows some physical properties of some possible plastics to be used in this design. Among these plastics, polycarbonate is chosen for all parts of the bioreactor because the properties of polycarbonate meet the design requirements. Medical grade stainless steel screws (Stainless steel grade 316L) are chosen for the screws needed in the bioreactor.

Table 4.1: Physical properties of various suitable plastics; (· · mean steam Autoclavable, **X** mean not autoclavable) [extracted from www.nuncbrand.com]

Material / Property	Polystyrene	Polypropylene	Acrylic	Teflon	High-Density Polyethylene	Nylon	PEEK	Polycarbonate
Steam Autoclavable	X	· ·	X	· ·	X	X	· ·	· ·
Heat Distortion Temperature (°C)	70	135	50	146	121	93	160	132
Water Absorption-24hrs (%)	0.1	0.01-0.03	0.3-0.4	0.01	0.01	1.2	0.15	0.15
Water Absorption-Saturation (%)	-	-	-	-	-	6.5	-	0.35
Transparency	Clear	Translucent	Clear	Opaque /translucent	Translucent	Clear	Opaque	Clear

4.3 Proposed Bioreactor design

A proposed design was made during this research. This design is a modified design of the bioreactor proposed by a final year undergraduate [Darrel, 2002/03]. In this design, 4 sheet form scaffolds could be strained at the same time. The spool is directly connected to the stepper motor at one end and another end of the spool is supported by a RVDT. One end of the scaffolds is attached to spool and another end attached to the scaffolds clamp system (Figure 4.1). The cyclic mechanical strain is applied to the scaffolds by rotating the motor.
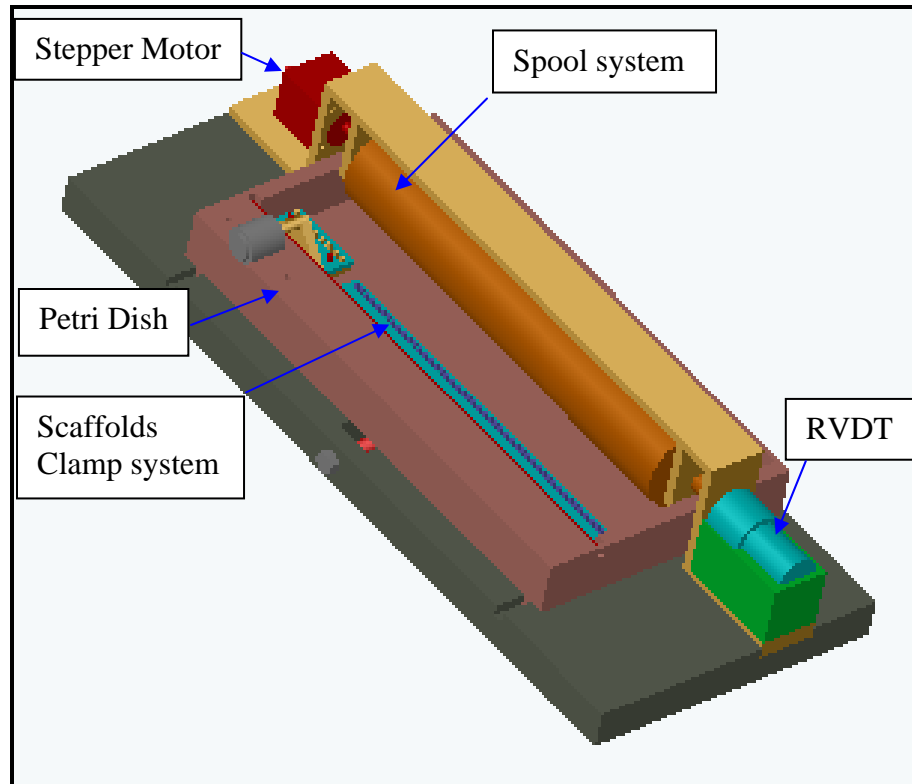
Figure 4.1: Proposed Bioreactor design.

There are two main disadvantages in this design:

a) The fabrication for scaffolds clamp system and spool assembled parts may too complicated and the part will face distortion after fabrication and

b) All scaffolds are stimulated in the same chamber

The scaffold clamp system and spool assemble parts from this design include many teeth which may be difficult to fabricate. When the scaffolds are attached to this part, these teeth may break some PLGA fibres from the scaffolds. The length of this clamp system is quite long while the thickness and width is quite small (Figure 4.2). This system will face distortion after fabrication. Another disadvantage of this proposed design is that all the scaffolds are stimulated in the same chamber (Petri dish). This may cause cross

contamination. If one scaffold gets contaminated, the rest of the scaffolds will be affected. If small separate chambers are used for each scaffold, we can reduce the chance of cross contamination.

(a)   (b)
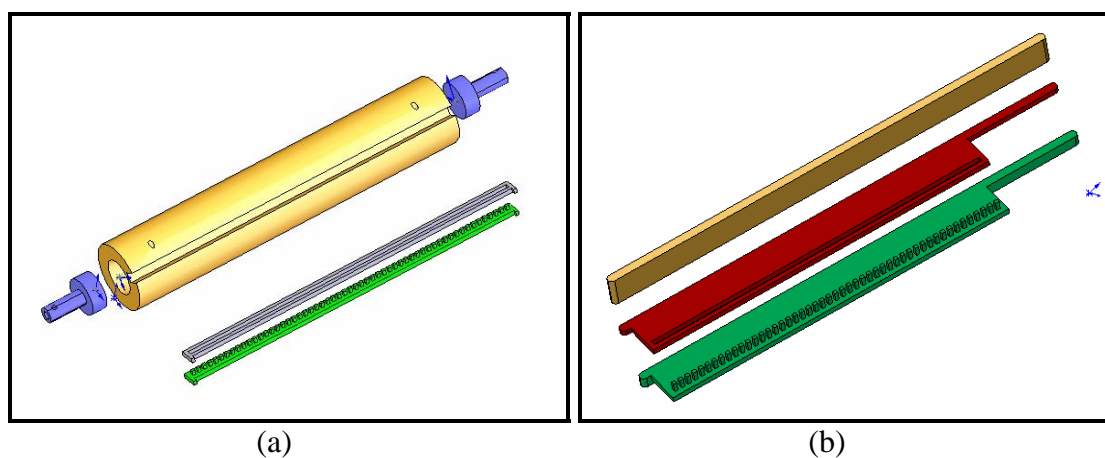
Figure 4.2: (a) Spool assembled parts; (b) Scaffolds clamp system

4.4 Fabricated Bioreactor design

In this design, the cyclic mechanical strain is applied to the scaffolds by the rotation of the spool, which is driven by a stepper motor. Three scaffolds can be loaded simultaneously in this design. Figure 4.3 shows the schematic diagram of the fabricated bioreactor.
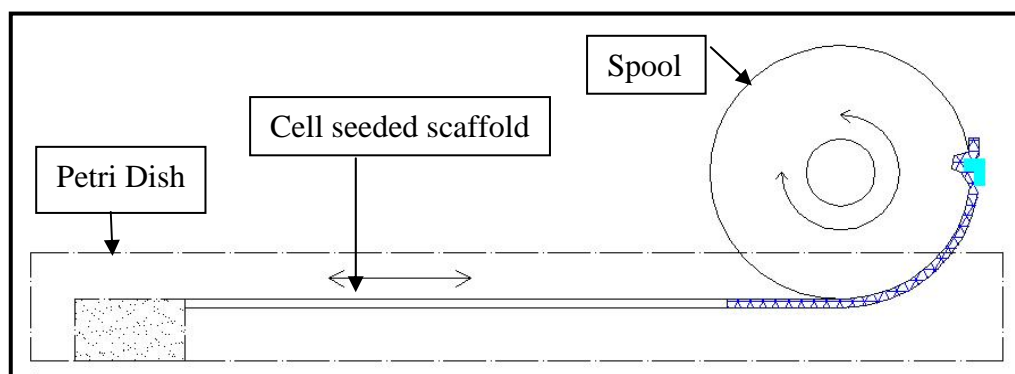
Figure 4.3: Schematic diagram of the bioreactor

4.4.1 Overall design
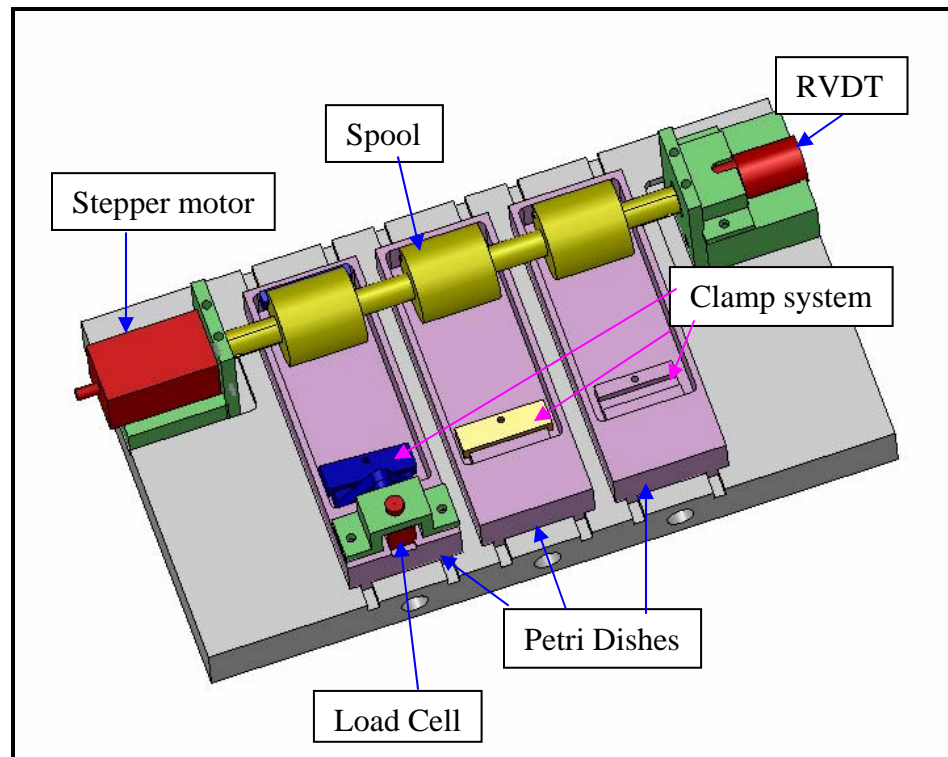
Figure 4.4: Design of the bioreactor

All parts of the bioreactor are fabricated from polycarbonate. There are three separate petri dishes for the three scaffolds. The scaffolds are attached to the spool at one end and another end is attached to the clamp systems housed in each petri dish. The motor is fixed to one end of the spool. The other end of the spool is attached to a rotary variable differential transducer (RVDT) which can measure the rotation of spool to counter check the accuracy of the control system (Figure 4.4). A load cell (PCB, Piezoelectrics, Model 208 C01) is fixed on one petri dish to monitor the load acting on the scaffolds. Three micrometer heads are used to adjust the length of scaffold by the moving petri dishes (Figure 4.5).
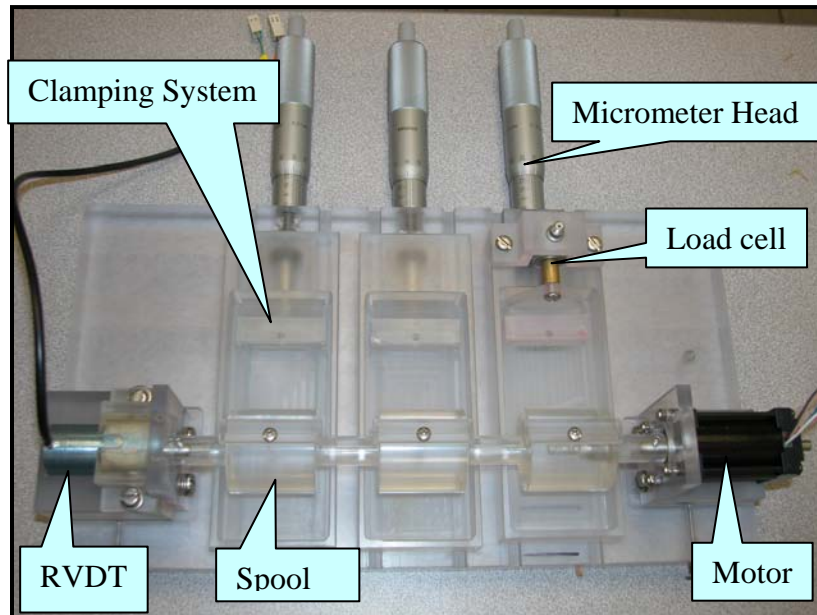
Figure 4.5: Picture of the bioreactor

4.4.2 The Actuating System

After considering various kinds of actuating system such as servo motor, rotary stepper motor and linear stepper motor, the rotary steeper motor is chosen. The circular motion of rotary motor can easily be converted to the required linear motion by means of the spool. The rotary stepper motor can give better torque than servo motor. Moreover, more accurate movement is achieved by using this rotary stepper motor instead of the linear stepper motor. The rotation of the motor is controlled through pulses sent to the motor which move the rotor by a basic step. There are two common types of stepper motor, the 2 phase stepper motor and 5 phase stepper motor. The 5 phase stepper motor has an additional pair of magnetic poles which give it the ability to run considerably smoother. There is less torque ripple and higher running torque.

The 5 phase stepper motor (MYCOM, PEE-535B) was used in this bioreactor. This motor has 500 basic steps per revolution (step angle = 0.72˚), giving smooth rotation and a very small rotor inertia to minimize vibrations.(Refer to Appendix-D for more detail specifications)
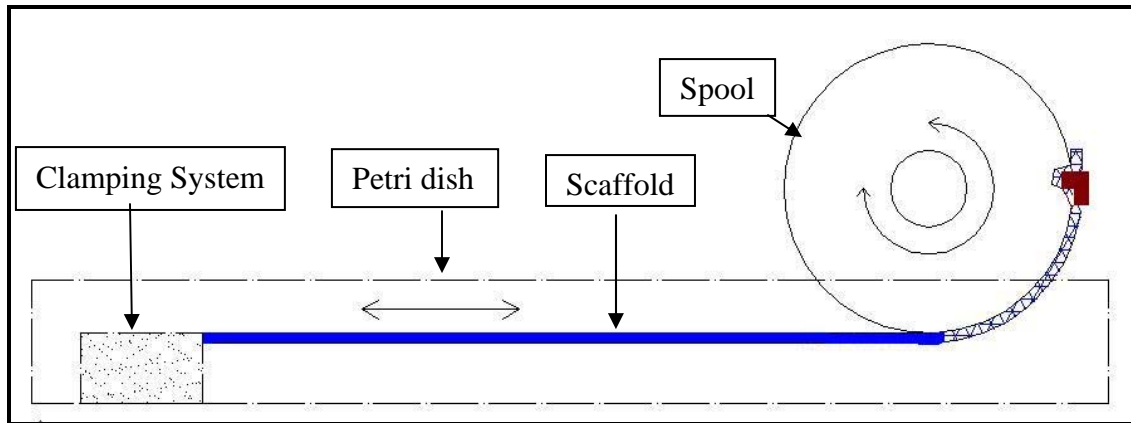
Figure 4.6: Schematic diagram of the bioreactor; blue colour shows the original length of scaffold.

The length of scaffold between the centre of the spool and the edge of the clamping system from petri dish was assumed as the original length of the scaffold (Figure 4.6). The strain amount can be calculated as follows;

$$\text{Strain} = \frac{\text{Extension of scaffold}}{\text{Original length of scaffold}} \hspace{3cm} \text{-----------------------(1)}$$

The original scaffold length is set to 59mm in this experiment. The strain value of 1.8% is used for the whole experiment, so the linear extension of 1.062mm is required to get this strain value. In this design, the extension of the scaffold is directly related to the rotation of spool by;

$$\text{Rotation angle (degree)} = \frac{\text{Desired extension (mm)}}{\pi \times \text{Diameter of spool (mm)}} \times 360^{\circ} \qquad \text{-----------------------(2)}$$

The diameter of spool in this bioreactor is 34mm, so when the spool is turned 3.58°, the desired extension of 1.062mm will occur. In this experiment, the bioreactor is programmed to turn 3.6° at a frequency of 0.1 Hz. (10 seconds for one complete cycle). The strain amount can be changed easily by changing the rotation angle of the spool.

4.4.3 Petri Dish- Base Assembly

An alternative way of adjusting the value of strain is to change the original scaffold length. The length of the scaffold is adjusted by translating the petri dish, to which one end of the scaffold is fixed, nearer or farther away from the spool. Figure 4.7 shows the petri dish-base assembly. A small piece of polycarbonate (Petri dish base) was glued under the petri dish. One aluminium ring, (micrometer head holder) was fixed at the shaft of micrometer head. By turning the micrometer head, the micrometer head holder will move forward and backward. The movement of the micrometer head holder makes the movement of the petri dish by pushing the petri dish base. There are two "grooves" on the base and two "legs" under petri dish which guide the movement of the petri dish (Figure 4.8).
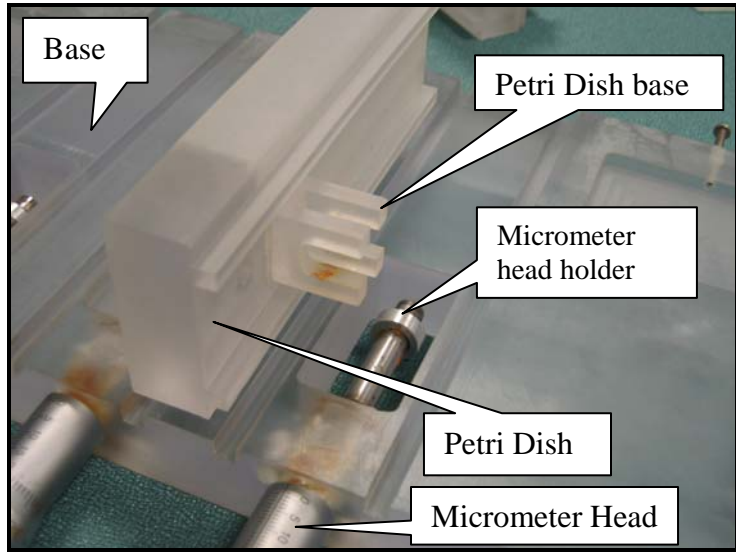
Figure 4.7: Photos of Petri dish-base assembly

(a)   (b)
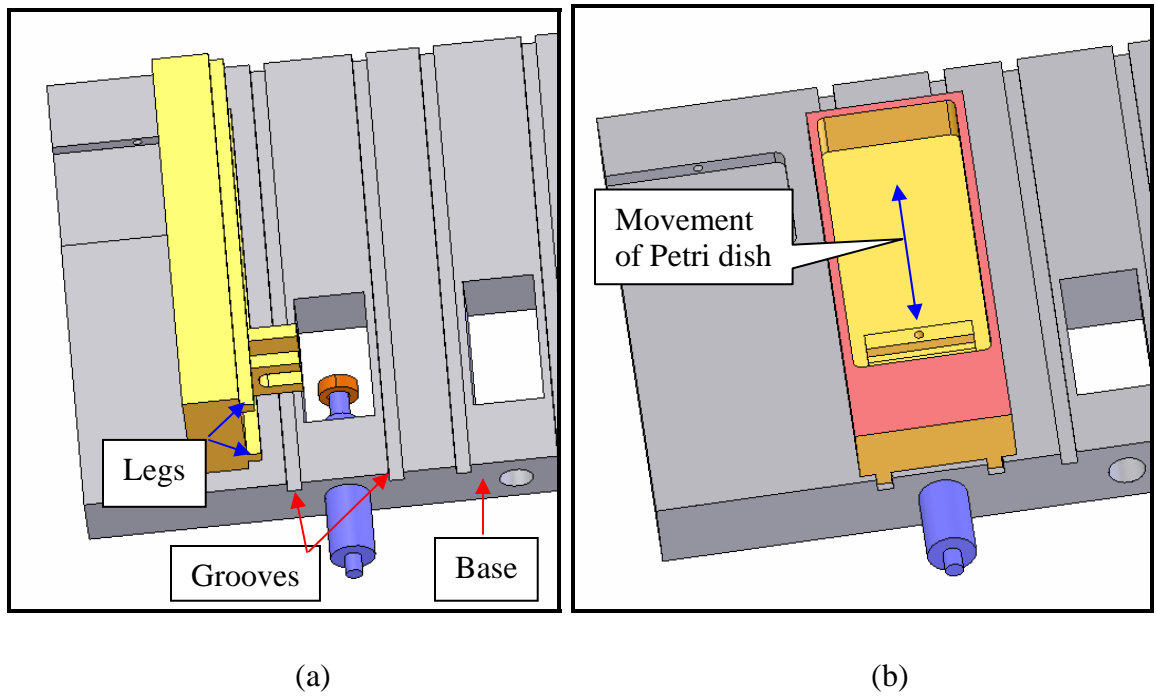
Figure 4.8: Petri dish-base assembly; (a) before assembly (b) after assembly

4.4.4 The clamping system
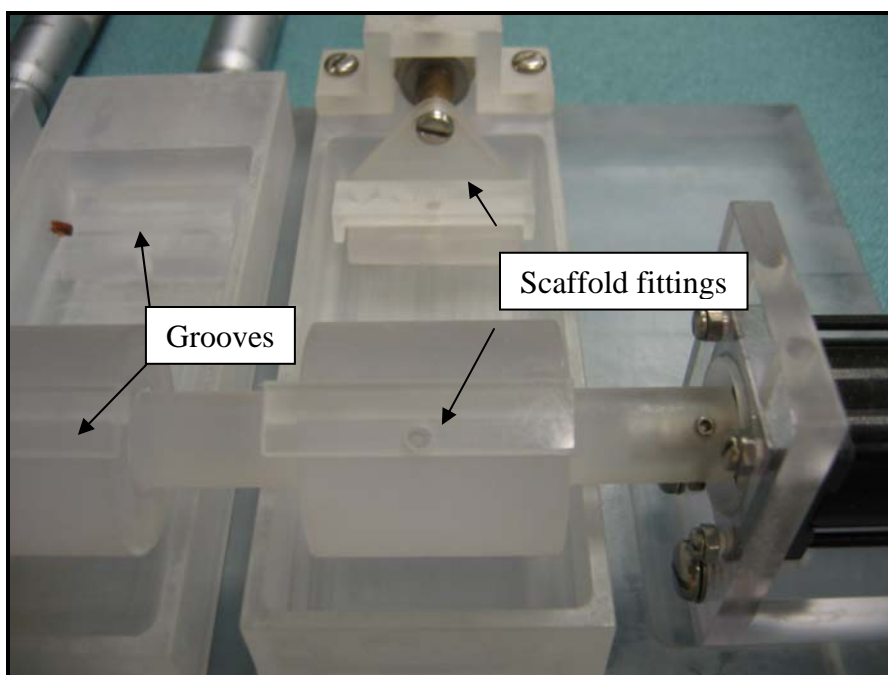
Figure 4.9: The clamping system on the spool and petri dish

The scaffold must be clamped properly to the set-up so as to prevent slipping. Grooves were created on both the spool and petri dishes. After the scaffold was placed in these grooves, scaffold fittings were used to clamp the scaffold (Figure 4.9). During the experiment, no scaffold slippage was detected.

For the unstrained samples, the clamping fixture as show in figure 4.10 is designed and fabricated. This is to ensure both strained and unstrained sample had similar stretched profile during the experiment.
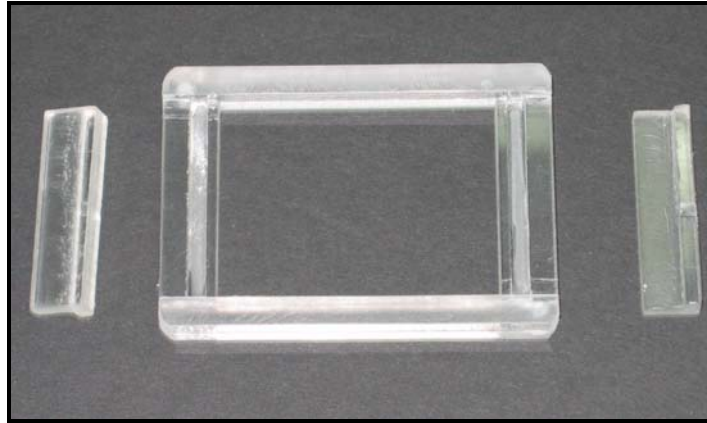
Figure 4.10: Clamping fixture for unstrained sample

4.4.5 The Control system

(a)　　　　　　　　　　　　　　(b)
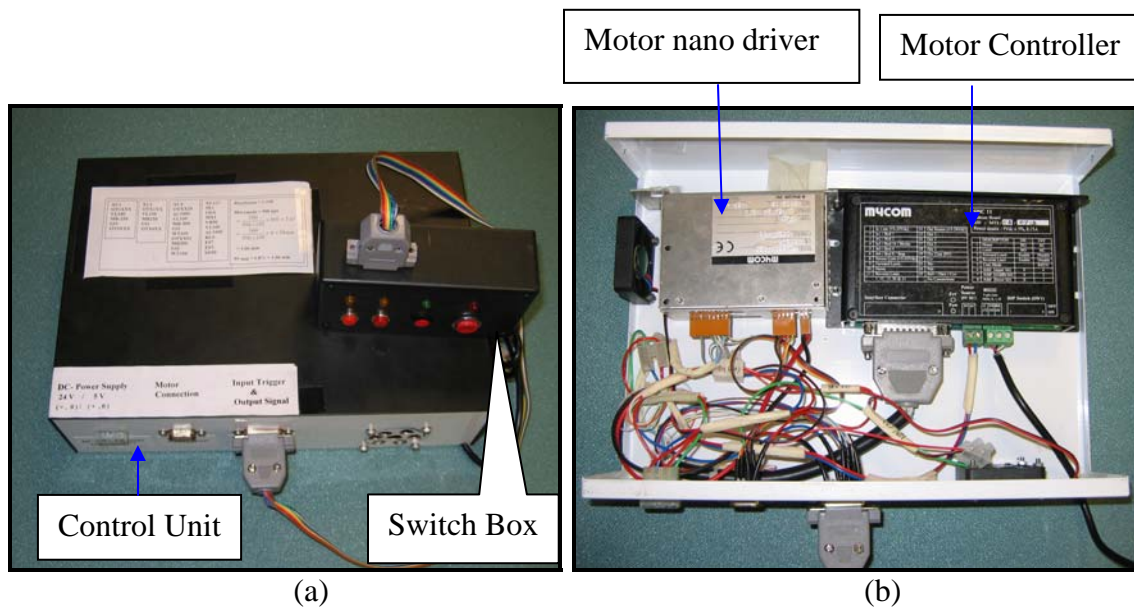
Figure 4.11: Control system: (a) Control unit and switch box, (b) Inside the control unit

The control system consists of a motor controller (mycom, SNC 11), a motor nano driver (mycom, INS500-020), input switches and output light emitting diodes (LED). The motor controller and motor nano driver are wired inside the control unit. The nano driver INS500-020 can give high resolution (up to 500,000 steps per revolution). The custom

made motion control program was written using the "Hyper–Terminal Software" from the Window 95-98 operation system. These motion control programs can be downloaded to the motor controller with RS 232 cable.

The resolution of the motor nano driver is set to 50,000 steps per revolution in this experiment. The motion control program is set for motor rotation of $3.6°$ in a 5 second time period and then goes back to original position with the same time interval. A total of 10 second is taken for one complete cycle (0.1 Hz). In the switch box, there are 4 input switches and 4 output LEDs, to indicate the working function. (Refer to Appendix-F for more detail programs and functions of control system).

4.4.6 Load and Displacement Monitoring System

A force and displacement monitoring system is integrated in the bioreactor system. To monitor the displacement input, a rotary variable differential transducer (RVDT, model R-30 D, sensitivity of 0.125V / degree of rotation, full range reading of $±30°$, Schaevitz Sensors) is fixed in another end of spool. This can counter check the reliability of the control system. To detect the load acting on the scaffold, the load cell (PCB, Piezoelectrics, Model 208C01, a sensitivity of 110mV / N, maximum 450N in tension) was fixed at another end of scaffold in one petri dish.

The output signals from the load cell and RVDT are being fed into the digital oscilloscope (4 Ch 100 Mhz Oscilloscope, model 54624A, Agilent Technologies). The output voltage results were recorded manually and results are analysed with calibration certificate supported by the producer.

From the results of RVDT, it shows that the strain input was fairly constant within 4 hour period. (As written program, 3.6° rotation and go back to its original position).

From the results of load cell, during the 1.8% strain value (1.06mm linear movement) no load was detected on the scaffold. The possible reason for this fact is that the knitted structure of scaffold was used in this experiment, which is not a rigid structure and only very few amount of movement was used. Another possible reason is that the sensitivity of the load cell used in this setup is quite high for the load acting on the scaffold. The possible way to overcome this problem is to use the more sensitive load cell (e.g. max load sensitivity 10 N).
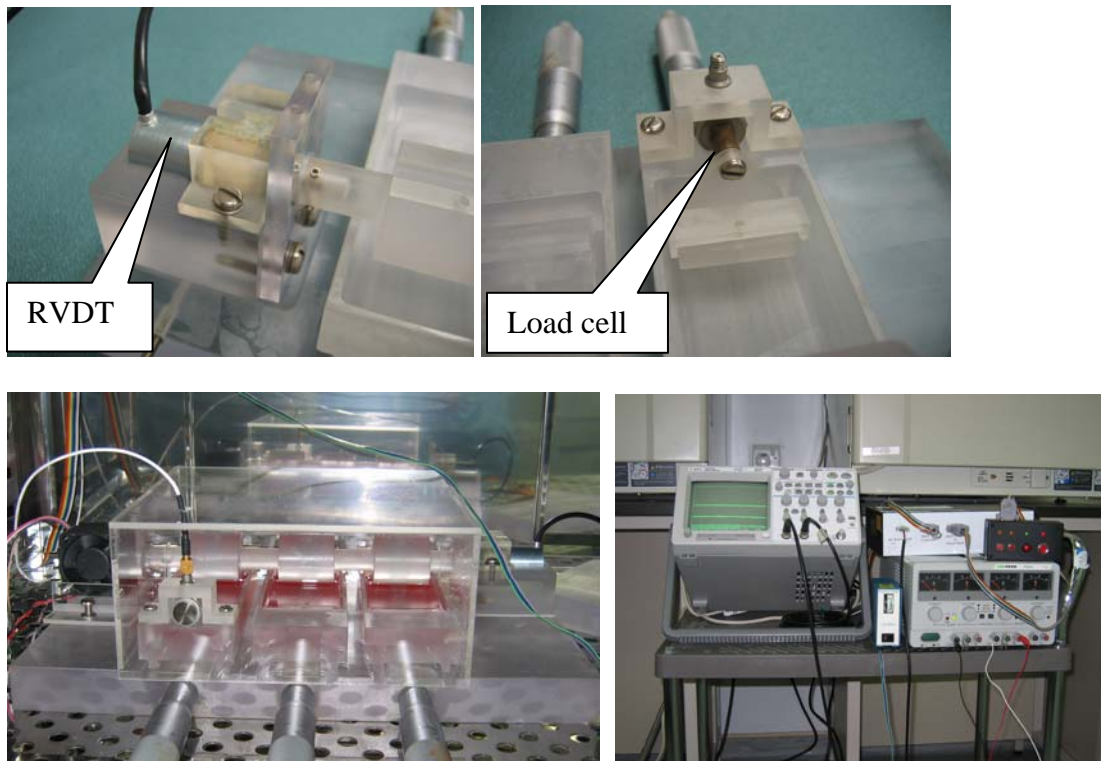
Figure 4.12: Photos for load and displacement monitoring system.

Chapter 5. Experimental Work

5.1 Cell Culture

Human dermal fibroblasts (HDFs) were used in this research. Cells were isolated from a 26 year-old female human skin samples. These isolated human dermal fibroblasts were then cultured and subcultured to get sufficient number of cells. HDFs cells were cultured in tissue culture flask at 37°C in a humidified incubator (SANYO) under 5% CO_2 in air. The culture medium, Dulbecco's Modified Eagles medium (DMEM) supplemented with 10% heat-inactivated fetal bovine serum (FBS, Hyclone Laboratories, Inc), penicillin-G (100 IU/ml), Streptomycin Sulfate (100 μg/ml), L-Glutamine (2 M/ml) and Fungizone (1.25 μg/ml) (Gibco/BRL Life Technologies, Inc) was used in cells culture. The medium was changed every three days to make sure that the nutrients were replenished and by products removed at regular intervals. When culture dishes became nearly confluent after about 7 days, the cells were detached with 0.25% trypsin and serially sub-cultured. Semi-confluent cells of ninth and tenth passage (P-9 and P-10) were used for cell seeding experiments.
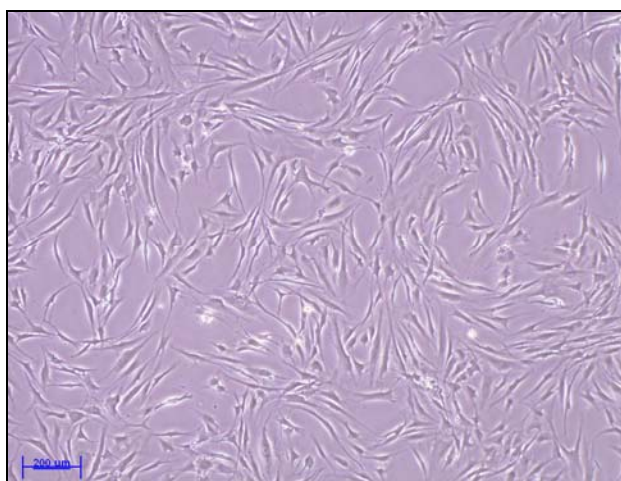
Figure 5.1: HDFs; Human Dermal Fibroblasts at sub-confluence (Magnification 100X, scale bar = 200 μm)

5.2 Scaffold Preparation

The use of biodegradable material as scaffolds is essential in tissue-engineering grafts both *in vitro* and *in vivo* environments [Ouyang et al, 2003]. Previous studies explored the use of different biodegradable materials as collagen, chitin, poly-glycolic acid (PGA) and poly-lactice acid (PLA) for tendon and ligament repair. Because of the limited internal space of braided fiber scaffold, new tissue ingrowths among the braided fibers were poor. [Zange et al, 1997]. Using collagen gel as scaffolds showed little ability to hold its three dimensional structure and resist mechanical strength [Young et al, 1998]. However, knitted scaffold was shown to possess sufficient porosity and mechanical strength [Zdrahala et al, 1996]. With regard to scaffold material, biocompatibility and toxicity studies suggest that PLA–PGA copolymers may be more suitable for orthopedic applications than PLA or PGA [Athanasiou et al, 1996]. Ouyang et al, (2002) also showed that bone marrow stromal cells (bMSCs) adhered to and grew faster on poly-lactice-co-glycolice (PLGA) film than on polycaprolactone (PCL), polylactic acid (PLA), or their copolymer films [Ouyang et al, 2002]. The PLGA fibre is able to maintain its mechanical integrity for a period of at least one month and the complete biodegradation duration is about 65-90 days. Base on these reasons, it was decided to use knitted PLGA scaffolds for all experiments.

The fibres used are made of PLGA fibre, produced by Tian Qing Biomaterials Co. Ltd, Shanghai, China. Each PLGA yarn is made of 16 filaments. The average diameter of each filament is 28 μm. The ratio of Poly lactic Acid (PLA) and Poly Glycolic Acid (PGA) in this PLGA co-polymer is 10:90. The scaffolds were knitted with 3 yarns of PLGA fibres on a knitting machine (Silver-reed SK270, Suzhou, China) (Figure 5.2) by using 12

needles to get 20mm scaffold width. The sizes of scaffolds are about 20mm × 60mm for unstrained group and 20mm × 80mm for strained group although the cell seeding area is same (20mm × 50mm). These scaffolds have a tendency to curl onto themselves into a tubular form. So, they were kept uncurled on custom-made U-shaped stainless steel wire frames, fabricated from 1mm diameter K wires (Global Orthopaedics, Hampshire, England.). (Figure 5.3)

Figure 5.2: Knitting machine used to fabricate knitted scaffolds from PLGA fibres; Inset: Bundle of PLGA yarn.
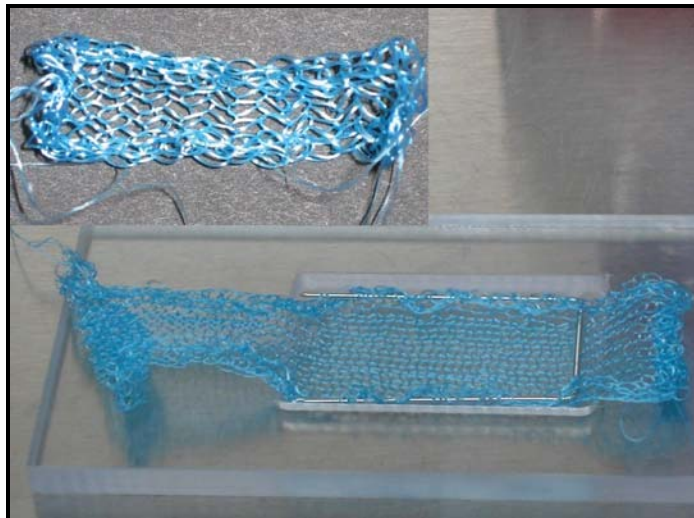
Figure 5.3: Scaffold in custom-made U-shaped stainless steel K wire frame; Inset: Curly scaffold without K wire frame

5.3 Bioreactor Setup

The whole bioreactor and clamping fixtures for unstrained samples were thoroughly sterilised prior to the commencement of experiment. All the polycarbonate parts of bioreactor and clamping fixtures were steam autoclaved. The rest metal parts of the bioreactor, e.g. motor, RVDT, micrometer head were sterilised by 30 minutes exposure to ultraviolet radiation, followed by the swabbing of 70% ethanol. After sterilising all the parts of bioreactor, the bioreactor was assembled in biological safety cabinet (BSC) and then all scaffolds were attached to bioreactor and clamping fixtures (Figure 5.4). To sterilise all PLGA scaffolds properly, all petri dishes in bioreactor were filled with 70% ethanol for 1 hour while round petri dish were used for control samples. After removing 70% ethanol from each petri dish, the scaffolds were left about 15 minutes to dry to make sure all ethanol were evaporated. Then the scaffolds were rinsed three times with 1X Phosphate-Buffered Saline (PBS).

(a)   (b)
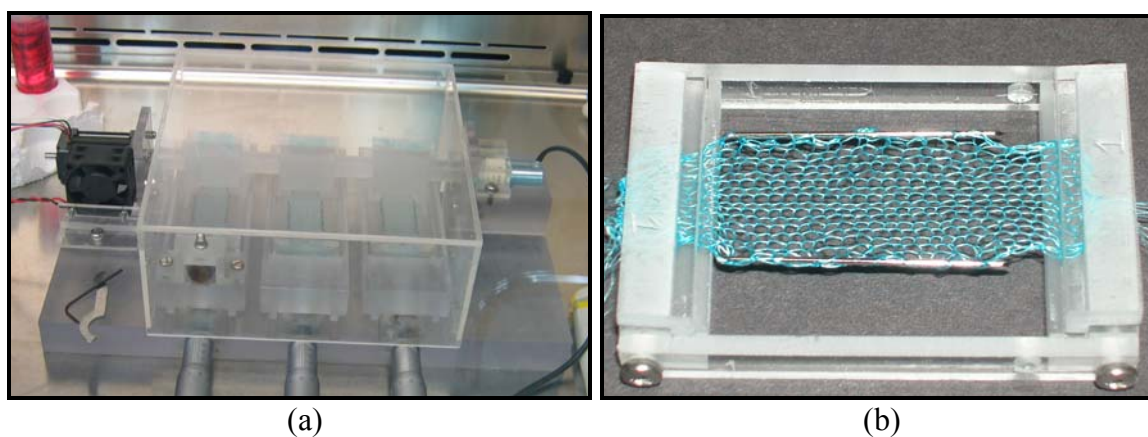
Figure 5.4: (a) Bioreactor setup with scaffolds in BSC (b) Clamping fixture for unstrained samples

After cells seeding, no cyclic straining was applied on the scaffolds within the first 3 days for a good cell adherence to be established before any straining was conducted. The U shaped K wire frames were removed from scaffolds two days after cell seeding. The machine was programmed to apply a cyclic strain of 1.8% for a period of 4 hours daily across a period of two weeks. The straining frequency used in straining regime was 0.1 Hz. Figure 5.5 shows the experimental setup inside the incubator and the data acquisition system and control system for bioreactor. In order to maintain a balanced level of nutritional contents of the medium, the culture medium was changed every three days.

(a)   (b)

(c)
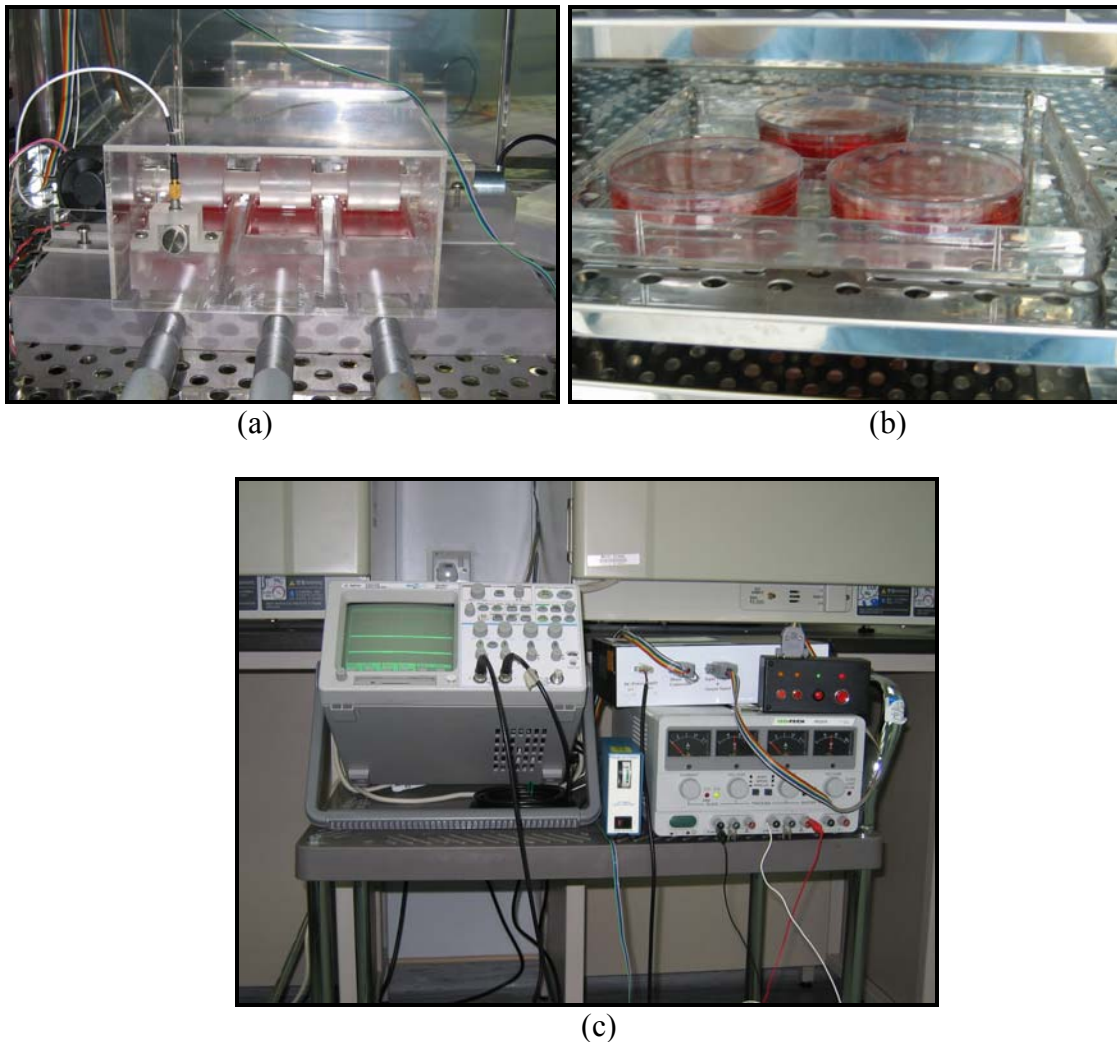
Figure 5.5: Experimental Setup (a) strained samples (b) unstrained samples (c) data acquisition and control system

5.4 Cell seeding

The cells were harvested upon reaching semi confluent condition in tissue culture flask around 7 days after sub culture. To harvest, the cells were washed with Phosphate-Buffer Saline (PBS) and dislodged from the tissue flask with 0.25% trypsin (Sigma, Chemical Co.). All the cell suspension from tissue culture flasks was collected in 50ml centrifuge tube and then counted with a Hemacytometer (Improved Neubauer Bright Light Counting Chamber, Hausser Scientific) to obtain the cell density. After cell counting, cell suspension was aliquot into 1.5ml tubes for each scaffold. Cell pellets were obtained by centrifuging the cell suspension at a speed of 1500 rpm for 5 minutes.

Fibrin glue (Tisseel[TM] Co. Hyland Immuno, Baxter) was used as a temporary biodegradable adhesive for the cells onto the scaffolds. Fibrin glue is a two components system, separate solutions of tisseel and thrombin/calcium. When the two solutions are combined, the resultant mixture mimics the final stages of the clotting cascade to form a fibrin clot within a short period of 3 minutes. According to the specification given by the producer, the biomatrix is developed by the glue and it can maintain for 7-10 days and beyond which it will begin to restore naturally through the process of hydrolysis.

The scaffolds were coated with 100μl tissel solution and followed by 100μl thrombin solution and left for 3 minutes. At this stage all the holes of scaffold were filled with fibrin glue (Figure 5.6). Then the cell pellet for each scaffold was mixed with 200μl of thrombin solution and loaded on each scaffold followed by 200μl tisseel solution by using

micropipette. Then all petri dishes were gently filled with 10% FBS complete culture medium (DMEM) and placed in the incubator. Approximately 6 millions HDFs cells were seeded on each scaffold, both strained and unstrained. (Figure 5.7)
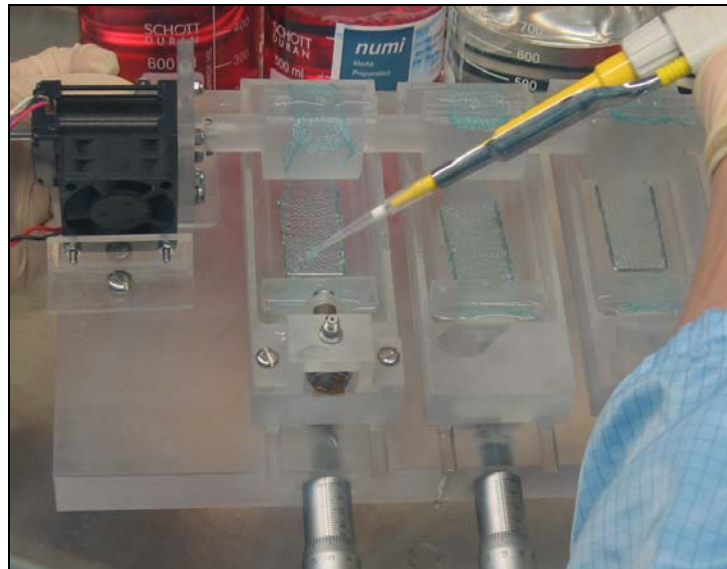
Figure 5.6: Filling with fibrin glue onto the strained samples scaffolds

(a)	(b)
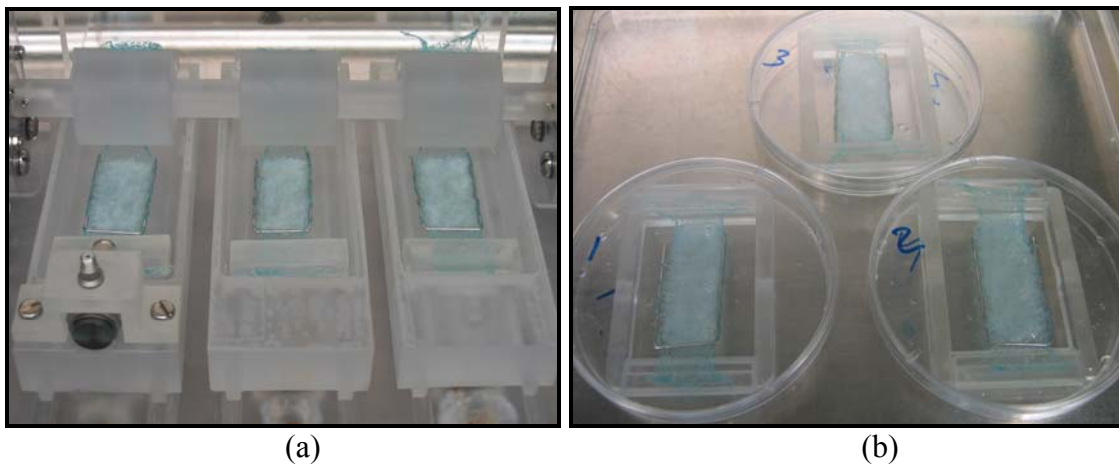
Figure 5.7: Scaffolds after cells seeding (a) strained samples (b) unstrained samples

5.5 Assessment of the Engineered Tissue

The "engineered tissues" were then assessed for:

a) Cell attachment, proliferation, ECM (SEM, LSCM)   Days 17

b) Cell proliferation (Alamar Blue Assay)   Days 3,17

c) Cell morphology, ECM (with H&E staining)   Days 17

d) ECM synthesis

- RT-PCR for ECM proteins   Days 17

- Collagen measurement (soluble collagen , Insoluble)   Days 3,17

- Immunohistochemistry(Antibody staining)   Days 17

e) Mechanical testing   Days 0,10

5.5.1 Cell attachment, proliferation (SEM/ LSCM)

After two weeks period of applying cyclic strain on the scaffolds, all the scaffolds from both groups (strained and unstrained) were taken out and assessed by Scanning Electron Microscope (SEM) and Laser Scanning Confocal Microscope (LSCM, Leica TCS SP2, Germany).

For Laser Scanning Confocal Microscope (LSCM), CMFDA stain was employed for live cells. The stock solution of CMFDA was warmed to 37°C, and 50 μl was diluted in 50ml of serum-free DMEM. Medium was pipette out from the wells of two scaffolds of each group, and replaced with this CMFDA-DMEM solution. After incubating for 30 minutes,

the medium was again changed to fresh DMEM, and the samples incubated for another 30-60 min in the CO_2 incubator at 37°C. The scaffolds were then taken out, rinsed with PBS, and fixed with 4% formaldehyde for 30 min, and rinsed with PBS again. They were then visualized under the LSCM. For LSCM, A/E of 492/517nm was employed.

For SEM, the samples were rinsed with PBS, fixed with 4% formaldehyde for 30 min and then rinsed with tap water. The samples were then dehydrated in graded concentrations of ethanol (30%, 50%, 70%, 90% and 100%), 10 minutes at each concentration, and then air dried for 30-60 min. The dried samples were sputter-coated with gold at 10mA, 10 psi, 50-60s (JFC-1200 Fine Coater, JEOL) and observed under the SEM at an accelerating voltage of 15 kV. (SEM, JEOL JSM-5800LV scanning microscope; Figure 5.8).

Figure 5.8: SEM, JEOL JSM-5800LV scanning electron microscope, Inset: JFC-1200 Fine coater, JEOL

5.5.2 Cell proliferation studies (Alamar Blue Assay)

Alamar Blue™ Assay (US Biological) was used to assess cell proliferation because it is non-destructive to the cells so it allows continuous monitoring of the same piece of cells-scaffold construct [Neidlinger et al, 2002]. Alamar Blue™ is composed of a blue dye called "resazurin", which can be reduced by the metabolic products of viable cells to form a fluorescent red dye called "resorufin". The amount of resazurin can be measured at 600nm absorbance wavelength while resorufin at 570nm wavelength. The percentage reduction of resazurin to resorufin was calculated with compensation for the culture medium background absorbance and this value will be reflective of cells viability [Phoo, 2003/04]. (Refer to appendix G for more detail)

Cells proliferation was studied on both strained and unstrained groups at Day 3 (before straining the scaffolds) and Day 17 (after two weeks straining). The Alamar Blue concentration used in this study was 5%. Procedure: Prepare 5% Alamar Blue with DMEM containing 5% FBS and put 15ml of that solution to each scaffold and incubated 3 hours in the incubator. For control, another 3-5 ml of 5% Alamar Blue was placed in round Petri dish and also incubated for 3 hours. Then mixtures from all scaffolds and control mixture were transferred to 96-well assay plate (100μl per well, 5 wells per samples), protected from light to record the absorbance value. The absorbance value at 570nm and 600 nm were recorded by using microplate reader (TECAN Microplate Reader, Magellan Instrument Control and data Analysis Software).The percentage reduction can calculate from these reading and this value give an indirect estimate of the number of cells in the scaffold.

5.5.3 Cell morphology, ECM (Histology with H&E staining)

The objective of histological observation is to investigate any possible cell morphology differences between the strained and unstrained samples. The observance of any cell morphology differences will be an indication of positive effect of the straining on the cell-seeded scaffolds. The cell morphology is being studied with the aid of Hematoxylin & Eosin staining. Histology was conducted after two weeks of straining. With the effect of straining, it was hypothesised that a change of cell morphology i.e. the alignment of cells in a particular direction should be observed at the end of the straining.

After two weeks straining, cell seeded scaffolds from both strained and unstrained groups were washed with PBS and then fixed in 4% formalin for one day. This was then followed by the dehydration process where the samples would go through 50%, 70%, 90% and 100% (twice) ethanol on an hourly basis. The samples were soaked in a solution of ethanol and toluene (volume ratio of 50:50) overnight and then in 100% toluene for 24 hours. The scaffolds were then paraffin embedded by transferring the samples through progressive grades of paraffin baths. The blocked paraffin samples were sectioned by microtome (Figure 5.9(a)) into 5 μm thickness and then mounted on microscope slides (Superfrost ® plus, ERIE Scientific Company, USA).

Histology was performed on both the transverse and longitudinal sections of the scaffolds. All the paraffin-embedded slide sections were dewaxed by transferring them sequentially to xylene (twice), xylene and toluene (volume ratio of 50:50), 100% (twice), 90%, 70% and 50% ethanol for 1 minute at each stage. Then, the slides were placed under tap water

and stained with Haematoxylin stain for 2-3 minute. After that, slides were differentiated in dilute HCL solution for 5-10 seconds. The slides were washed with water again and followed by Eosin stain for 30-45 seconds. After staining with H&E, all slides were dehydrated by transferring them sequentially to 70%, 90%, 100% alcohol (twice), xylene + 100 % alcohol (50:50, volume) and 100% xylene (twice) for 1 minute at each stage. Then xylene based mounting medium (permount) was applied on the slide and cover with coverslip. In H&E staining, the fibrin glue and ECM were stained red by Eosin while the cell nuclei became dark purplish blue by the Haematoxylin.

(a)   (b)
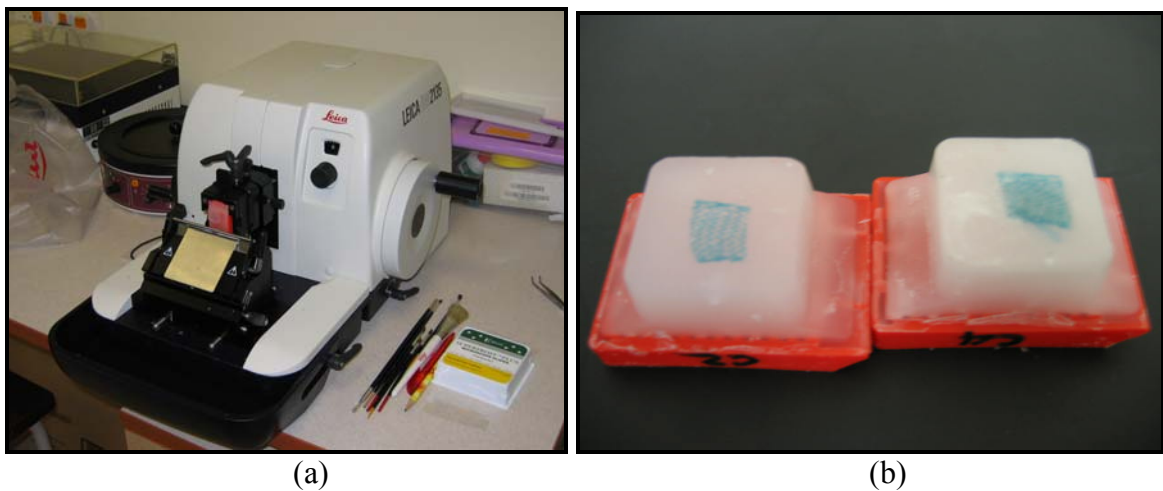
Figure 5.9: (a) Microtome to section paraffin block (b) Paraffin embedded scaffolds

Changes in the shape and alignment of the cells were examined using Inverted Light Microscopy (ILM) (Olympus Optical) after being stained with H&E stain. Quantitative analysis like measurement of the length and orientation of the cell nuclei was done with the help of image-processing software (MicroImage 4.5.1, Olympus Optical Co). The cell nuclei of interest were selected by colour selection as defined by the user. In this context, purplish blue was used as the selection tool (Figure 5.10).
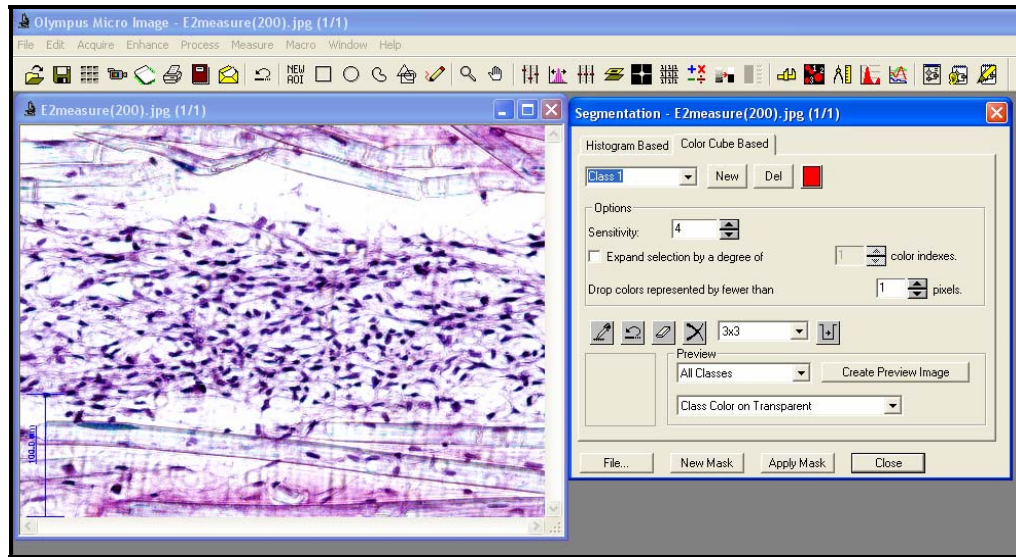
(a)
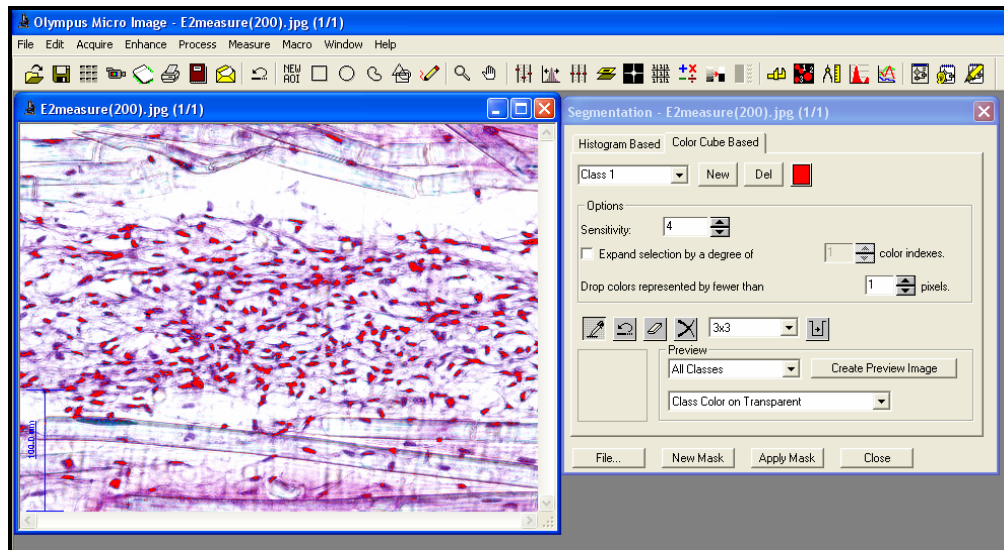
(b)

Figure 5.10: Colour selection was used to select the cell nuclei of interest ;(a) Before colour selection, (b) after colour selection.

5.5.4 PCR Analysis of ECM Proteins

5.5.4.1 RNA Extraction using Qiagen RNeasy Kit®:

After two weeks of straining, 2 samples from each of strained and unstrained groups were separately washed with PBS, cut into half and the wet weights of engineered tissue were recorded. In this experiment the wet weight of engineered tissues were adjusted to 0.3g each. The total RNA was isolated from the engineered tissue by using "Qiagen Rneay Kit®". This kit consists of (i) buffer RLT, (ii) buffer RW 1, (iii) buffer RPE (iv) RNase-free water and (v) RNeasy mini spin columns.

The weighted engineered tissue samples were cut into small pieces with scissors and placed in labeled 2ml micro centrifuge tubes. 600μl of lysis buffer RLT was added to these tubes and the samples were homogenized with tissue homogenizer (TH-220, Omni International, Inc) with separate generator probes. The samples were then centrifuged at 13,000 rpm for 3 minutes and the supernatant was transferred to new tubes and an equal volume of 70% ethanol was added to these tubes.

About 700μl of the solution was applied to RNeasy mini spin columns in 2 ml centrifuge tubes and the column were centrifuged at 13,000 rpm for 15 seconds. The flow through was discarded. The rest of the solution (buffer RLT + 70% ethanol) was loaded again and centrifuged again. 700μl of buffer RW1 was added to the columns and centrifuged at 13,000 rpm for 15 seconds. The flow through was discarded.

The RNeasy mini spin columns were transferred to new 2ml centrifuge tubes. Then, the column was washed with buffer RPE by adding 500μl of buffer RPE and centrifuged at 13,000 rpm for 15seconds and the flow through was discarded. The washing step with buffer RPE is repeated again with 500μl of buffer RPE and centrifuged at 13,000 rpm for 2 minutes.

After discarding the flow through, the column was transferred to new 1.5ml centrifuge tube. 50μl of RNase-free water was pipette directly onto the silica-gel membrane of the column and the tube was centrifuged at 13,000 rpm for 1 minute to elute. The elution step was repeated with another 50μl of RNase-free water. The final RNA solution was then assessed for its purity and concentration of RNA by spectrophotometer (Biowave S2100 UV/Vis Diode Array Spectrophotometer, WPA Ltd, UK), and stored at -80°C.

5.5.4.2 Reverse Transcriptase–PCR using "Qiagen® One-Step RT-PCR Kit"

RT-PCR was performed for the following ECM proteins: Collagen I, Collagen III, Tenascin-C, β-actin, and Glyceraldehyde Phosphate Dehydogenase (GAPDH). Normally both β-actin and GAPDH can be employed as the reference house-keeping gene. In this research only GAPDH gene was used as the reference house-keeping gene. The primer sequences were obtained from published literature, Collagen I, GAPDH [Martin et al, 2001], Collagen III, Tenascin-C [Altman et al, 2001] and were synthesized by Research Biolabs, Singapore. The details of the primers are given in Table 5.1.

Table 5.1: Primer sequences used in RT-PCR; 1: Forward primer; 2: Reverse primer;

bp: base pairs; AT: Annealing Temperature; Cycle: number of PCR cycles; GAPDH:

Glyceraldehyde Phosphate Dehydogenase.

Primer	Sequence	bp	AT (˚C)	Cycle
Collagen I	1-CAG CCG CTT CAC CTA CAG C 2- TTT TGT ATT CAA TCA CTG TCT TGC C	83	55	30
Collagen III	1- ACA CGT TTG GTT TGG AGA GTC C 2- CTG CAC ATC AAG GAC ATC TTC AG	88	60	30
Tenascin C	1-TCT CTG CAC ATA GTG AAA AAC AAT ACC 2-TCA AGG CAG TGG TGT CTG TGA	118	60	30
β-actin	1- CTG GAA CGG TGA AGG TGA CA 2- AAG GGA CTT CCT GTA ACA ATG CA	139	55	30
GAPDH	1-ATG GGG AAG GTG AAG GTC G 2-TAA AAG CAG CCC TGG TGA CC	70	55	30

RT-PCR was performed using "Qiagen® One-Step RT-PCR Kit". This kit consists of (i) RT-PCR Enzyme mix (ii) dNTP Mix (iii) 5X RT-PCR buffer and (iv) Rnase-free water.The template RNA, primer solutions, deoxynucleotides (dNTP) mix, 5X Buffer solution and RNase-free water were thawed. A master-mix was prepared by adding 5X Qiagen buffer (10 μl), dNTP mix (2μl), RT-PCR Enzyme mix (2μl) for each PCR reaction. Primer solution (3μl, both forward and reverse primers, 100 uM) was diluted 10 times. Then 14 μl of master-mix, 3 μl of diluted primer solution and 5 μl of RNA were mixed thoroughly in each labeled PCR tube and make a total volume of 50μl with RNase-free water. For negative control, extra 5 μl of RNase-free water was used instead of RNA solution. All these reactions were set up on ice. The PCR machine (iCycler, Bio-Rad

Laboratories, Inc) was programmed and pre-heated to 50°C, and then the PCR tubes were placed in it and RT-PCR was performed.

5.5.4.3 Analysis of RT-PCR products by Agarose Gel Electrophoresis

The RT-PCR products were analyzed by separation on 2% agarose gel electrophoresis. Procedure; 2.5g of agarose was added to 125ml 1X TBE electrophoresis buffer in a conical flask and dissolved by boiling in a microwave oven. The solution was allowed to cool to about 55°C when ethidium bromide was added to it at a concentration of 0.5μg/ml. The gel tray was set-up on a horizontal surface and a 20 teeth comb was placed in it. The agarose solution was poured into the gel-tray and allowed to gel for around 30 min. The comb was then removed; the gel-tray was transferred into the horizontal electrophoresis chamber and submerged under 1X TBE buffer with ethidium bromide at a concentration of 0.5μg/mL. 2μl of 6X Gel loading dye was mixed with 10 μl of PCR product (DNA solution) and loaded into each well. 2μl of the loading dye was mixed with 10μl of the 100bp DNA ladder (Promega Corp, USA) and loaded to the outermost wells on both sides. The pattern of sample loading was recorded. The electrodes were connected and electrophoresis was started at a voltage of 100V. It was stopped when the orange band from the loading dye reached the end of the gel. The gel was then visualized and photographed in a Gel Documentation system (Gel Doc 2000, Bio Rad) (Figure 5.12).

The Densitometry analysis of PCR products bands was performed with the help of imaging software (Quality-one 4.4.0, Bio Rad). First, create lane frames on photo, detect

all the bands and then the average density of bands were measured (Figure 5.13). GAPDH gene was used as house keeping gene in this research, the average density of each target gene was normalized with that of GAPDH gene (both in strained and unstrained sample). The resulting data of strained sample was expressed as a ratio to the value of unstrained sample denoted as one.

Figure 5.11: Gel Documentation system (Gel Doc 2000, Bio Rad)
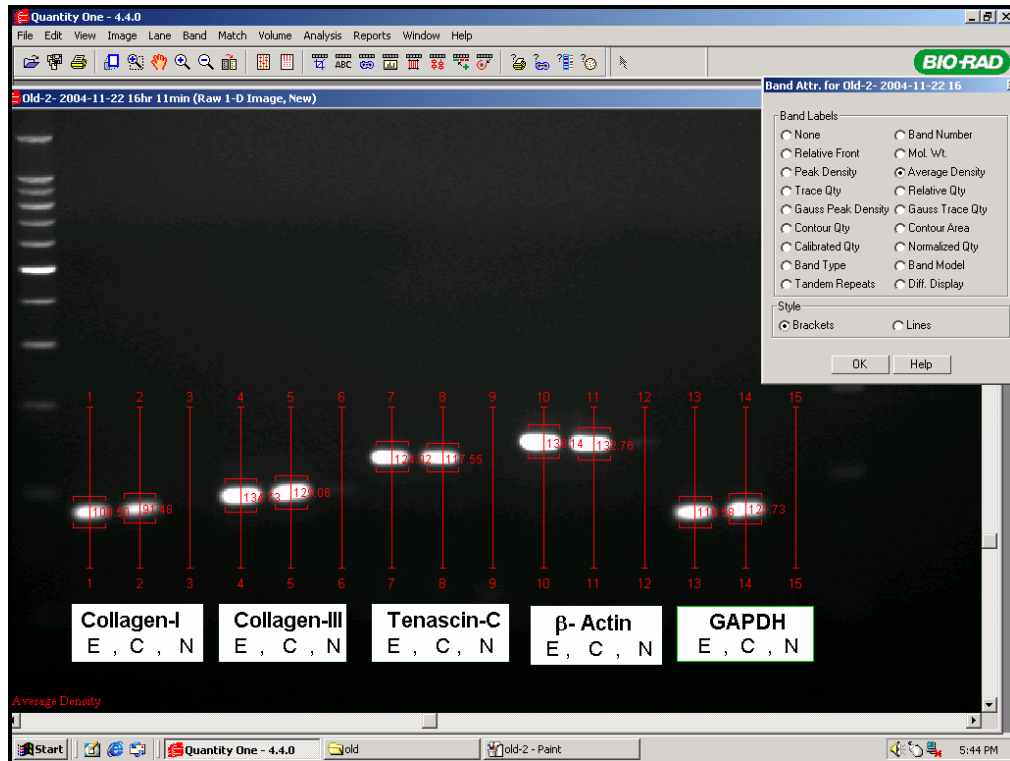
Figure 5.12: Detection and measuring the average density of PCR product Bands;
E=strained sample band, C=unstrained sample band, N= negative control band (no RNA
template)

5.5.5 Collagen Assay (Soluble & Insoluble)

The total soluble collage synthesized and secreted into the culture medium and insoluble
collagen deposited on the scaffold after two weeks straining were determined by
biochemical assay using commercial kit, Sircol® Assay for collagen (Biocolor Ltd,
Northern Ireland).

5.5.5.1 Collagen Assay (Soluble collagen released into Medium)

The collagen released into the medium was measured on 3rd and 17th day of experiment. The Sircol® Collagen Assay, a dye-binding method, does not require the isolation of collagens from other soluble tissue proteins; the collagen released into the medium can be directly measured, without any prior extraction, a minimum concentration of $2.5\mu g/100\mu l$. The Sircol® Dye Reagent selectively binds to the [Gly-X-Y]n tripeptide sequence found within the triple helix sequence of mammalian collagens. The culture medium was replaced on day 1 (for 3rd day measurement) and 15th day (for 17th day measurement) with fresh DMEM with 5%FBS. On the 3rd day and 17th day, the medium was collected from the petri dish into separate labeled 1.5 ml centrifuge tubes. Collection of 2 days' medium ensures that only freshly synthesized soluble collagen is obtained.

To obtain standards values and a reagent blank, 25, 50, and $100\mu L$ of Standard Collagen (rat-tail; 0.5 mg/ml standard in 0.5ml acetic acid) and 200 μL of fresh culture medium respectively, were taken in duplicate 1.5 ml centrifuge tubes. Distilled water was added to make a total volume of 200 μl. For test samples, 200 μL of culture medium from three strained samples and three unstrained samples were taken in separate labeled micro centrifuge tubes. 1 ml of the Sircol Dye Reagent was added and the contents of the tube mixed by inversion, and then in a mechanical mixer for 30 min. After that centrifuged at 13,000 rpm for 10 minutes, the supernatant was decanted away, and any excess supernatant was removed by an absorbent paper. Then, 1 ml of Alkali reagent was added, and the tubes were vortexed for 5 min. 200 μL of the solution obtained was aliquot into separate wells of a 96-well microplate (3 well per sample), and the absorbance values of the samples were measured with a microplate reader at a wavelength of 540nm.

Comparing the absorbance values with the standard curve, the concentration of collagen in the medium was known and results were expressed as µg/ml of collagen secreted in 2 days.

5.5.5.2 Collagen Assay (Insoluble collagen deposited on the scaffold)

The amount of insoluble collagen deposited on the scaffolds after two weeks straining were also measured by using Sircol® Collagen Assay. After two weeks straining, 1 sample each from both strained and unstrained groups were taken and wash separately with PBS and cut it half. The wet weight of samples is adjusted to 0.22g. Then the scaffolds were cut into small pieces with scissors and placed in labeled 2ml micro centrifuge tubes. 900 µl of PBS was added to the tube and scaffolds were homogenized with tissue homogenizer (TH-220, Omni International, Inc) with separate generator probes.

Dissolve pepsin from porcine mucosa (4000U/mg, Sigma) in 0.5M acetic acid to a stock concentration of 1mg/ml and vortex frequently. After all pepsin dissolve in 0.5M acetic acid, add 100 µl of pepsin solution to labeled 2ml micro centrifuge tubes and incubate for 2 hour at room temperature. This makes the working concentration of pepsin 100 µg/ml in 0.5M acetic acid. Then 100 µL of 1N NaOH (equal amount with pepsin solution) was added to stop pepsin digestion. By this stage all non-collagenous proteins should have been shredded and only collagen triplehelix should have survived. Then 200 µl of that solution was taken and followed the procedure as mention in section 5.5.5.1. The results were expressed in µg, amount of collagen deposited in 0.22g of engineering tissue.

5.5.6 Immunohistochemistry (Antibody Staining)

Immunohistochemistry was conducted on the micro-sections of scaffolds from both strained and unstrained groups, harvested on the 17th day of the straining regime. The detection kit used in this research constituted a labeled Streptavidin-biotin immunoenzymatic antigen detection system (CHEMICON IHC Select TM). This technique involved the sequential incubation of the specimen with an unconjugated primary antibody specific to the target antigen, a biotinylated secondary antibody (Goat Anti-Mouse) which reacted with the primary antibodies, enzyme-labeled streptavidin and substrate-chromogen. The primary antibodies used were mouse anti-human collagen type I and collagen type III for the detection of collagen type I and III respectively.

After two week of straining, engineered tissues were washed with PBS and then fixed in 4% Formalin for one day. Then the specimens were transferred into 15% sucrose solution until the specimens sinks. Place samples on freezing medium and solidified by liquid nitrogen. Then the samples were section into 5μm thickness using cryostat (Leica CM 3050 S) (Figure 5.14). All slides were divided into three groups: one group will be stained with the antibody for collagen type I, one with collagen type III and the last group without any primary antibody (Table 5.2).

The cut sections were then blocked with 5% normal goat serum for one hour in an enclosed, highly humid environment. After blotting the serum, the sections were incubated in primary antibody (Dilution 1:100) overnight. After washing with PBS for 4 times, all

the sections were then incubated with the secondary antibody, biotinylated goat anti-mouse IgG, for 10 minutes at room temperature, followed by washing with PBS and the incubation with streptavidin horseradish peroxidase (HRP) for another 10 minutes. After washing with PBS for 4 times, all the slides were incubated with a DAB solution {1:25 ratio of DAB chromogen A (3,3' Diaminobenzidine) and DAB chromogen B (hydrogen peroxide)}. The cell nuclei for all the slides were then counterstained with Hematoxylin (appear dark purplish). Then all the slides were placed in deionizer water after that apply aqueous-based mounting media to the slide and apply coverslip. Both collagen types were stained brown in the immunohistology.

Figure 5.13: Cryostat (Leica CM 3050 S)

Table 5.2: Grouping of specimens for immunohistochemistry.

Group	Treatments
Collagen Type I	Treated with mouse anti-human collagen type I primary antibody, followed by anti mouse secondary antibody
Collagen Type III	Treated with mouse anti-human collagen type III primary antibody, followed by anti mouse secondary antibody
BLANK	Treated with PBS (instead of a primary antibody), followed by anti mouse secondary antibody

5.5.7 Biomechanical Testing

The scaffold fibres bear the mechanical load before the engineering tissue can be generated by the cells. In an ideal case, the scaffolds should degrade *in-vivo* at a predefined rate so that the 3D space occupied by the initial scaffold material is replaced by regenerated host tissue. Prior to the complete regeneration of the engineered tissues, the cell-polymer constructs need to withstand the hostile in-vivo physiological conditions. For an example, in the case of the anterior cruciate ligament, the estimated force that the ligament experiences in ascending a ramp is 67N [Wright et al, 1993]. By understanding the tensile strength prior to *in-vivo* implantation, appropriate rehabilitation programs can be planned to improve the recovery rate of the implants.

The biomechanical tests were done on cell-scaffold constructs of both strained and unstrained groups (n=3 each) at 10th day experiment (after 1 week straining) and PLGA scaffold alone at day 0(n=4, without cell and any other treatment). Mechanical properties were measured with a universal testing machine , UTM, (Instron$^{®}$ 3345 Tester, Series IX and Merlin Software, Instron Corp., MA, USA) (Figure 5.15) with a 1000 N load cell, by loading to failure at room temperature. Test specimens of width of 20mm, a gauge length of 10mm were stretched to failure at a crosshead speed 10mm/minute, without any pretension and preconditioning. Masking tape was used to prevent any slippage of the scaffold from the machine grips during testing (Figure 5.16). The samples were kept moist by spraying PBS and the load (N) and extension (mm) were recorded. The data of load and extension from the Instron machine were recorded by the computer, and the load-

extension graph was drawn by using these data. The ultimate tensile load (F_{max}) is defined as the highest load in load-extension graph. The structural stiffness of the scaffolds was obtained from the gradient of the line which fitted to the best linear region of the load-extension graph (Refer to Appendix H) and expressed in N mm^{-1} [Cacou et al, 2000].

Data were analyzed by statically analysis software, SPSS release 11.5, and mean, standard deviation and level of significance (p-values) obtained by Paired Sample T-tests (when samples are of same size) or Independent Sample T-tests (if samples are of different sizes). *P* values in excess of 0.05 were considered to be insignificant.

Figure 5.14: Universal testing machine (UTM) (Instron® 3345 Tester)
Inset: Close up view of sample on clamp

Figure 5.15: Samples for mechanical test with masking tape

Chapter 6. Results and Discussions

6.1 Cell attachment, proliferation (SEM/ LSCM)

After two weeks straining, HDFs cell seeded scaffolds were observed under phase contract microscope. On phase contrast microscopy, the cell seeded scaffold revealed that cells were attached and growing well on scaffold. Most of the pore areas of scaffolds were covered with cell and fibrin gel matrix. Fibrin gel also still remains in some parts of scaffold after 17 days period. In strained sample scaffold, the shape of pore becomes more elongated due to the cyclic strain while the shape of unstrained sample still remains in round shape.

(a)   (b)
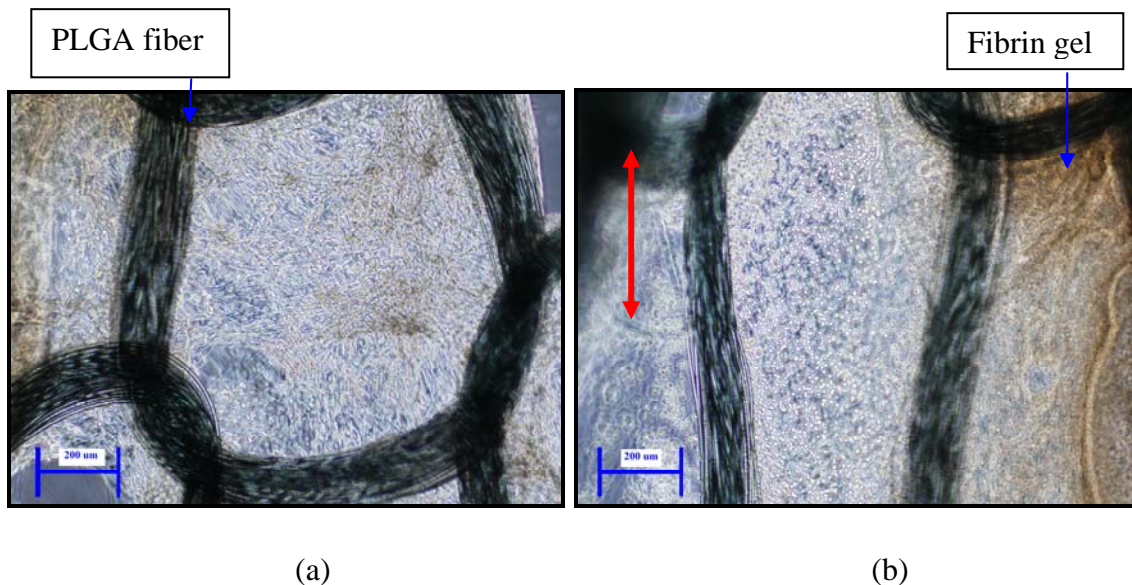
Figure 6.1: Cell attachment on the PLGA scaffolds after two weeks straining (Magnification 40 X, scale bar =200 µm).(a) Unstrained sample, rounded pore shape, (b) Strained sample, elongated pore shape, red colour arrow shows the direction of straining

SEM analysis (Figure6.2) also shows that the cells were growing both on PLGA fibre and on the fibrin gel. As the cells were embedded within the fibrin gel, SEM analysis did not

reveal cell morphology and cell alignment. The SEM images show that there is slightly higher cell density in strained sample compare with unstrained sample.

(Unstrained sample)   (Strained sample)
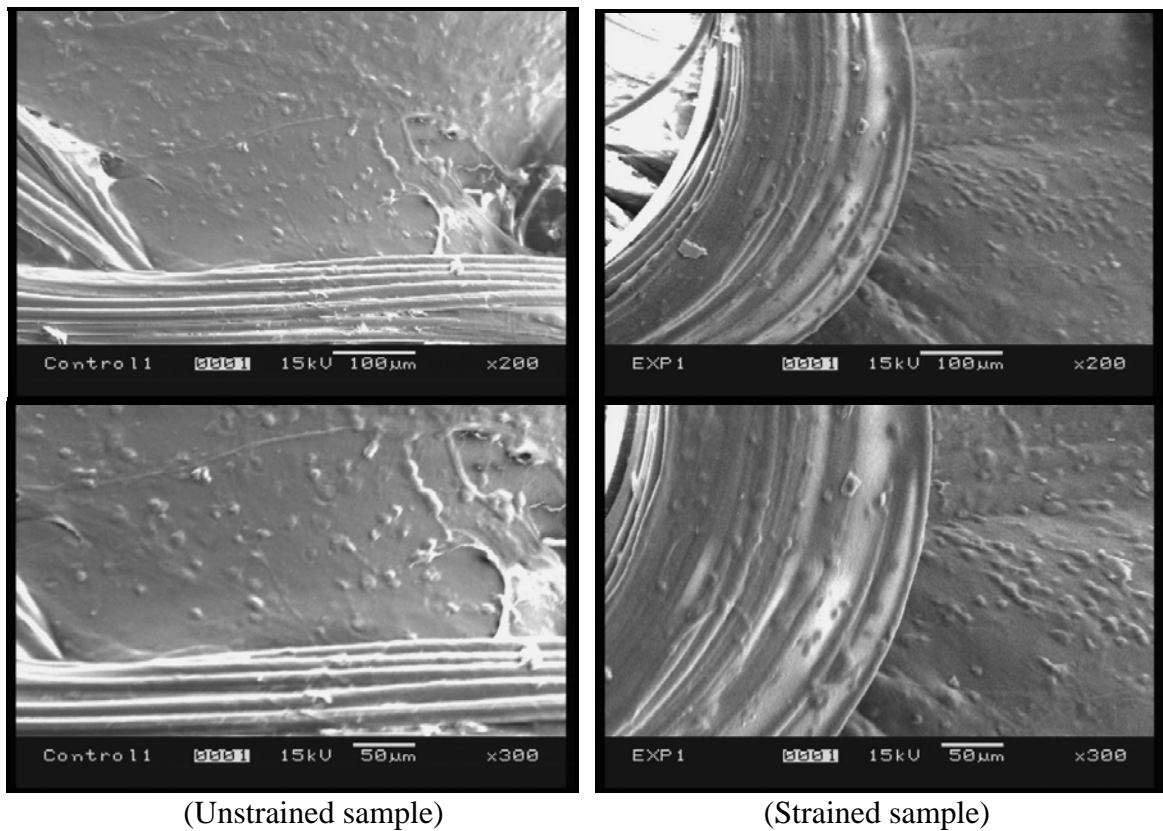
Figure 6.2 SEM digital image done on Day 17: (left) Unstrained sample (right) Straining sample showing slightly higher cell density

After fluorescent staining with CMFDA at day 17, cell seeded scaffolds from both groups were observed under Laser Scanning Confocal Microscope (LSCM). CMFDA is a specific dye stained to viable cell only and show green colour under 492/517nm. LSCM images (Figure 6.3) shows cell density was slightly higher in strained sample. The presence of viable cells in both groups after the experiment period also indicated the biocompatibility of the bioreactor. According to SEM images and LSCM images, cell density in strained sample is slightly higher than unstrained sample.

(a)   (b)
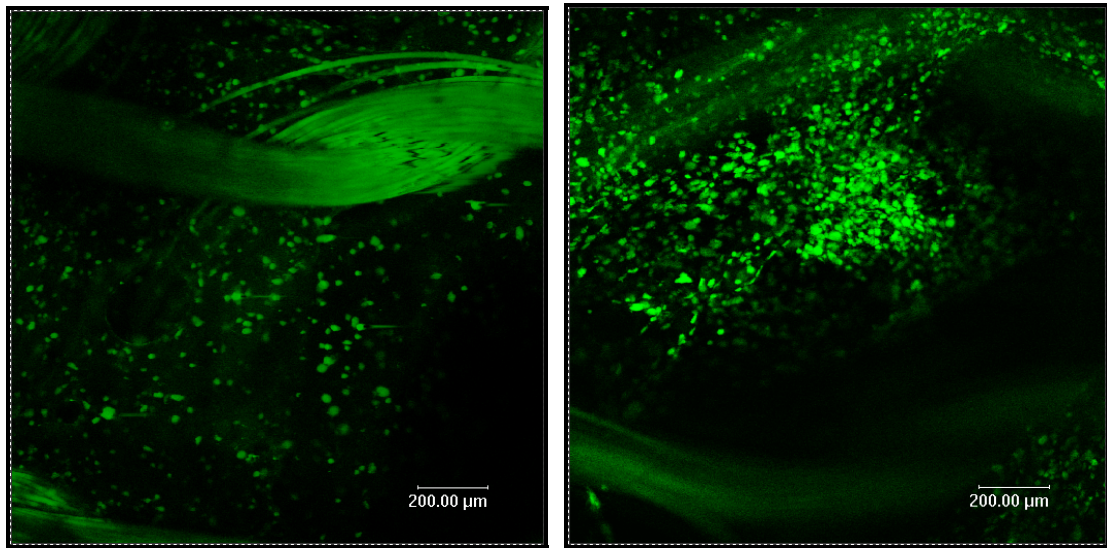
(Magnification 100 X)

(c)   (d)
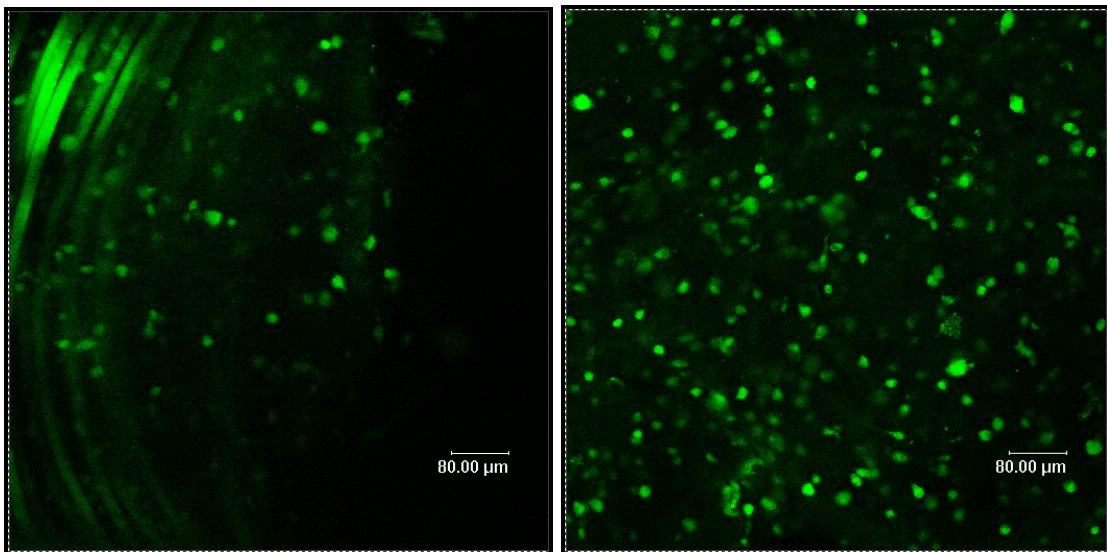
(Magnification 200 X)

Figure 6.3: LSCM images in different magnification (100X & 200X): (a, c) Unstrained sample, (b, d) Straining sample showing slightly higher cell density

6.2 Cell proliferation studies (Alamar Blue Assay)

The cell proliferation was studied by using Alamar Blue assay. 3 samples each from both strained and unstrained group were conducted for cell proliferation study on day 3 (before straining) and day 17 (after two weeks straining). An increase in percentage of Alamar Blue reduction between two time points demonstrates the cell proliferation of the sample within this time interval.
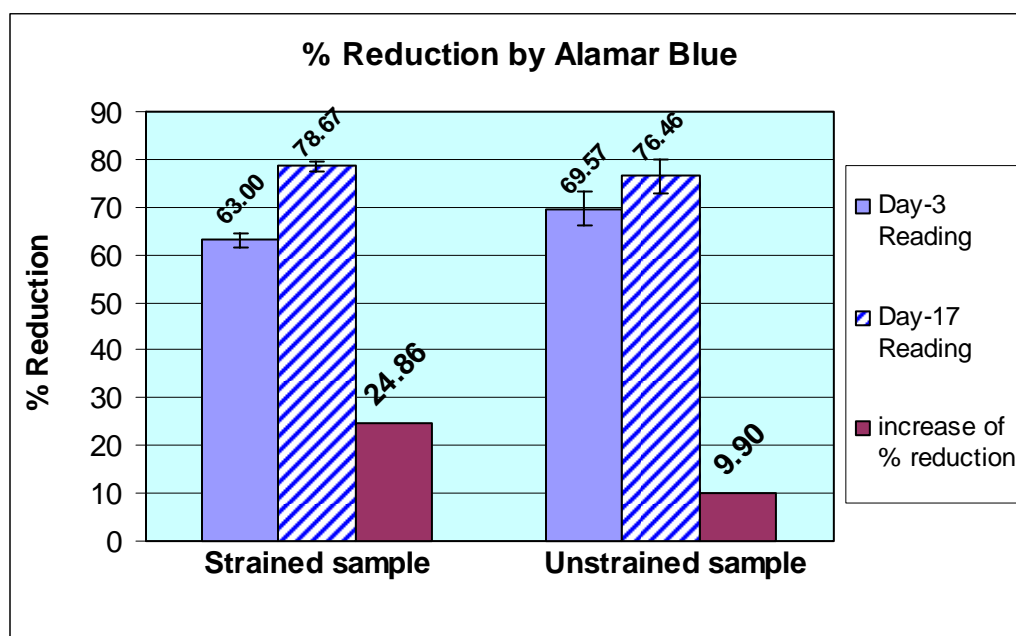
Figure 6.4: Comparison of % Reduction of Alamar Blue on both groups at different times

At day 3, percent reduction of Alamar Blue in strained and unstrained samples were 63.0 ± 1.62 and 69.57 ± 3.58 respectively (Mean value ± Standard Deviation). After two weeks straining, percent reduction of Alamar Blue in strained sample group reach to 78.67 ± 1.06, while that of unstrained sample group remain in 76.46 ± 3.59. Within this two weeks period, percent reduction of Alamar Blue in strained sample increase 24.86%. On the

other hand, percent reduction of Alamar Blue in unstrained sample increase only 9.9% in two weeks period.

The results show higher proliferation rate occurs in strained sample. This observation suggests that cyclic strain on the cell seeded scaffolds have positive effect on cell proliferation.

6.3 Cell morphology (Histology with H&E staining)

6.3.1 Transverse section

(Magnification 40 X),
Scale bar = 500 µm

(Magnification 200 X),
Scale bar = 50 µm
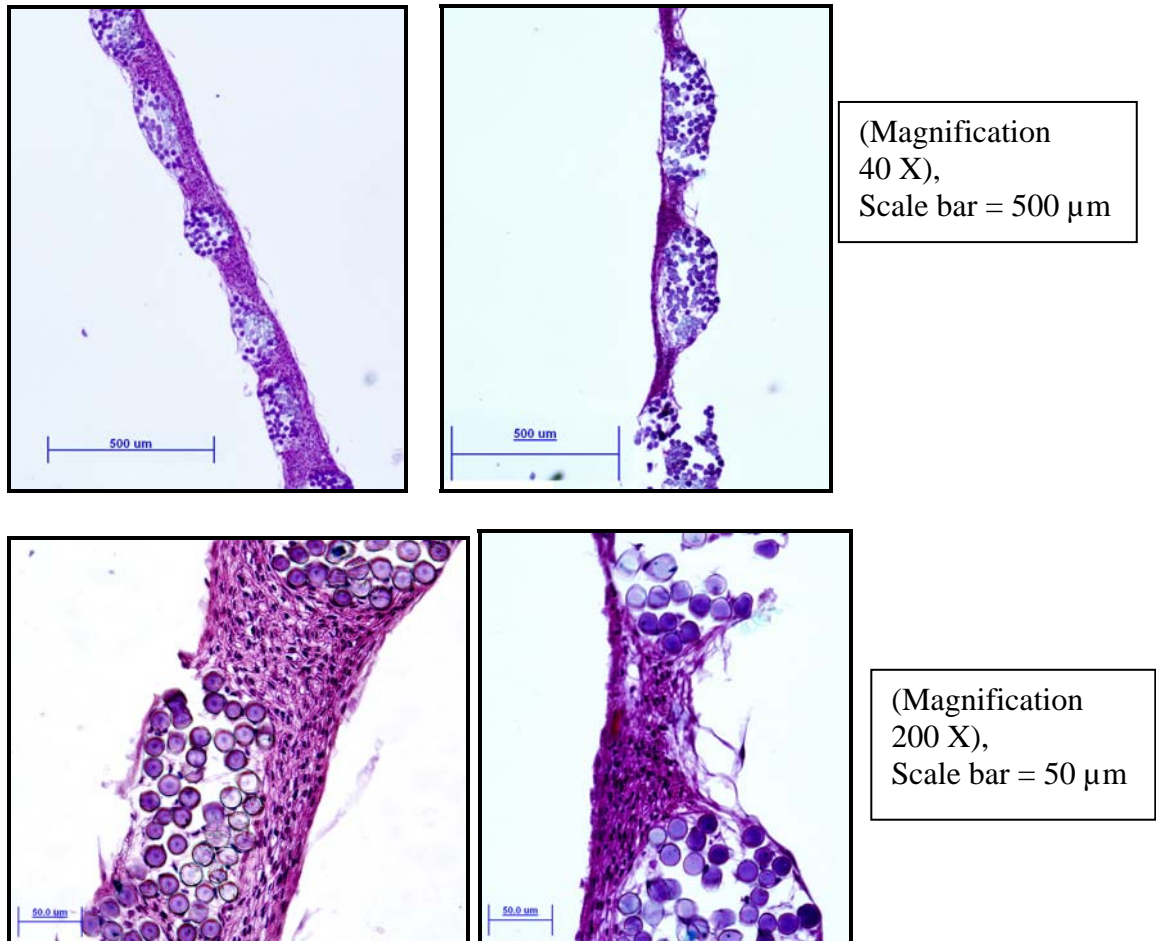
Figure 6.5: Transverse Section Histology in different magnification ;(left column) unstrained sample, (right column) strained sample

Figure 6.5 shows the transverse sections of cell seeded scaffolds with Hematoxylin & Eosin staining. These photos show that HDFs cell are growing well on the PLGA scaffolds. Cells are filled to the area between PLGA fibers.

6.3.2 Longitudinal Section

(a) (b)
(Magnification 100X, Scale bar = 100 µm)

(c) (d)
(Magnification 200X, Scale bar = 50 µm)
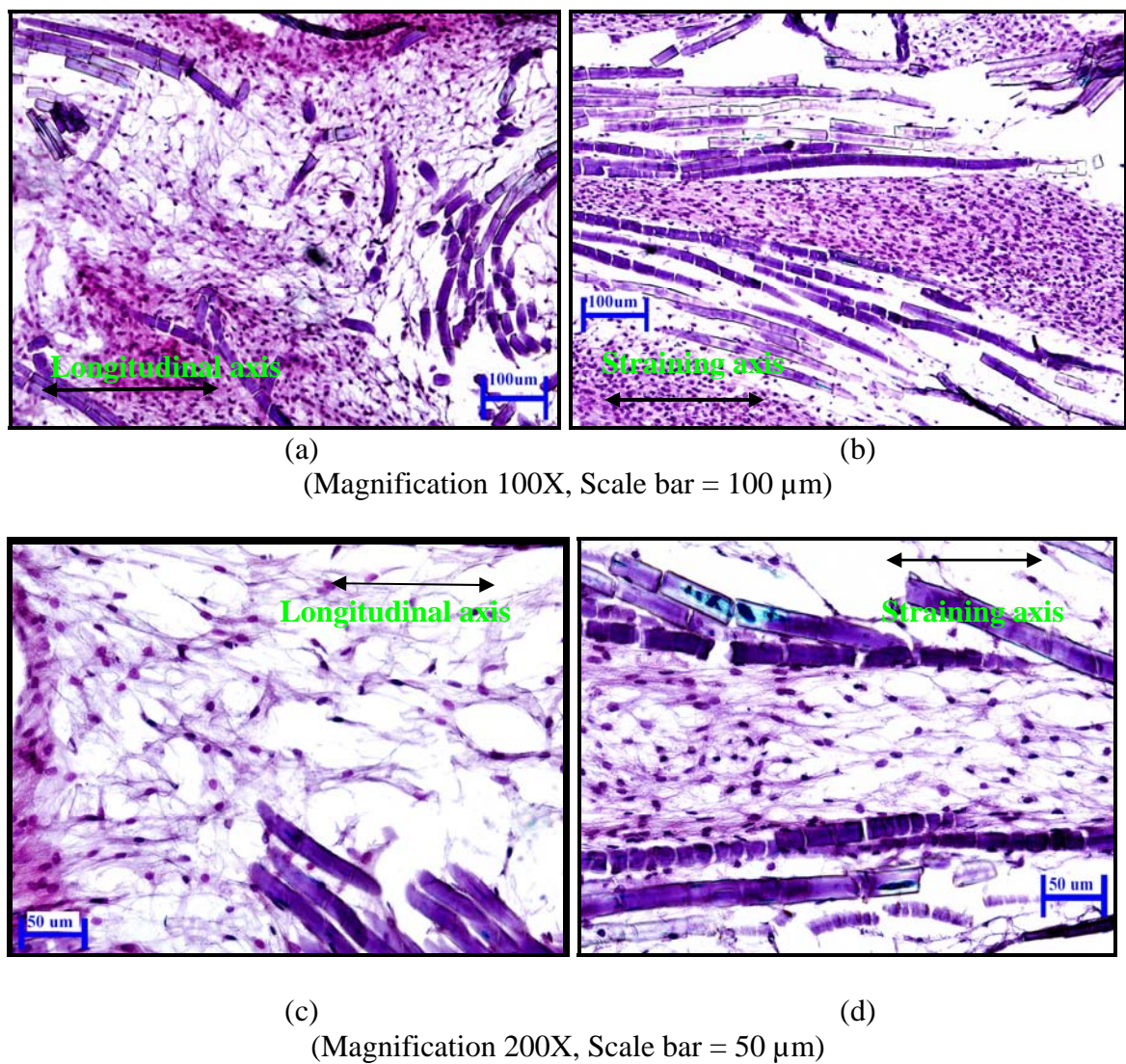
Figure 6.6: Longitudinal sections Histology of scaffold at Day 17 ;(a, c) unstrained sample, (b, d) strained samples

Under microscopic view of longitudinal sections, samples harvested after 2 weeks straining show different cell morphology (Figure 6.6). The cells from strained sample show slightly more elongated morphology. Moreover, most of the cell from strained sample also aligned in the straining axis. This observation may suggest that there are a change in the cell alignment and morphology under the effect of mechanical straining.

According to quantitative measurements results, the cells from unstrained samples were found to have a mean nuclei length of 7.46μm (n=1935) with a standard deviation of 2.35μm. For the strained sample, the mean nuclei length of cell is 8.05μm (n=1776) with a standard deviation of 2.39 μm. That is the cell length in strained sample is 7.9% longer than unstrained sample (Figure 6.7).

In the case of cell alignment, more cell population from strained sample fall in specific orientation angles compare with unstrained sample. For example, 19% of cell population falls in the orientation angle of ±5° while only 5.9% of cell population from unstrained sample falls in this orientation angle. This observation suggests that the cells from strained sample have better alignment than that of unstrained sample due to apply cyclic strain.

Weiss et al (1945) suggested that cells in many cases oriented and migrated along fibres or ridges in the surface and this phenomenon was known as contact guidance. The observed alignment in strained sample might be the product of contact guidance, especially when the fibres were made to align in the straining direction by the straining mechanism. The

difference between strained sample and unstrained sample is that the fibres in strained sample will be further stretched during the straining regime (Figure 6.1).

Eastwood et al (1998) predicted that the orientation of the fibroblasts along the maximum strain will reduce the perceived strain across the cell. This will be further minimized by the long thin bipolar morphology. This cell arrangement is often seen in the densest collagenous tissues such as tendons and ligaments. Altman et al (2001) also observed that the mechanical stimulation of ligaments based on bone marrow-derived cells had induced elongated, ligament-like cell morphology, and cell alignment in the direction of loading, in contrast to the round and randomly distributed cells in static controls. Cell alignment in the direction of the mechanical loading is 2.5 times higher than that of the controls.

Margolis and Popov (1991) proved cell processes can be induced by the action of a local force. They induce cell processes in round mouse embryo fibroblasts by pulling the cells with two tungsten microelectrodes. This forced caused cell processes to be formed within 20 seconds of its application and parallel with the applied force. The model of Margolis and Popov (1991) thus supported the hypothesis of cells aligned along the direction of principal strain. The cell processes formed were in the direction of the applied force, which would also be the direction of the maximum principal strain. Takakuda et al (1996) suggested that the alignment of collagen fibres in the direction of the tensile stress will have a positive feedback loop on the adhered cells to align in the similar direction as they proliferate.

The finding of this research suggested that HDFs cell had response to the cyclic mechanical strain by aligning themselves in the direction of straining and forming more elongated morphology compare with unstrained sample.
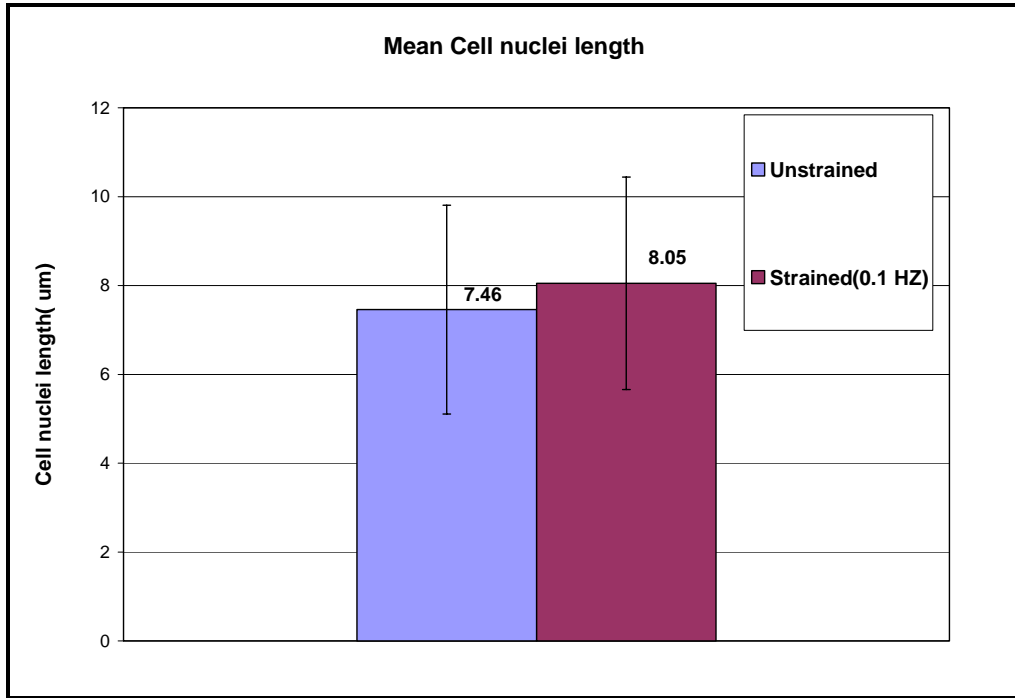
Figure 6.7: Graph showing cell nuclei length from different groups
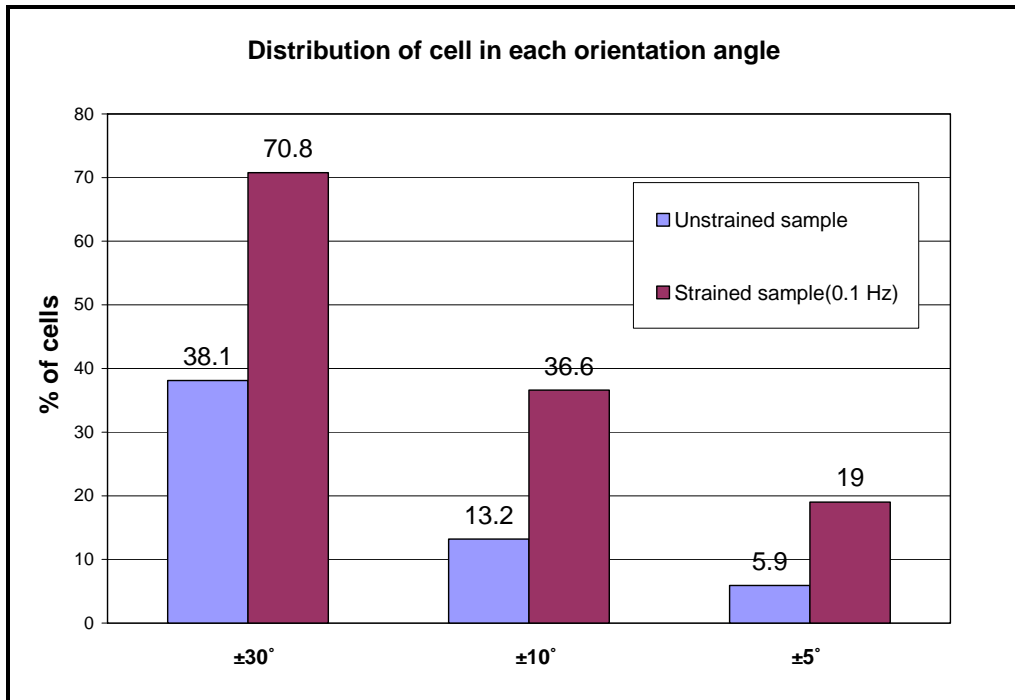
Figure 6.8: % of cells in each orientation angles for all groups

6.3.3 Comparative Study on Different Frequency of Straining (0.1 Hz & 1 Hz)

(a; scale bar= 200 µm)　　　　　　　(b; scale bar= 100 µm)

(Magnification 100X)

(c; scale bar =100 µm)　　　　　　　(d; scale bar = 50 µm)

(Magnification 200X)
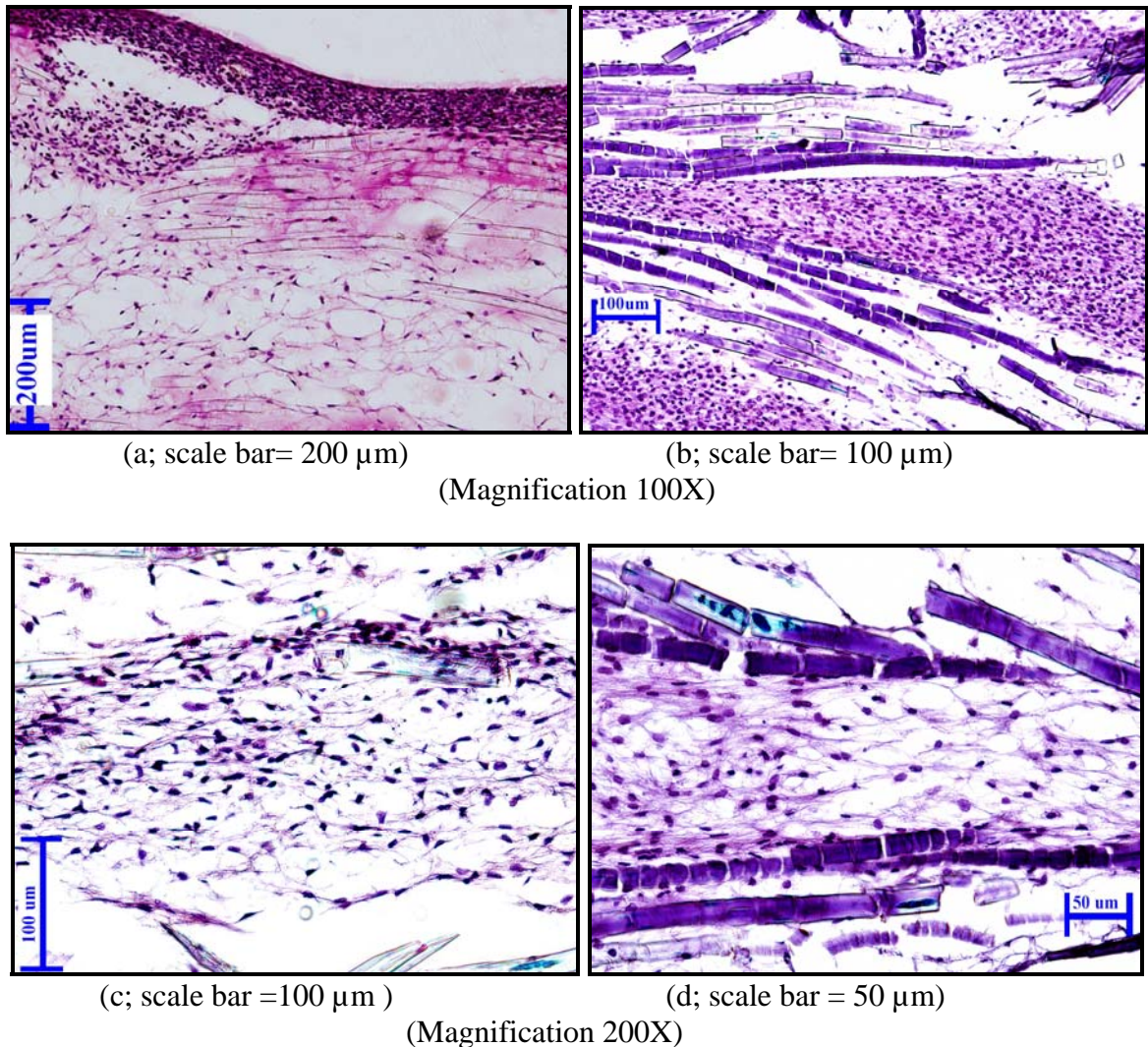
Figure 6.9: Longitudinal sections Histology of scaffolds in different frequency at Day 17; (a, c) Strained sample with 1Hz, (b, d) Strained samples with 0.1 Hz

The comparative study was conducted on scaffolds from strained samples which are strained at different frequencies. The rest straining parameters are the same in both groups. (e.g. Strain amount =1.8%, strain period = 4 hours per day for 2 weeks.) The effect of strain frequency on the cell morphology was investigated by observing the cell nuclei length and cell orientation angle. Figure 6.9 shows longitudinal sections of scaffold from different strain frequencies groups.
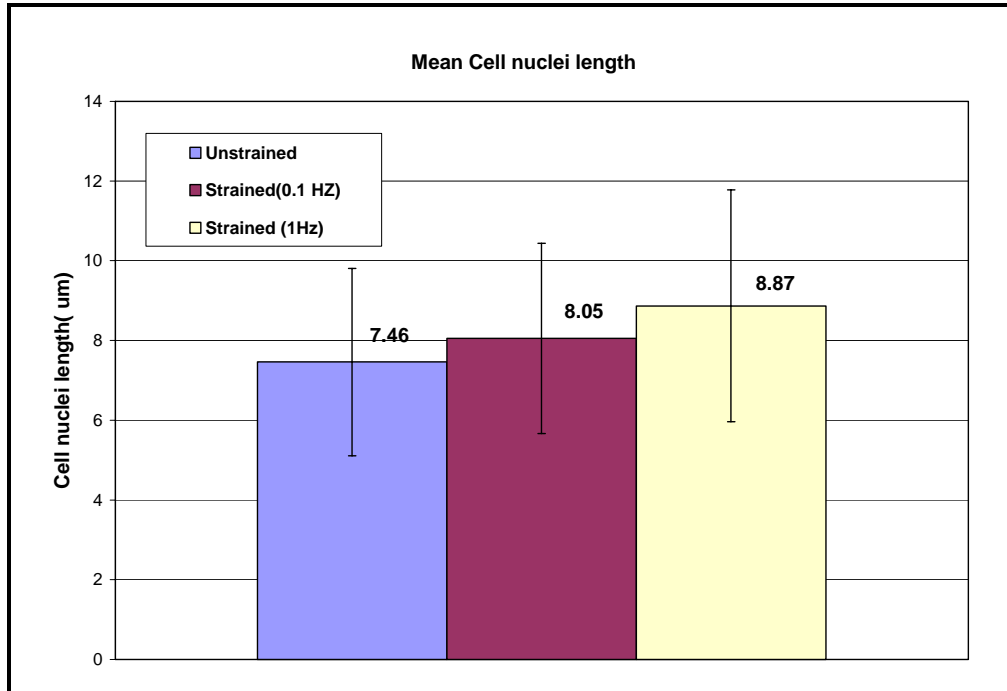
Figure 6.10: Graph showing cell nuclei length from different strain frequency groups
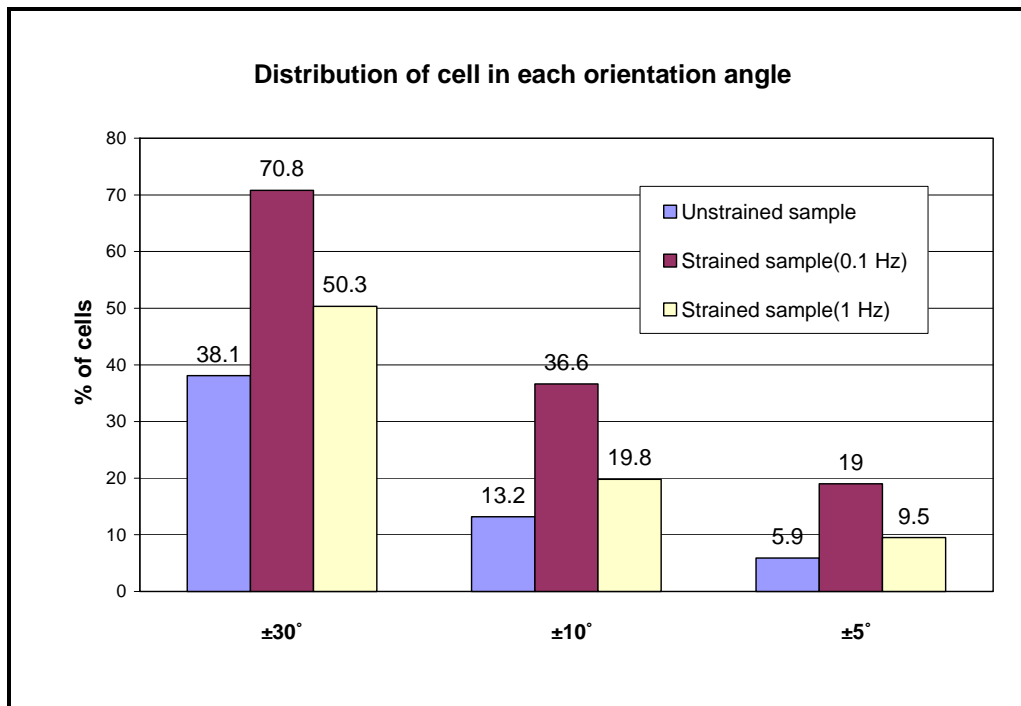
Figure 6.11: Percentages of cells from different frequencies strained groups in each orientation angle

The quantitative results show that the cells from 0.1Hz frequency strained samples were found to have a mean nuclei length of 8.05 μm (n=1776) with a standard deviation of 2.39μm. For the 1 Hz frequency strained sample, the mean nuclei length of cell is 8.87 μm (n=1825) with a standard deviation of 2.91μm (Figure 6.10). In the case of cell orientation angle, 19 % of cell from 0.1 Hz frequency strained sample fall in ± 5° orientation angle while only 9.5 % cell from 1 Hz frequency strained sample fall in this range. Figure 6.11 shows percentage of cells from different frequencies strained groups in each orientation angle. From this observation, it seems that lower frequency may give better cell alignment. However more experiments will be needed to confirm this finding. By observing effect of other straining parameters (e.g. strain value, strain frequency) we may find out the optimal strain parameters for engineering tissue *in-vitro* condition.

6.4 PCR Analysis of ECM Proteins

The observation on mRNA expression of collagen type I, collagen type III and tenascin-C was done in this research. These genes, collagen type I, collagen type III and tenascin-C are typical markers of ligament cells [Amiel et al, 1986, Mackie et al, 1996]. All negative control lanes from both sample-1 and sample-2 did not show any bands (Figure 6.12). This proves that the whole RT-PCR process was free from cross contamination. As GAPDH genes was used as house keeping gene in this research, all mRNA expression of targeted gene were normalized with GAPDH value. The resulting data were then expressed and illustrated as a ratio of the unstrained sample. Table 6.1 shows detail calculation of mRNA expression and figure 6.13 shows the final results of mRNA expression. The ratio of strained sample to unstrained sample values of collagen type I,

collagen type III and tenascin-C are 1.136, 1.076 and 1.143 respectively. According to limited sample number, only two samples were done for RT-PCR analysis, statically analysis could not do for this result.
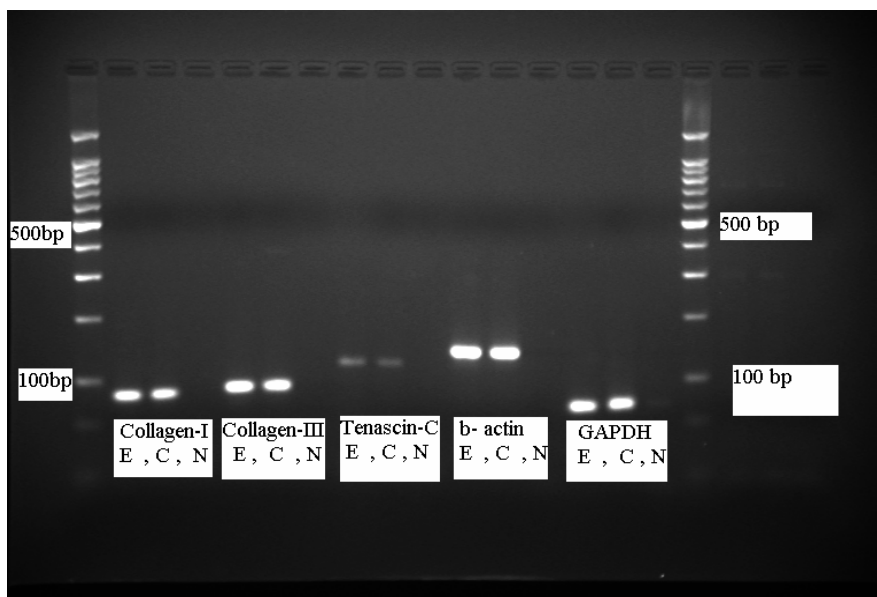
(a)
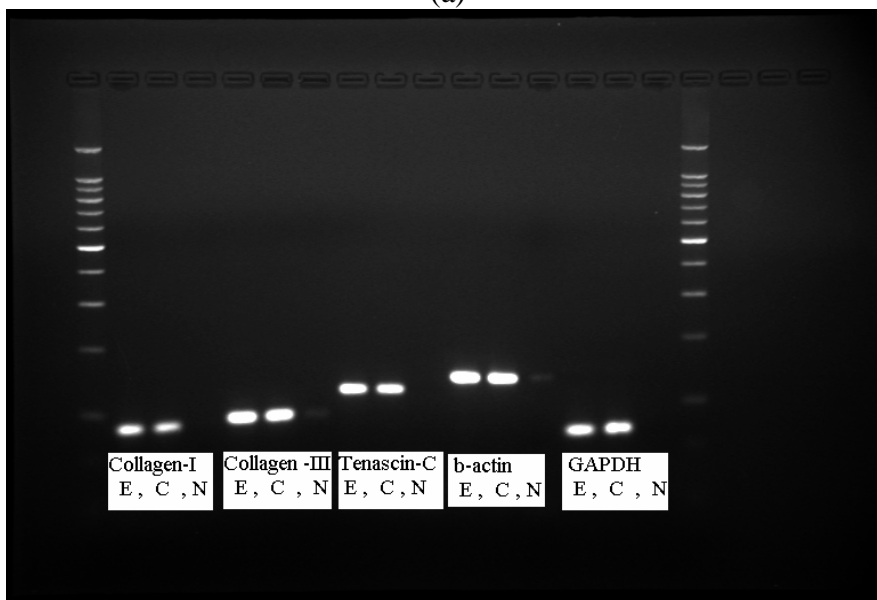
(b)

Figure 6.12: Gel-electrophoresis images after separation of RT-PCR products; (a) sample-1, (b) Sample-2. E: Strained scaffold, C: Unstrained scaffold, N: negative control (no DNA template)

Table-6.1: The result data of RT-PCR products: S: strained sample, US: unstrained sample

		Collagen-I		Collagen-III		Tenascin-C		GAPDH	
		S	US	S	US	S	US	S	US
Sample-1	Average Density value	114.59	101.49	112.10	114.49	37.94	31.91	113.27	112.79
	Normalize with GAPDH value	1.012	0.900	1.078	1.015	0.335	0.283	1.000	1.000
	Normalize with US value	**1.124**	**1.000**	**1.062**	**1.000**	**1.184**	**1.000**		
Sample-2	Average Density value	100.50	91.48	134.73	129.06	124.03	117.55	116.58	121.73
	Normalize with GAPDH value	0.862	0.751	1.156	1.060	1.064	0.966	1.000	1.000
	Normalize with US value	**1.148**	**1.000**	**1.091**	**1.000**	**1.101**	**1.000**		
Average value of S-1 & S-2		**1.136**	**1.000**	**1.076**	**1.000**	**1.143**	**1.000**		
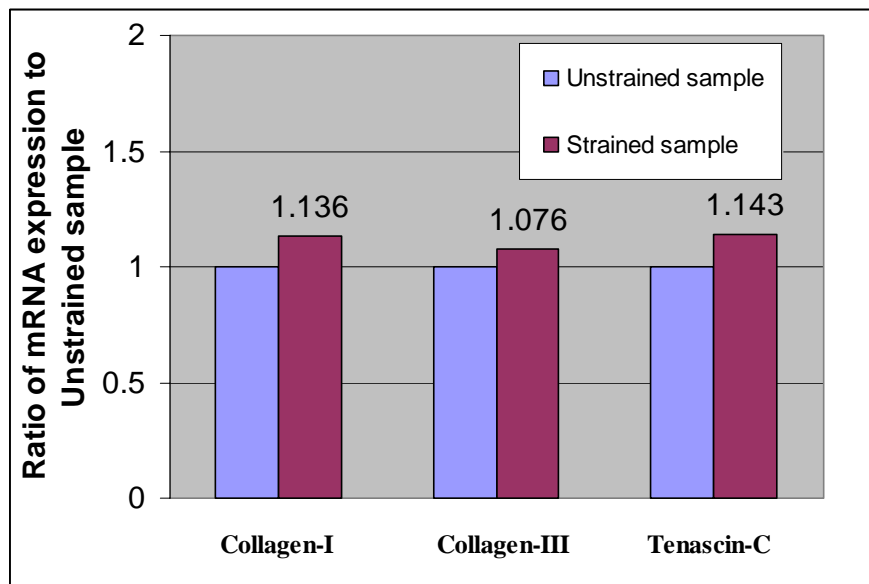
Figure 6.13: The resulting data of RT-PCR for Collagen type I, Type III and Tenascin-C expressed as a ratio of unstrained sample

Similar observations were done by Altman et al (2001) and Kim et al (2002). Altman et al (2001) seeded the Bovine bone marrow cell (BMSC) on type I collagen gel and stimulated translationally (10% strain, 2mm) and torsionally (25%, 90˚) at a frequency of 0.0167 Hz over a period of 21 days. Real-time RT-PCR was done on day 14 and the mRNA levels of collagen type I, collagen type III and tenascin-C were normalized with GAPDH value and results are expressed as a fraction of the average expression levels measured in native ligaments. After 14 days of culture, the difference of mRNA levels became statistically significant ($P< 0.05$) and mRNA levels in mechanically stimulated ligaments approached those quantified in native ligaments [Altman et al, (2001)].

Kim et al (2002) built a system which can applied for uniaxial cyclic stretch to cultured ACL fibroblasts cells on a silicon membrane. Uniaxial cyclic stretch was applied on ACL fibroblasts cells at 10 cycles/min with 10% length strength for 24 hour and RT-PCR was done for collagen type I and collagen type III. GAPDH was used as an internal control. Densitometric analysis was performed using NIH imaging after resolving on 2% agarose gel strained with ethidium bromide. The resulting data were expressed as a ratio to the control value denoted as one. The results show that the ratio of stretch to control values of collagen type I and collagen type III were 1.63±0.21 and 2.69±0.39 respectively. These observations show that mechanical stimulation cause increased in mRNA levels of collagen type I, collagen type III and tenascin-C. Our finding shows consistency with these observations.

6.5 Collagen Assay (Soluble & Insoluble)

6.5.1 Collagen Assay (Soluble collagen released into Medium)

The results of Sircol[®] Collagen Assay show that the cell seeded scaffold from strained sample synthesized an average of 86.2 µg/ml (SD=9) of soluble collagen between 1st day and 3rd day, while an average of 58 µg/ml (SD=6.1) was synthesized by unstrained samples. Between 15th day and 17th day, the strained sample synthesized 97.3 ± 13.5 µg/ml (Mean ± SD) and only 50.5 ± 0.4 µg/ml was synthesized by unstrained samples. This results show that the amount of soluble collagen synthesized by strained sample was increased 12.8% after 2 weeks straining. On the other hand, the amount of soluble collagen synthesized by unstrained sample was decreased 12.9% after the same period.
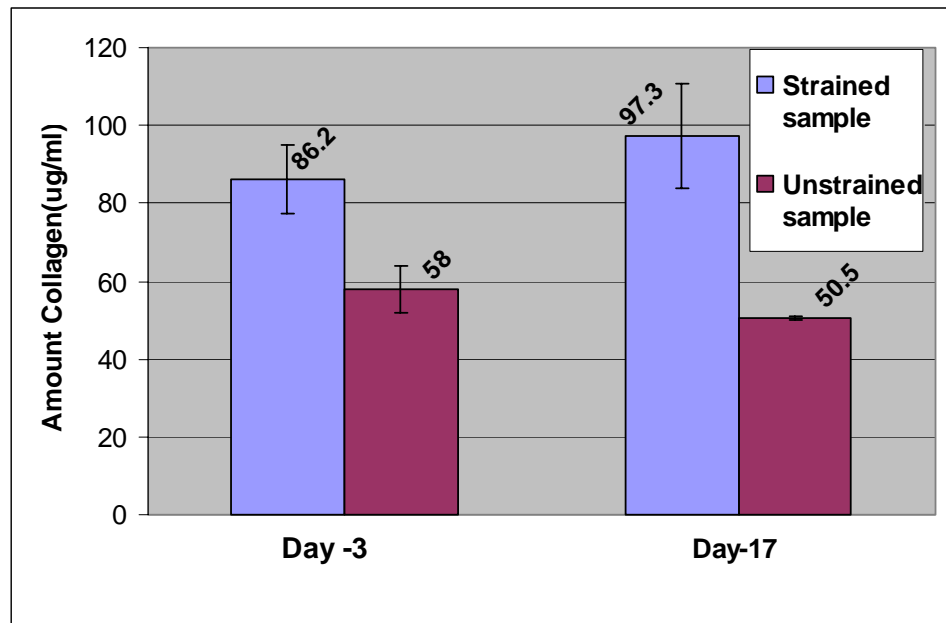
Figure 6.14: Total soluble collagen production from strained and unstrained scaffold between 1st to 3rd day and 15th to 17th day.

6.5.2 Collagen Assay (Insoluble collagen deposited on the scaffold)

The study of amount of insoluble collage deposited on the scaffold was done after two weeks straining. The investigation was done on one sample from both strained and unstrained groups. The wet weight of tissue sample for this study is 0.22g. The results were shown in mg of collagen based on 0.22g wet tissue weight. Figure 6.15 shows 747.2µg was deposited from strained sample while only 548.45 µg was deposited from unstrained sample.
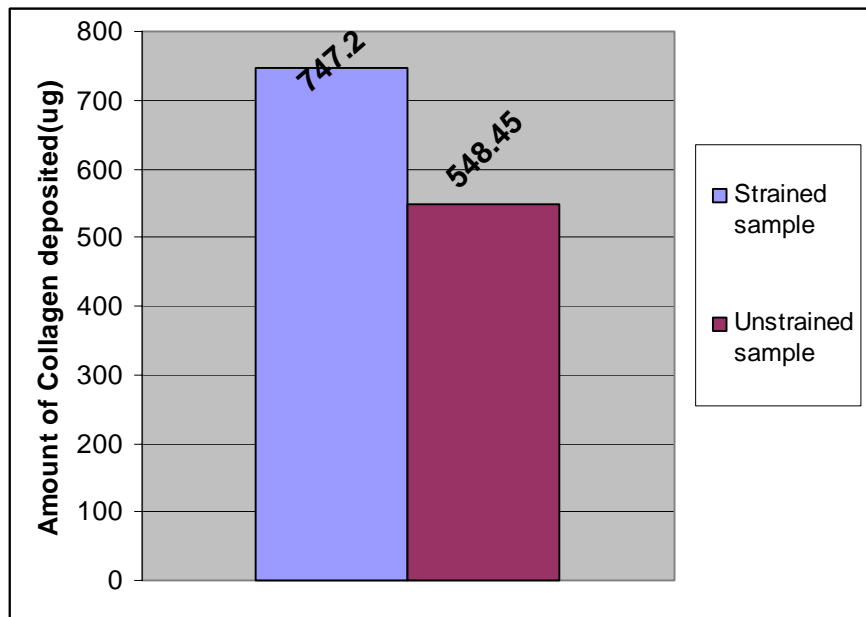
Figure 6.15: Amount of insoluble collagen deposited from strained and unstrained scaffold at day 17

According to the results of collagen assay, both soluble and insoluble, it suggest that the cyclic mechanical strain on the cell seeded scaffold have positive effect on collagen formation of engineered tissue *in vitro* condition.

6.6 Immunohistochemistry (Antibody Staining)

Extra-Cellular Matrix (ECM) is a molecular complex surrounding living cells that has as basic components collagens and other proteins, hyaluronic acid, proteoglycans, glysaminoglycans, and elastins. Cell-ECM interactions are believed to be directly involved in promoting cell-adhesion, mitigation, growth, differentiation, and programmed cell death, as well as in modulation of the activities of cytokines and growth factors, and in directly activating intracellular signaling [Boudreau et al, 1995]. The presence of ECM could be used as a good indication of the viability of the cells. Collagens comprise a family of fibrous glycoproteins that are only present in ECM. Collagen types I and type III in the extra cellular matrix were observed in this study as they are the major collagens found in skin tissue primarily produced by the fibroblasts.

The results had indicated the presence of collagen types I and III (stained brownish in colour) in the extra cellular spaces (Figures 6.16). No specific stain (brown) was found in blank sample. Both collagen type I and type III were detected in both unstrained and strained sample. The Immunohistochemistry images did not reveal any alignment of collagen in this result.
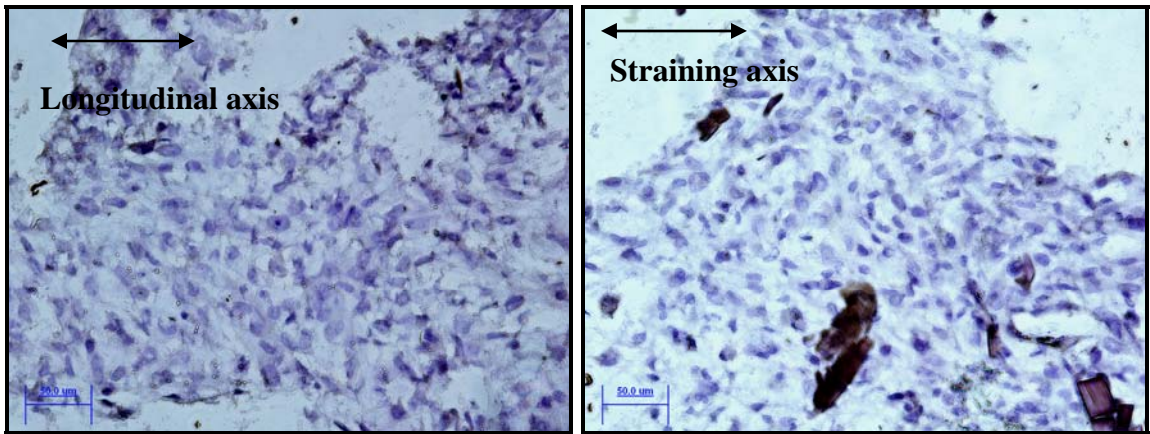
(Blank)
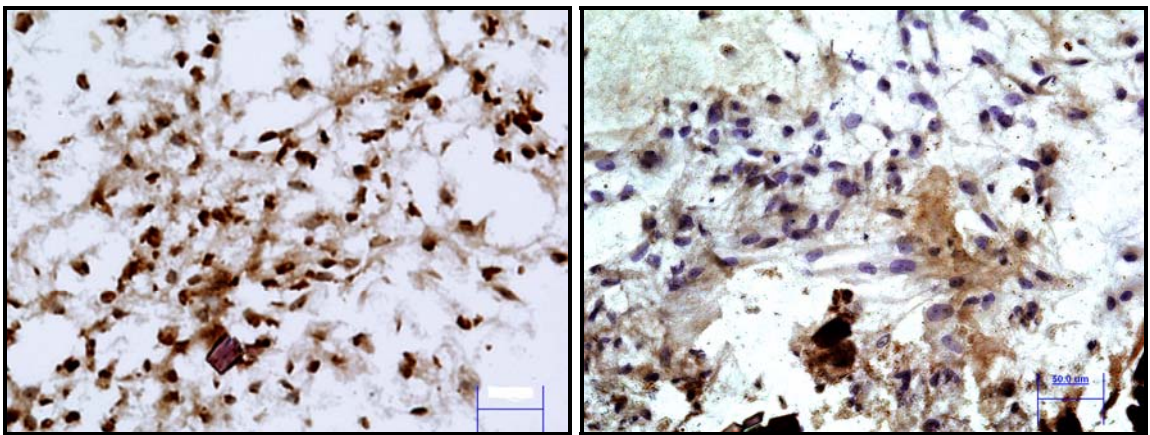
(Collagen Type I)
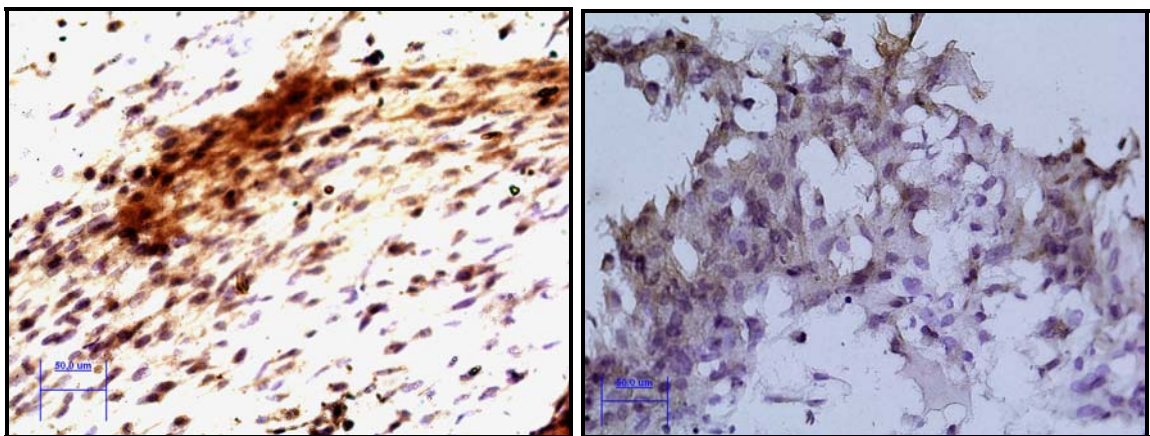
(Collagen Type III)

Figure 6.16: Immunohistochemistry (Antibody Staining) (left column) Unstrained sample, (right column) Strained sample. (Magnification 200X, scale bar = 50 µm)

6.7 Biomechanical Testing

According to the biomechanical test results, (Table 6.2, Figure 6.17, and Figure 6.18) the cell seeded scaffold from strained samples had lower structural stiffness (12.01 ± 1.35) than that of the unstrained samples (16.51 ± 1.34) .i.e. approximately 37.5% lower (P=0.015). On the other hand, the ultimate tensile force of that strained sample is slightly higher (31.9 ± 3.1) than that in unstrained samples (30.3 ± 1.6). The difference is insignificant (P=0.489).

The alignment formation of the fibroblast due to the mechanical straining is similar as slip plane manner, which is common in engineering materials [Eastwood et al, 1998]. Engineering materials fail along these slip planes as it represent the minimum energy required for failure to occur. When fibroblasts became aligned due to the applied mechanical load they themselves would create local minimum potential energy wells in a similar manner to that seen in the slip planes. It may be seen that cells will be energetically drawn towards the same slip planes and, further increasing the alignment. According to the existence of this slip plane, the fewer loads are required to deform the cells in this slip plane as compare to the absence of the slip plane. This may be one reason of why the strained samples occupied lower structural stiffness. Another possible reason is that the straining did increase the degradation of the PLGA fibres itself in the culture medium and so the structural stiffness of strained samples is lower than unstrained samples.

PLGA was degrading in aqueous medium according to hydrolysis action, where PLGA were broken down into by–products, Lactic acid and Glycolic acid. This reaction causes

reduction in its mechanical integrity. Our results also argue on this, the initial ultimate tensile load for PLGA scaffold is 70.8 ± 7.8 N. After 10 day in culture medium, the cell seeded PLGA scaffold possesses only 42% of its original ultimate tensile load.

Table 6.2: Ultimate Tensile Force and Structural Stiffness for each group (mean $\pm$ SD)

Groups	Ultimate Tensile Force, F_{max} (N)	Structural Stiffness, M (N/mm)
PLGA scaffold at day 0 (n=4)	70.8 ± 7.8	18.16 ± 1.24
Scaffold from strained sample at day 10 (n=3)	31.9 ± 3.1	12.01 ± 1.35
Scaffold from unstrained sample at day 10 (n=3)	30.3 ± 1.6	16.51 ± 1.34
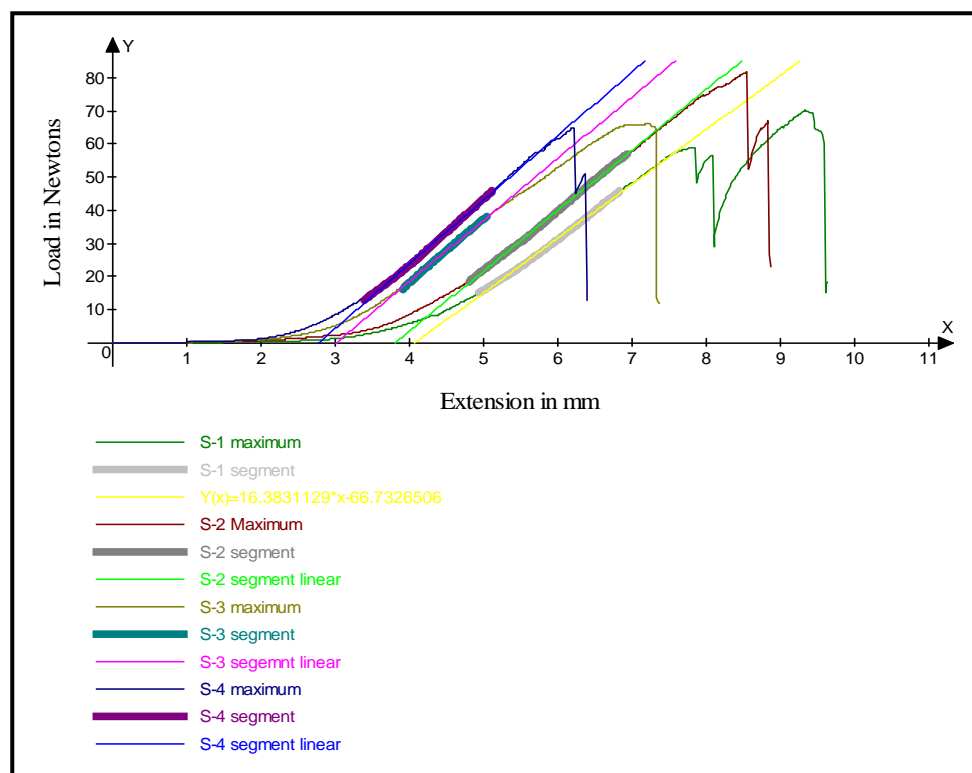
Figure 6.17 Load-Extension graph for PLGA scaffold at day 0: Thick line segment show the segment of most linear region of the graph
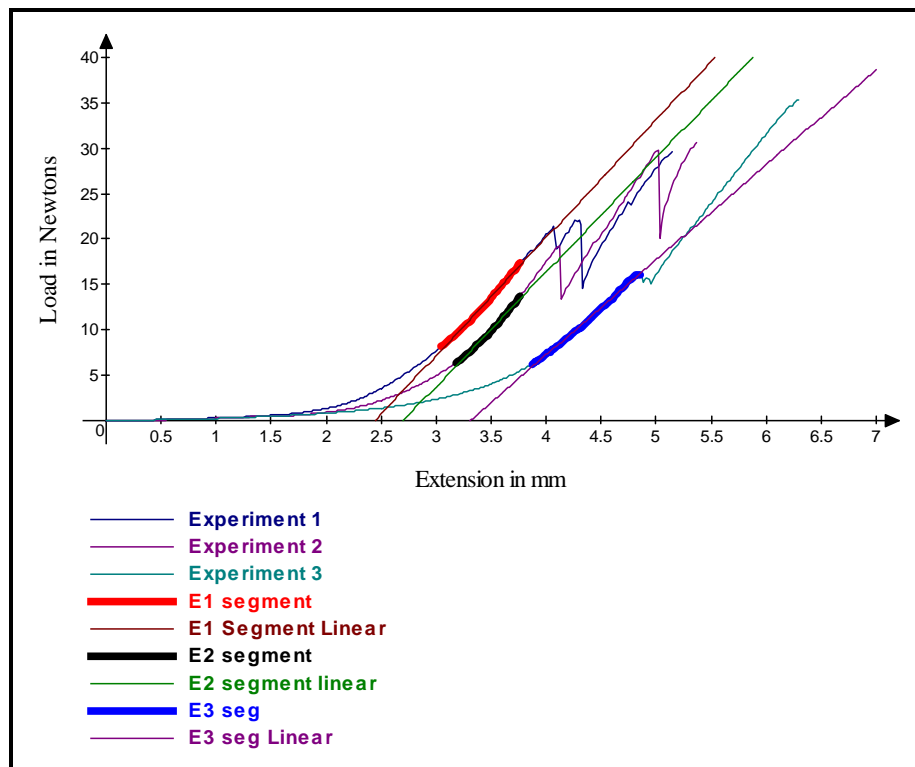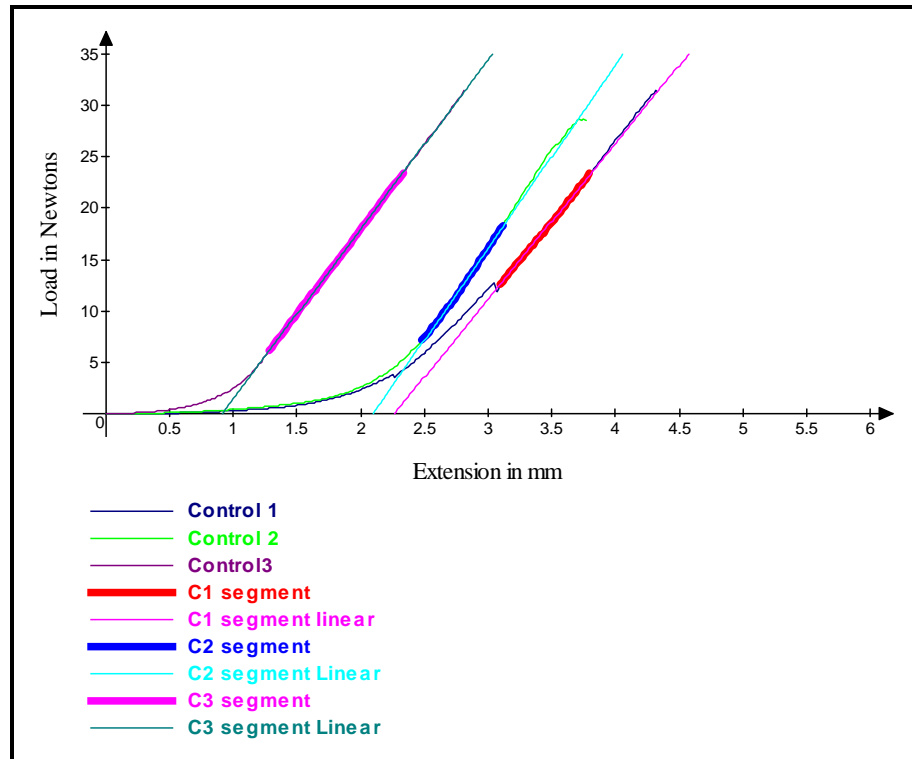
Figure 6.18 Load-Extension graphs for cell seeded PLGA scaffold at day 10 (top) unstrained samples (bottom) strained samples: Thick line segments show the segments of most linear region of the graph

Chapter 7. Conclusions and Recommendations

7.1 Conclusions

According to the LSCM images, there are viable cells in both strained and unstrained group. This finding shows that the whole experimental setting is biocompatible. In this study, application of cyclic mechanical strain on the cell seeded PLGA scaffold shows positive effect on cell growth *in-vitro* condition. According to microscopic examination and cell proliferation study, it is clear that cell proliferation rate in strained sample is higher than unstrained sample. Alamar Blue assay result shows the percent of reduction of Alamar Blue, which reflect the cell proliferation, of strained sample group increased 24.86% after two weeks period of straining while unstrained samples increase only 9.9% in the same period. The results show that higher proliferation rate occurs in strained samples.

In the study of cell morphology, cell from strained sample (0.1 Hz frequency) possesses more elongated morphology than unstrained sample. The mean nuclei length of cell from strained sample is 7.9% longer than unstrained sample. The mean cell nuclei lengths of strained and unstrained sample are 8.05±2.39 μm and 7.46 ± 2.35 μm respectively. Moreover, the more percentage of cells from strained sample fall in specific orientation angle than unstrained sample. This finding suggests that cyclic mechanical strain also causes better alignment of cell formation.

In comparatives study of different strain frequencies sets (0.1 Hz and 1 Hz), lower strain frequency cause better alignment while higher frequency result in more elongated cell nuclei length.

The observation on mRNA expression level by RT-PCR analysis show that the mRNA level of typical markers of Ligament gene, i.e. Collagen type I, Collagen type III and Tenascin–C are higher in strained samples. That suggests that cyclic mechanical strain possible to induce the fibroblast cell to ligament like cells. Moreover, cyclic mechanical strain help in formation of collagen on the scaffold and released soluble collagen. The collagen assay results show higher amount of collagen are detected in culture medium and also on the scaffold for strained sample.

In immunohistochemistry study, antibody staining, both collagen type I and collagen type III are detected in both strained and unstrained group. The results images did not reveal any alignment of collagen.

The biomechanical result shows that the strained sample has lower structural stiffness and slightly higher in ultimate tensile force as compare with unstrained sample. The difference of this ultimate tensile force between strained sample and unstrained sample is not significant. Another finding suggested that PLGA scaffolds degrade in the culture medium. After 10 day culture, the ultimate tensile force of PLGA scaffold possesses only 42% of its original ultimate tensile load. Previous degradation test shows that the ultimate tensile force of PLGA scaffold at day 18 is 1.06±0.32 N only [Lau, 2003-04]. This fact shows that mechanical integrity of pure PLGA scaffold is not enough for tissue implantation.

Generally the main advantage of the designed bioreactor is all the straining parameters (both frequency and strain amount) could be changed easily. By changing the motor speed, the frequency of straining could be set up easily. The possible minimum frequency of straining in this system is 0.01 Hz. The straining amount also easily can set up by changing the rotation angle of motor. Another advantage of the system is biocompatible,

compactable and easy to access. More machines could be fabricated for muti-station testing.

7.2 Recommendations for Future Research

According to biomechanical test result and previous degradation test results, PLGA fiber shows short time degradation. After two weeks in culture medium, PLGA lose most of the mechanical integrity. This shows that another polymer which has longer degradation time is required in future experiment. Poly -l-lactic acid is recommended for future experiment because of its slower degradation rate. Hybrid scaffolds such as 2 yarns of PLLA and 2 yarns of PLGA will be ideal structure because PLLA possess longer degradation rate and good mechanical integrity while PLGA is recommended for better cell attachment.

/Another find out in this research is cell seeding technique. In this research, Fibrin Glue (Tisseel) is used for cell seeding. The usage of fibrin glue is not an ideal technique for cell seeding. Although it has a lots advantage, there are also some limitations. First, by using fibrin glue for cell seeding, it is difficult to achieve uniform cell distribution on the entire scaffolds area. Another disadvantage is that some fibrin glue still remains in tissue formation process after two weeks period. Sometimes, the remaining fibrin glue interfere the staining process of tissue slides. This may be because of using extra amount of fibrin glue. So we need to find out the optimal amount of fibrin glue base on scaffold area and seeded cell numbers. Another recommended way to solve this problem is using nano

scale fibre scaffolds instead of micro scale fibre scaffolds. Now a day, nano scale fibre scaffolds are achieved by using electro spinning technology.

According to limited specimen numbers for the bioreactor, only two sets of straining frequency are tested in this research. In future some more experiments should be done for different straining parameters such as strain amount, straining period (e.g. increasing straining period to 8 hour per day instead of 4 hour per day). Then, we may find out the optimal straining parameters for tissue growth *in-vitro* condition.

REFERENCES

Journal Articles:

1. Altman, G.H., Rebecca L. Horan, Ivan Martin, Jian Farhadi, Peter R. H. Stark,Vladimir Volloch, John C. Richmond, Gordana Vunjak-Novakovic, and David L.Kaplan. (2001): Cell Differentiation by Mechanical Stress; Federation of American Societies for Experimental Biology (FASEB) Journal 16:270-272

2. Altman, G.H., Lu, H.H., Horan, R.L., Calabro, T, Ryder, D., Kaplan, D.L., Stark, P.,Martin, I., Richmond, J.C. and Novakovic, G.V. (2002): Advanced Bioreactor with Controlled Application of Multi-Dimensional Strain for Tissue Engineering; Journal of Biomechanical Engineering 124:742-747

3. Amiel, D., Kleiner, J. B., Roux, R.D., Harwood, F.L., and Akeson, W. H. (1986) The phenomenon of "ligamentization": anterior cruciate ligament reconstruction with autogenous patellar tendon. *J. Orthop. Res* 4**,** 162-172

4. Athanasiou, K.A., Niederauer, G.G., and Agrawal, C.M.Sterilization, toxicity, biocompatibility and clinical applications of polylactic acid/polyglycolic acid copolymers. Biomaterials 17, 93, 1996.

5. Boudrea, N., Werb, Z., Bissell, M.J. (1995): From Lamini to Lamin: Regulation of Tissue-Specific Gene Expression by the ECM; Trends Cell Biol 5:1-4

6. Cacou, C., Palmer, D., Lee, D.A., Bader, D.L. and Shelton, J.C. (2000): A System for Monitoring the Response of Uniaxial Strain on Cell Seeded Collagen Gels; Medical Engineering & Physics 22:327-333

7. Catherine, C.B., Julia, C.S., Dan, L.B. and David, A.L.(2003): Influence of External Uniaxial Cyclic Strain on Oriented Fibroblast-Seeded Collagen Gels; Tissue Engineering 9,613-623.

8. Dehoff PH. 1978. On the nonlinear viscoelastic behavior of soft biological tissue. Journal of Biomechanics.11:35-40

9. Eastwood, M., Mudera, V.C., McGrouther, D.A. and Brown R.A. (1998). Effect of Precise Mechanical Loading on Fibroblast Populated Collagen Lattices: Morphological Changes; Cell Motility and the Cytoskeleton 40:13–21

10. Fu F.H., Bennett CH, Lattermann C, Menetrey J, Lattermann C. 1999. Current trends in anterior cruciate ligament reconstruction, part I. Biology and biomechanics of reconstruction. *Am. J. Sports Med.* 27: 821–30

11. Jackson DW, Grood ES, Goldstein JD, Rosen MA, Kurzweil PR, et al. 1993. A comparison of patellar tendon autograft and allograft used for anterior cruciate ligament reconstruction in the goat model. *Am. J. Sports Med.* 21:176–85

12. Karamuk E, Mayer J, Düring M, Wagner B, Bischoff B, Ferrario R, Billia M, Seidl R, Panizzon R, Wintermantel E. Embroidery technology for medical textiles. *Medical Textiles*, Proceedings of the 2nd International Conference, Bolton, 1999.

13. Ker RF. The design of soft collagenous load-bearing tissues. *The Journal of Experimental Biology*, 1999, 202: 3315–24.

14. Ker RF, Wang XT, Pike AVL. Fatigue Quality Of Mammalian Tendons:*The Journal of Experimental Biology*, 2000, 203: 1317–27.

15. Kim, B.S., Putnam, A.J., Kulik, T.J. and Mooney, D.J. (1997): Optimizing Seeding and Culture Methods to Engineer Smooth Muscle Tissue on Biodegradable Polymer Matrices; Biotechnology and Bioengineering 57(1): 46-54

16. Kim, B.S. and Mooney, D.J. (2000): Scaffolds for Engineering Smooth Muscle under Cyclic Mechanical Strain Conditions; Journal of Biomechanical Engineering 122:210-215

17. Kumar K, Maffulli N. 1999. The ligament augmentation device: an historical perspective. *Arthroscopy* 15:422–32

18. Langer R, Vacanti JP. Tissue engineering. *Science*, 1993, 260: 920–6.59) [Laurencin et al, 1999] Laurencin CT, Ambrosio AMA, Borden MD, Cooper JA. Tissue engineering: Orthopedic applications. *Ann Rev Biomed Eng*, 1999, 01: 19-46.

19. Lee TQ, Woo SLY. A new method for determining cross-sectional shape and area of soft tissues. *J Biomech Eng*, 1988, 110: 110–14. 76

20. Mackie, E. J. and Ramsey, S.(1996) Expression of tenascin in Joint-associated tissues during development and postnatal growth. *J. Anatomy* 188, 157-165

21. Maffullin N. Rupture of the Achilles tendon. *J Bone Jt Surg Am*, 1999,81: 1019–36.

22. Margolis L.B., Popov, S.V. (1991): Induction of Cell Processes by Local force; Journal of Cell Science; 98:369-373

23. Markolf KL, Pattee GA, Strum GM, Gallick GS, Sherman OH, Dorey FJ. 1989. Instrumented measurements of laxity in patients who have a Gore-Tex anterior cruciate ligament substitute. *J. Bone Jt. Surg.* 71:887–93

24. Martin, I., Jakob, M., Schaefer, D., Dick, W., Spagnoli, G., Heberer., M.(2001) Quantitative analysis of gene expression in human articular cartilage from normal and osteoarthritic joints. *Osteoarth. Cartil.*9**,**112-118

25. Monti RJ, Roy RR, Zhong H, Edgerton VR.2003. Mechanical properties of rat soleus aponeurosis and tendon during variable recruitment in situ. The Journal of Experimental Biology, 206: 3437-45.

26. Moyen BJ, Jenny J-Y, Mandrino AH, Lerat JL. 1992. Comparison of reconstruction of the anterior cruciate ligament with and without a Kennedy Ligament-Augmentation Device. *J. Bone Jt. Surg.* 74:1313–19

27. Neidlinger-Wilke C., Grood E., Claes L., Brand R., *Fibroblast orientation to stretch begins within 3 hours, J. of Ortho. Research.*, 20:953-956 (2002)

28. Noyes FR, Butler DL, Grood ES, Zernicke RF, Hefzy MS. 1984. Biomechanical analysis of human ligament grafts used in knee-ligament repairs and reconstructions. *J. Bone Jt. Surg.* 66:344–52

29. Ouyang, H.W., Goh, J.C.H., Mo, X.M., Teoh, S.H., and Lee, E.H. Characterization of anterior cruciate ligament cells and bone marrow stromal cells on various biodegradable polymeric films. Mater. Sci. Eng. C 520**,** 63, 2002

30. Ouyang HW, Goh JCH, Thambyah A, Teoh SH, Lee EH. Knitted polylactide- co-glycolide scaffold loaded with bone marrow stromal cells in repair and regeneration of rabbit achilles tendon. *Tissue Eng*, 2003, 9(3): 431-9.

31. Ouyang, H.W.,Goh, J.C.H.,Thambyah, A.,Teoh, S.H., Lee, E.H.: Knitted Poly-lactide-co-glycolide Scaffold Loaded with Bone Marrow Stromal Cells in Repair and Regeneration of Rabbit Achilles Tendon; Tissue Engineering;9:431-451

32. Richmond JC, Manseau CJ, Patz R, Mc-Conville O. 1992. Anterior cruciate reconstructionusing a Dacron ligament prosthesis. A long-term study. *Am. J. Sports Med.* 20:24–28

33. Schechtman H, Bader DL. Fatigue damage of human tendons. J*ournal of Biomechanics*, 2002, 35: 347–53.

34. Takakuda, K., Miyairi, H. (1996): Tensile Behaviour of Fibroblasts cultured in Collagen Gels. Biomaterials 17:1393-1397

35. Van Eijk, F., Saris, D.B.F., Riesle, Willems, W.J., Van Blitterswijk, C.A.,Verbout, A.J, and Dhert, W.J.A., Tissue Engineering of Ligaments: A Comparison of Bone Marrow Stromal cells, Anterior Cruciate Ligament, and Skin Fibroblast as Cell Source. Tissue Engineering Vol 10 , Number 5/6, 2004

36. Viidik, A.,(1973). Functional properties of collagenous tissue. International Review of Connective Tissue Research, 6, 127-215.

37. Weiss, P. (1945): Experiments on Cell and Axon Orientation In-Vitro: The Role of Colloidal Exudates in Tissue Organisation; J. Exp. Zool. 100: 353-386

38. Weiss JA, Gardiner JC. Computational modeling of ligament mechanics. *Critical Reviews in Biomedical Engineering*, 2001, 29(3):1-70.

39. Weitzel PP, Richmond JC, Altman GA, Calabro T, Kaplan DL. 2002. Future direction of the treatment of ACL ruptures. *Orthop. Clin. North Am.* 33:653–61

40. Woo SLY, Debski RE, Zeminski J, Abramowitch SD, Saw SSC, Fenwick JA. Injury and repair of ligaments and tendons. *Annu Rev Biomed Eng*, 2000, 02: 83–118.

41. Yang S, Leong KF, Du ZH, Chua CK. The design of scaffolds for use in tissue engineering, *Tissue Eng*, 2001, 7: 679-89.

42. Yost, M.J., Simpson, D., Wrona, K., Ridley, S., Ploehn, H.J., Borg, T.k. and Terracio, L. (2000): Design and Construction of a Uniaxial Cell Stretcher; Am. J. Physiol. Heart Circ. Physiol. 279:H3124-H3130

43. Young, R.G., Butler, D.L., Weber, W., Caplan, A.I., Gordon, S.L., and Fink, D.J. Use of mesenchymal stem cells in a collagen matrix for Achilles tendon repair. J. Orthop.Res. 16**,** 406, 1998.

44. Zange, R., and Kissel, T. Comparative in vitro biocompat-ibility testing of polycyanoacrylates and poly(D,L-lactideco-glycolide) using different mouse fibroblast (L929)biocompatibility test models. Eur. J. Pharmacol. Biopharmacol.44, 149, 1997.

45. Zdrahala, R.J. Small caliber vascular grafts. I. State of the art. J. Biomater. Appl. 10, 309, 1996.

B. Eng Thesis:

46. Darrel, L.C.L.,(2002-03) Development of Bioreactor for Tissue Engineering Application

47. Lau, S.Y., (2003-04) Characterization of Collagen Coated Knitted PLGA Scaffolds.

48. Phoo, W. W., (2003-04) Development of an Effective Cell Seeding System for Ligament Tissue Engineering Application

M.Eng Thesis:

49. Kwan, M. S.,(2003)Design and Development of a bioreactor for the in-vitro engineering of soft tissues

BOOKS:

50. Akeson, W.H., Woo, S.L-Y., Amiel, D. and Frank, C.B. (1984). The chemical basis of tissue repair. In L.Y. Hunter and F.J. Funk (Ed.) Rehabilitation of the Injured Knee (pp. 93-104). St. Louis: C.V. Mosby Company.

51. Amiel D, Billings E Jr, Akeson WH.1990. Ligament structure, chemistry, and physiology. In *Knee Ligaments: Structure, Function, Injury, and Repair*, ed. DM Daniel, WH Akeson, JJ O'Connor, pp. 77–91. New York: Raven

52. Fauci AS, Brawnwald E, Isselbacher KJ, Wilson JD, Martin JB, Kasper DL, Hauser SL, Longo DL eds. *Harrison's Principle of Internal Medicine*. 14th edn., 2001, McGraw-Hill, New York.

53. Fung YCB. 1972. Stress-strain-history relations of soft tissues in simple elongation. In *Biomechanics: Its Foundations and Objectives*, ed. YCB Fung, pp. 181–208. Englewood Cliff

54. Goulet F, Germain L, Rancourt D, Caron C, Normand A, Auger FA. Tendons and ligaments. In: Lanza R, Langer R, Chick W. eds., *Principles of Tissue Engineering*, 1997, Academic Press, San Diego, CA, USA: 631–44.

55. McCarthy DM, Tolin BS, Schwenderman L. 1993. *Anterior cruciate ligament: Current and future concepts*, pp. 343–56. New York: Raven

56. Singer KM, Jones DC. Soft tissue conditions of the ankle and foot. In The *Lower Extremity and Spine in Sports Medicine*, ed. JA Nicholas, EB Hershman, 1986, Mosby, St. Louis, MO, USA, 1: 498–525.

57. Woo SLY, Buckwalter JA, eds. 1988. *Injury and Repair of the Musculoskeletal Soft Tissues*, pp. 45–101. Park Ridge, IL: Am. Acad. Orthop. Surg.

58. Woo SLY, Levine RE. Ligament, tendon and fascia. *Handbook of Biomaterial Properties* - Black J, Hastings G. eds., 1998, Chapman and Hall, London, B3:59-65.

59. Wright, V and Radin, E.L. Mechanics of Human Joints: Physiology, Pathophysiology and Treatment 163-195, New York Marcel Dekker 1993

PUBLICATIONS

### *International Journal:*

1- <u>Ouyang HW</u>, Toh SL, Goh JCH, Tay TE, Moe K, Phan-Thien N. **Assembly of bone marrow stromal cell sheets with knitted Poly (L-Lactide) scaffold for ligament tissue engineering.** Accepted for publishcation in Journal of Biomedical Material Research partB -Applied Biomaterials

International Conference:

1- <u>Kyaw Moe</u>, Tay TE, Goh JCH, Ouyang HW, Toh SL. **Cyclic Mechanical Strain on knitted PLGA Scaffolds.** Poster Presentation proceedings of 7th World Biomaterials Congress 17-21 May 2004, Sydney, Australia

2- <u>Kyaw Moe</u>, Tay TE, Goh JCH, Ouyang HW, Toh SL.**Cyclic uniaxial strains on Fibroblasts-seeded PLGA scaffolds for tissue engineering of Ligaments.** Oral Presentation proceedings of The 3rd International Conference on Experimental Mechanics 29th Nov-1st Dec 2004, Singapore.

Appendix A. Technical drawing of the Bioreactor(all dimensions are in mm)
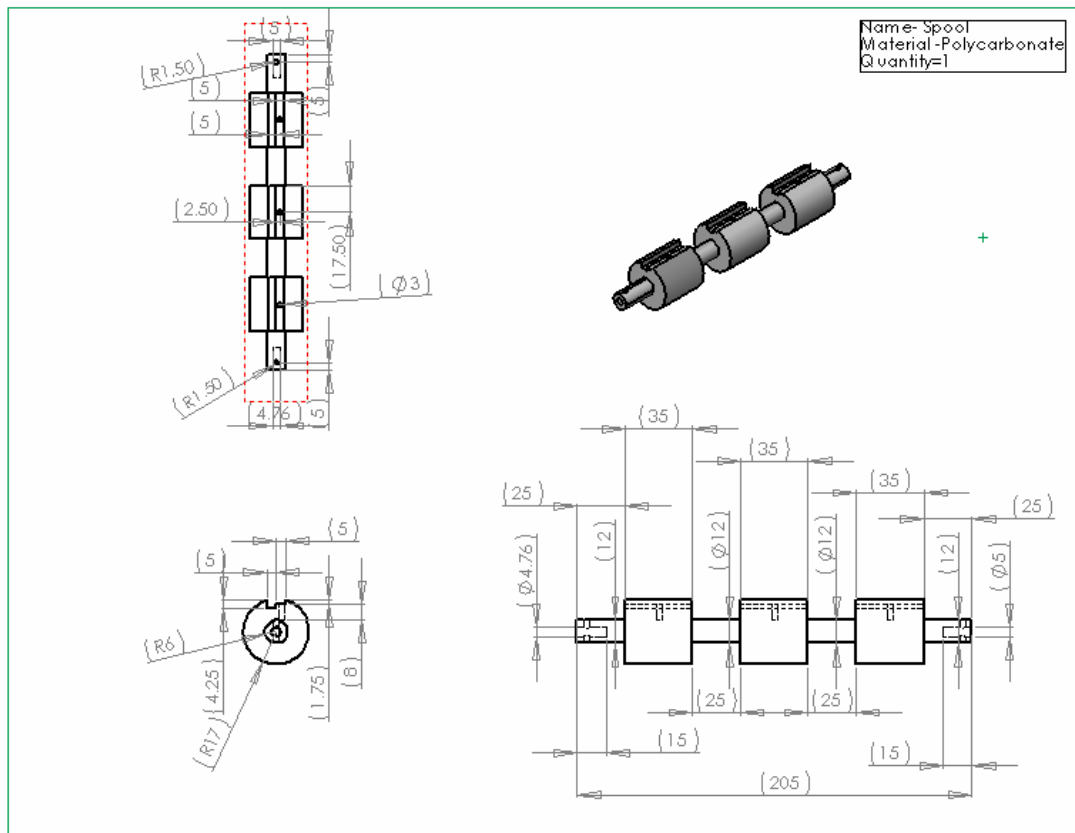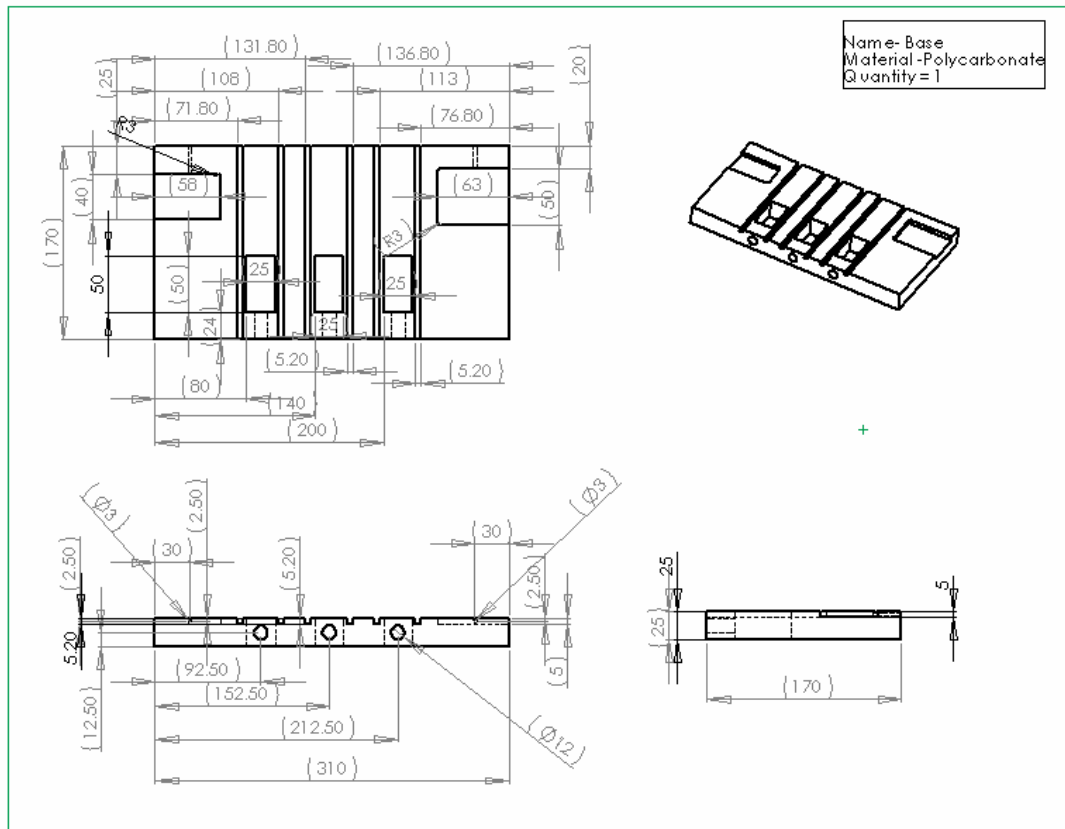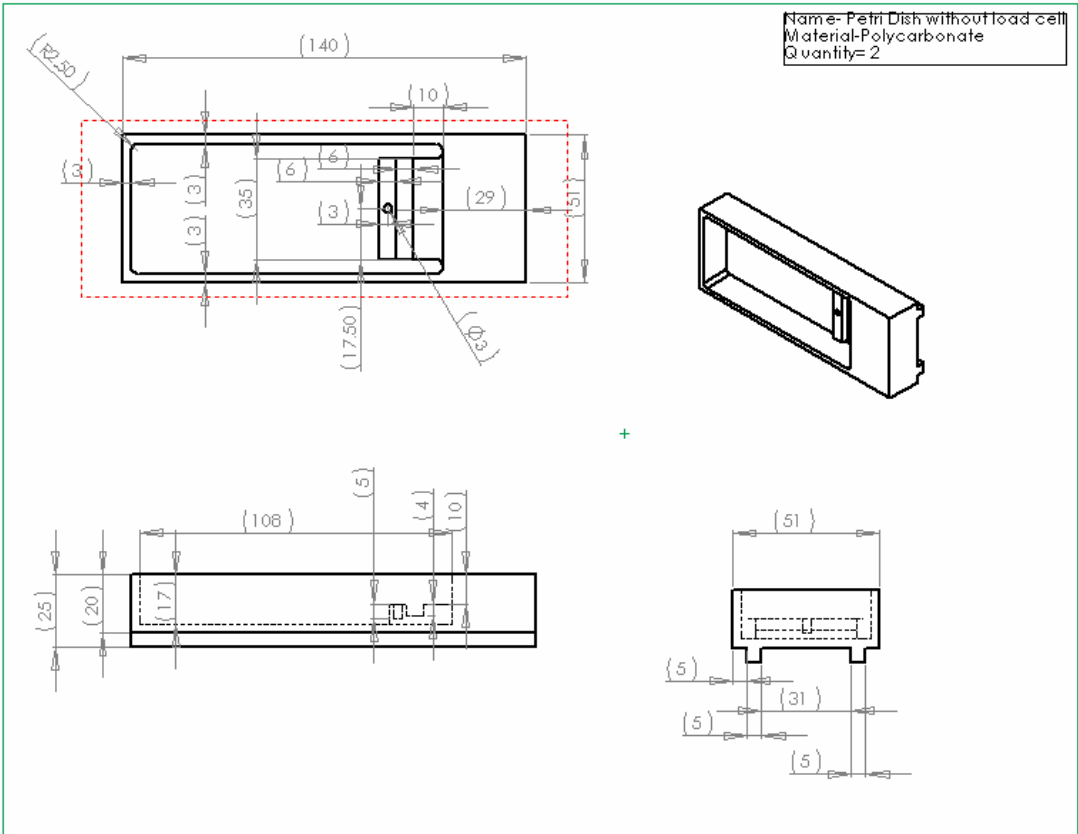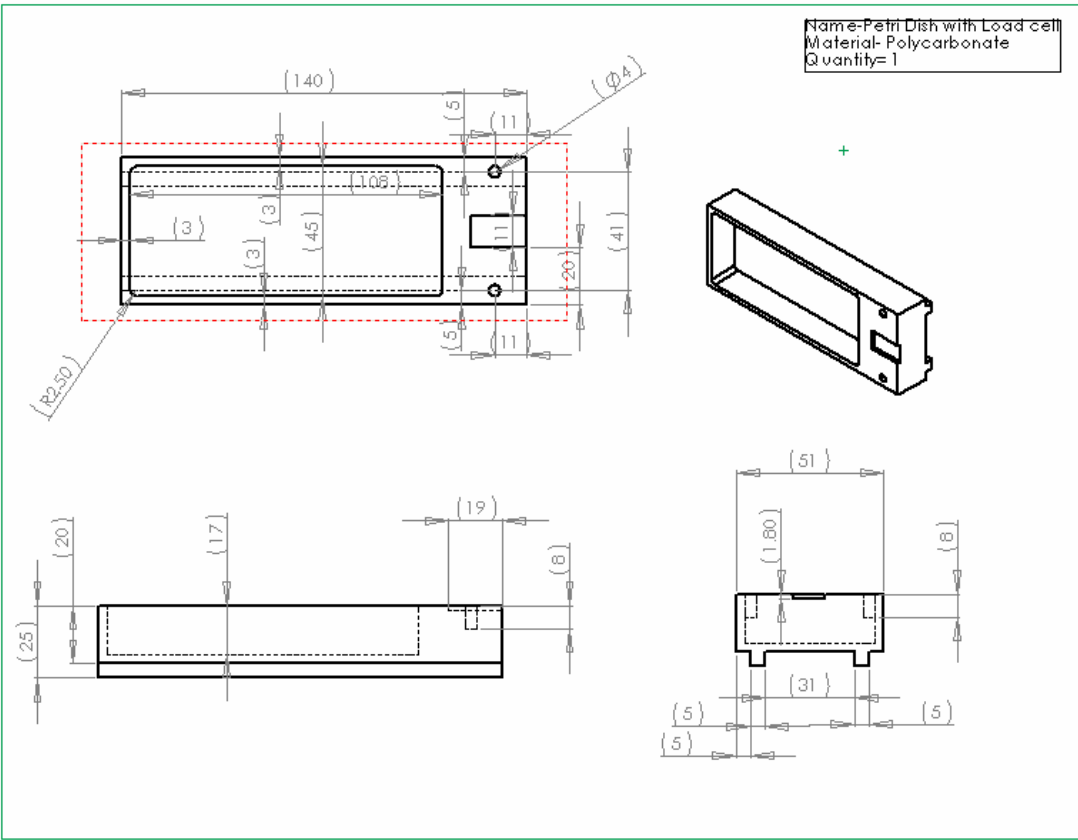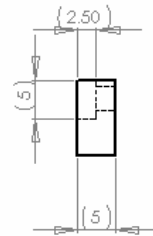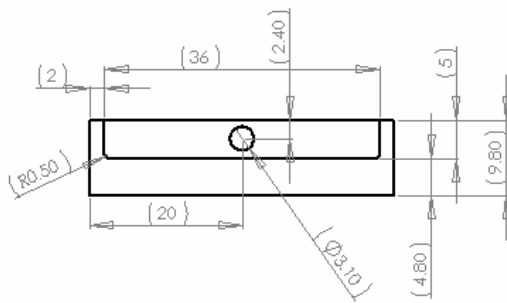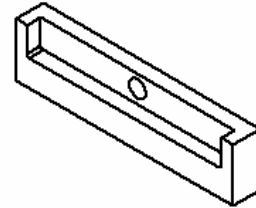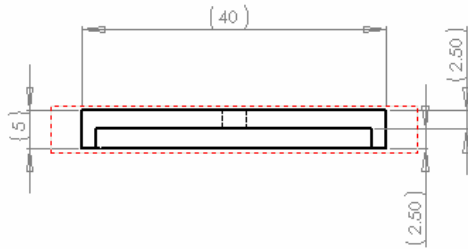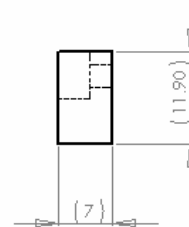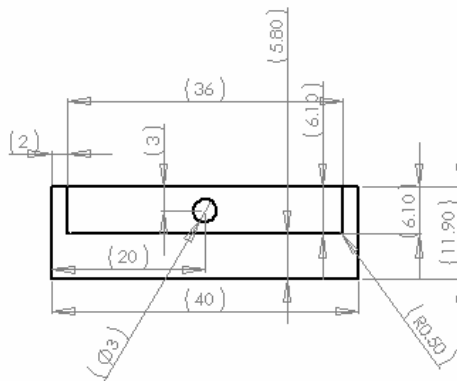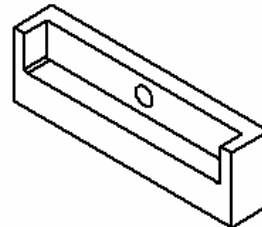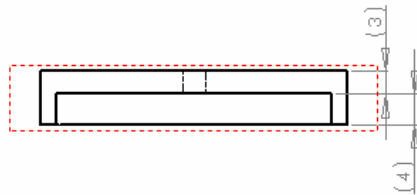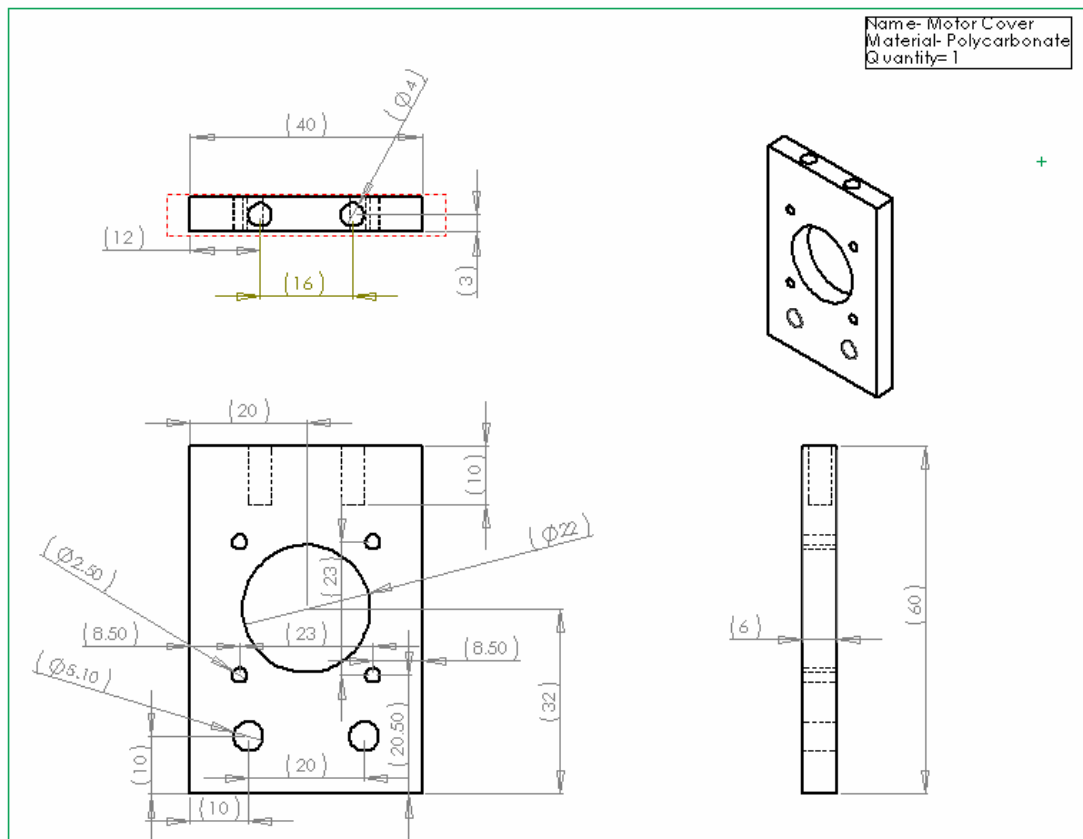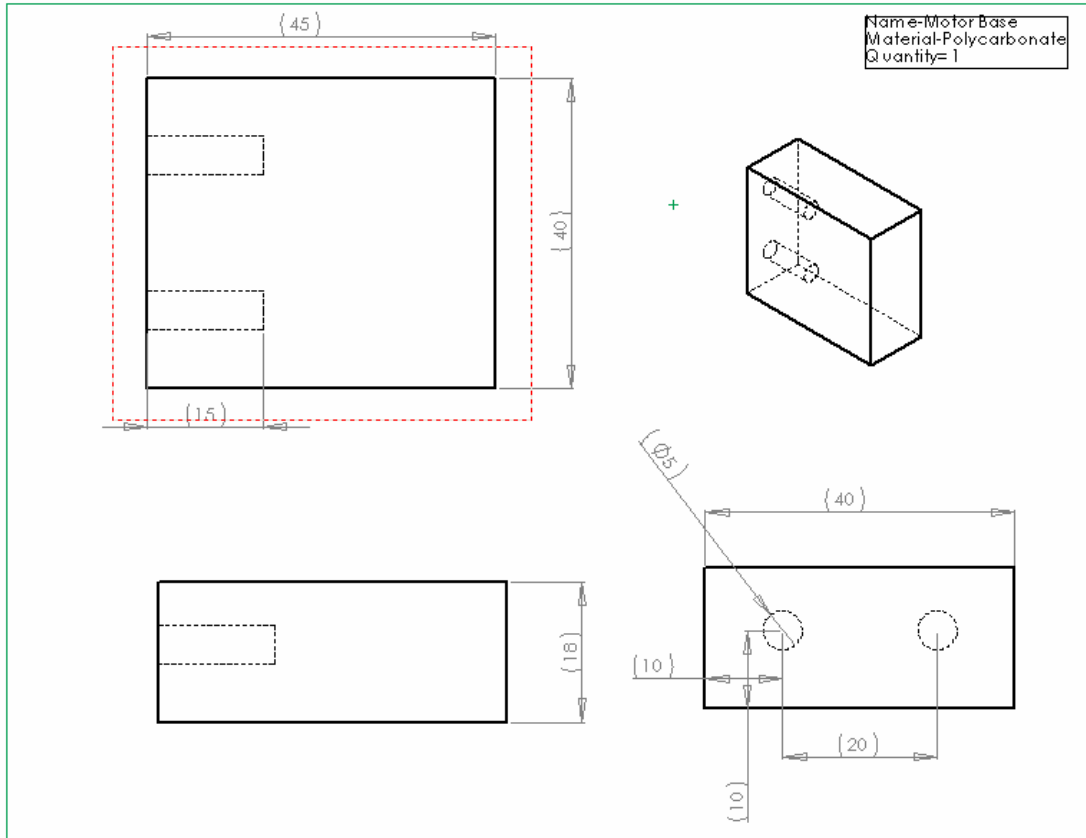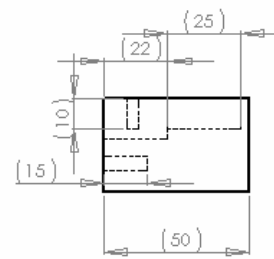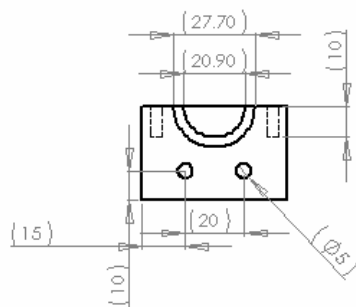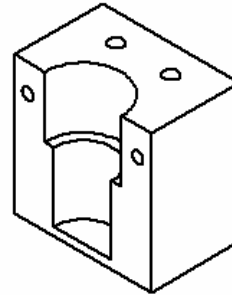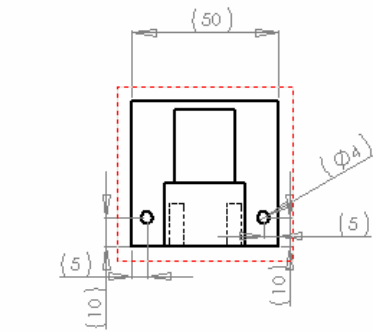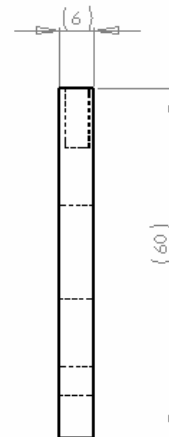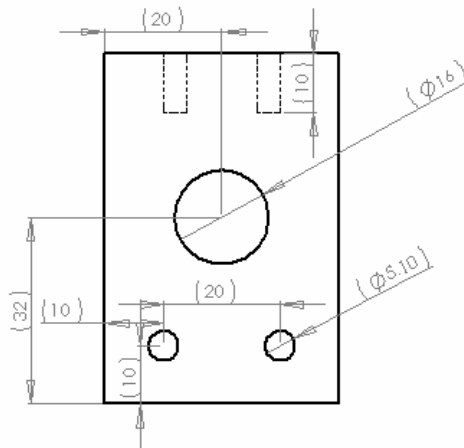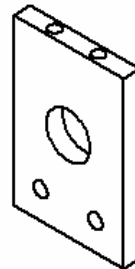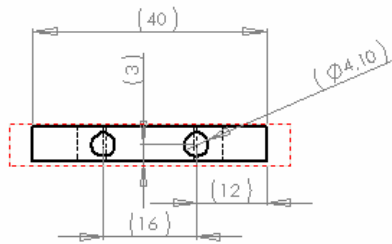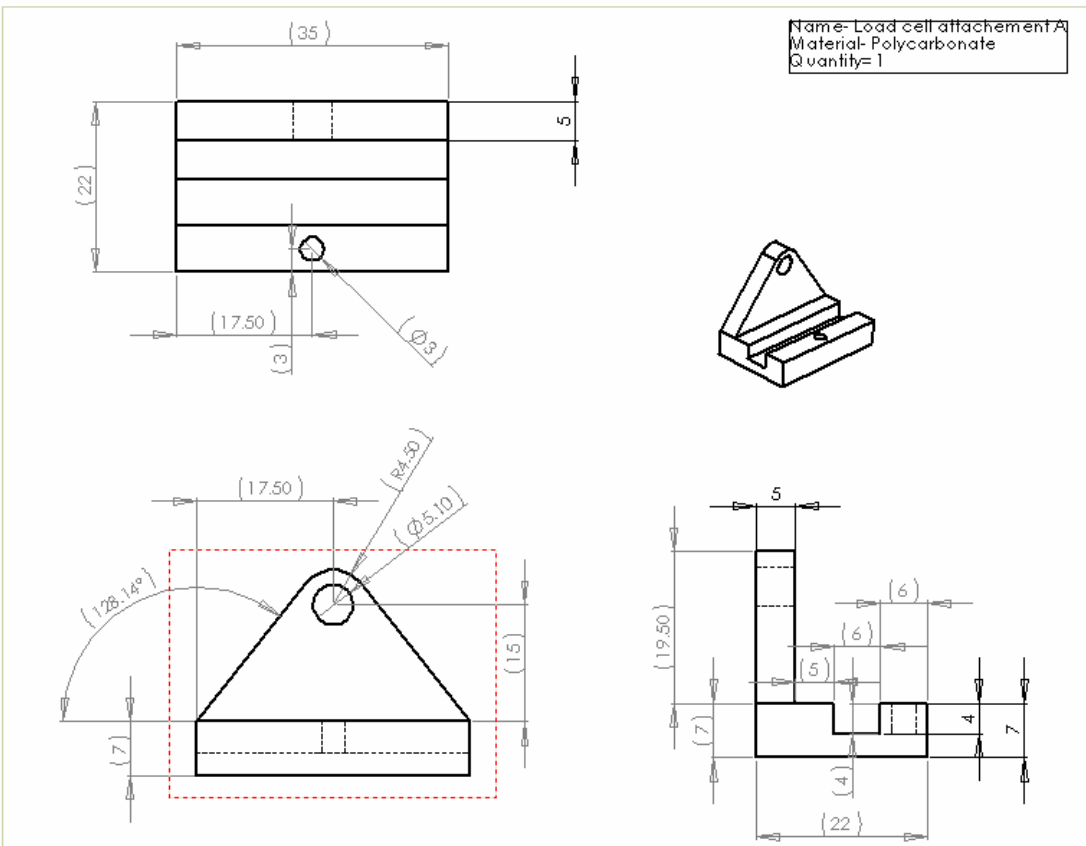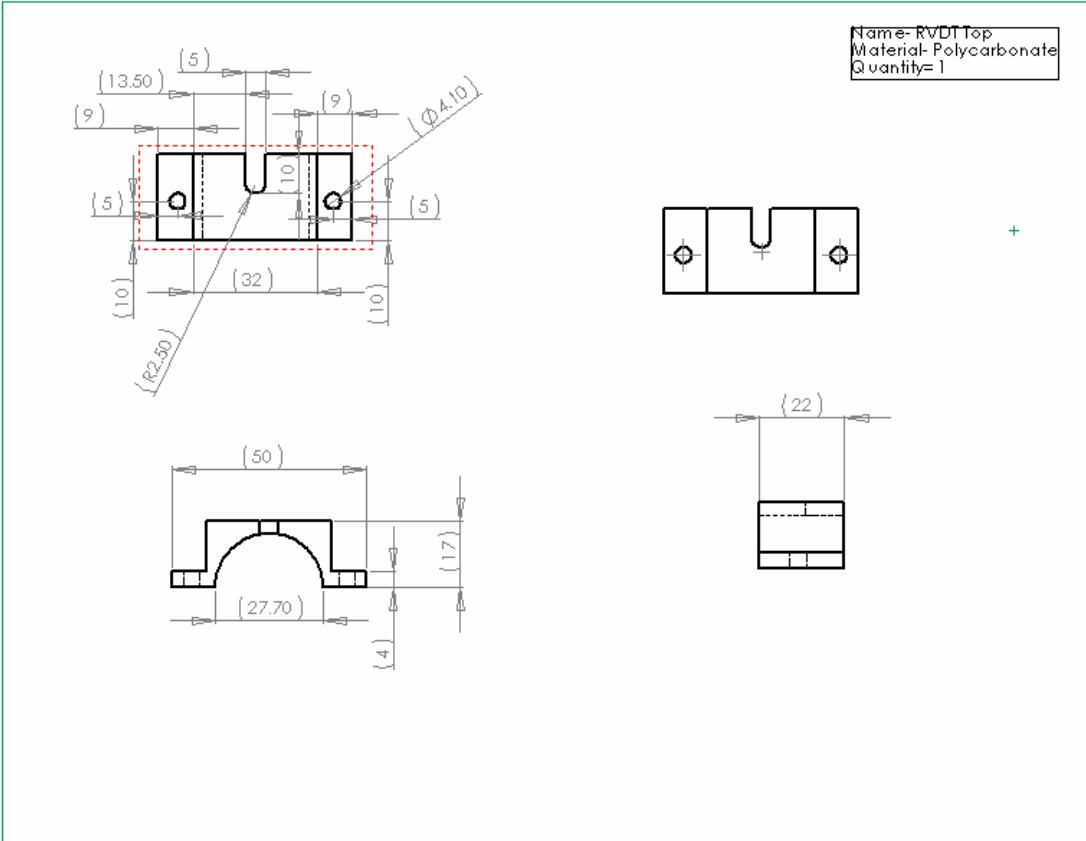
Name-Petri Dish with Load cell
Material- Polycarbonate
Quantity= 1

Name- Petri Dish without load cell
Material-Polycarbonate
Quantity= 2

115

Name-Motor Base
Material-Polycarbonate
Quantity= 1

(45)
(40)
(15)
(18)
Ø5
(40)
(10)
(20)
(10)

Name- Motor Cover
Material- Polycarbonate
Quantity= 1

(40)
Ø4
(12)
(16)
(3)
(20)
(10)
Ø22
Ø2.50
(23)
(23)
(8.50)
(8.50)
Ø5.10
(32)
(60)
(6)
(10)
(20)
(20.50)
(10)

(50)

(Ø4)

(5)

(5)

(10)

(10)

(27.70)

(20.90)

(10)

(15)

(20)

(10)

(Ø5)

(25)

(22)

(10)

(15)

(50)

(40)

(3)

(Ø4.10)

(12)

(16)

(6)

(20)

(10)

(Ø16)

(32)

(10)

(20)

(Ø5.10)

(10)

(60)

117

(5)
(13.50)
(9)
(9)
Ø4.10
(5)
10
(5)
(10)
(32)
(10)
R2.50

(50)
(17)
(27.70)
(4)

(22)

(35)
5
(22)
(17.50)
(3)
Ø3

(17.50)
R4.50
Ø5.10
(128.14°)
(15)
(7)

5
(19.50)
(6)
(6)
(5)
(7)
(4)
4
7
(22)

(11)

(Ø5.10)

(Ø9)

(11)

5

M- 3

Ø8

R7

14

Name_ Petri Dish Base
Material- Polycarbonate
Quantity= 3

(20)
(16)
(16)
(22)
R3
(9)
(15)
(18)
(6)
(5.50)
(5.50)
(5)
(5)

Part 1

Part 2

PART 3

70
70
6
8
40
3
6
10
40
3
40
40
3.50
5
6
40
40
10

NAME- Control Clamp
Material - POlycarbonate
Quantity= Part 1- 6pcs
Part 2- 6pcs
Part 3- 6pcs

120

R30D RVDTs

DC-Operated Rotary Variable Differential Transformers

RVDTs incorporate a proprietary noncontact design that dramatically improves long term reliability when compared to other traditional rotary devices such as syncros, resolvers and potentiometers. This unique design eliminates assemblies that degrade over time, such as slip rings, rotor windings, contact brushes and wipers, without sacrificing accuracy.

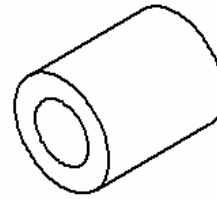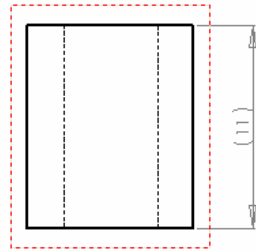High reliability and performance are achieved through the use of a specially shaped rotor and wound coil that together simulates the linear displacement of a Linear Variable Differential Transformer (LVDT). Rotational movement of the rotor shaft results in a linear output signal that shifts ±60 (120 total) degrees around a factory preset null position. The phase of this output signal indicates the direction of displacement from the null point. Noncontact electromagnetic coupling of the rotor provides infinite resolution, thus enabling absolute measurements to a fraction of a degree.

Although capable of continuous rotation, most RVDTs are calibrated over a range of ±30 degrees, with nominal nonlinearity of less than ±0.25% of full scale (FS). Extended range operation up to a maximum of ±90 degrees is possible with compromised linearity.

R30D

The R30D RVDT is a DC operated noncontacting rotary transducer. Integrated signal conditioning enables the R30D to operate from a bipolar ±15 VDC source with a high level DC output that is proportional to the full range of the device. Calibrated for operation to ±30 degrees, the R30D provides a constant scale factor of 125 mVDC/ degree. Nonlinearity error of less than ±0.25% FS is achieved while maintaining superior thermal performance over -18°C to 75°C.

The DC excitation is internally converted to an AC carrier signal which excites the transducer's primary coil. An integrated demodulator amplifier and filter convert the differential secondary output into a smooth, high level, DC output signal that is linear with the shaft angle position. Resolution is infinite enabling measurements to a fraction of a degree.

The R30D features a rugged aluminum size 11 housing making this rotary transducer ideal for applications where integrated signal conditioning and small size are required. Typical applications include hydraulic pump control, rotary actuator feedback, and throttle lever position feedback.

Specifications

Input Voltage (nom)	±15 Vin DC
Output Voltage (nom)	±3.75 VDC
Input Current (max)	35 mA
Output Current (max)	5 mA
Frequency Response	500 Hz @ -3 dB
Linearity Error	±0.25% of full scale output
Storage Temperature Range	-65°F to 250°F (-55°C to 125°C)
Operating Temperature Range	0°F to 170°F (-18°C to 75°C)
Temperature Coefficient of FS	±0.02% of FS/20°F to 160°F (±0.04% of FS/-5°C to 70°C)
Moment of Inertia	.53 x 10^{-6} lb • in • sec²
Lead Wires	28 AWG, Teflon® insulation, 4 wire, minimum 12" long
Torque	0.015 in-oz (1.08 gm-cm)
Weight	1.9 oz (53 gm)
Mounting	Size 11 servo mount BU-ORD
Bearings	Shielded ABEC 3 precision
Shaft Diameter	3/16 in (4.76 mm)
Axial Shaft Bearing Load Capability	10 lbs (4.54 kg)
Radial Shaft Bearing Load Capability	8 lbs (3.6 kg)
Casing Material	Aluminum

Appendix C- Technical Specifications of Load cell

ICP® FORCE SENSOR

Series 208C General Purpose Force Sensors

The 208 Series quartz force sensors are general purpose medium range sensors for dynamic measurements such as compression, impact, reaction, and actuation forces in testing, vibrating, tensioning, balancing, striking, welding, rolling, cutting, coining, pressing, machining, punching, and similar operations. They measure dynamic and short-term static forces from 0.0002 to 5000 pounds at any level within this range.

These sensors have a side-exit connector with 10-32 tapped mounting holes on the top and bottom surfaces. They easily install to the test structure with 10-32 mounting studs. The high stiffness of these sensors allows them to become an integral part of the structure under test. A removable curved impact cap for use in drop testing applications is supplied with each sensor.

DYNAMIC PERFORMANCE

Measurement Range:			
Compression (for +5V output)	lb [kN]	10 [0,04448]	
Tension (for -5V output)	lb [kN]	10 [0,04448]	
Useful Overrange:			
Compression (for +10V output)	lb [kN]	20 [0,08896]	
Tension (for -10V output)	lb [kN]	20 [0,08896]	
Maximum Static Force:			
Compression	lb [kN]	100 [0,4448]	
Tension	lb [kN]	100 [0,4448]	
Broadband Resolution (1 Hz to 10 kHz)	lb-rms [N-rms]	0.0001 [0,00045]	[3]
Low Frequency Response (-5%)	Hz	0.01	[1]
Upper Frequency Limit	Hz	36,000	[5]
Amplitude Linearity	%FS	≤1	[2]

ENVIRONMENTAL

Temperature Range	°F [°C]	-65 to +250 [-54 to +121]	
Temperature Coefficient	%/°F [%/°C]	≤0.05 [≤0,09]	

ELECTRICAL

Sensitivity	mV/lb [mV/kN]	500 [112 410]	[±15%]
Discharge Time Constant (at Room Temperature)	sec	≥50	
Power Requirements: Voltage	VDC	18 to 30	[4]
Constant Current	mA	2 to 20	
Output Impedance	ohms	≤100	
Output Bias Voltage	VDC	8 to 12	
Spectral Noise: 1 Hz	lb/√Hz [N/√Hz]	1.26E-5 [5,62E-5]	[7]
10 Hz	lb/√Hz [N/√Hz]	4.24E-6 [1,89E-5]	[3]
100 Hz	lb/√Hz [N/√Hz]	1.49E-6 [6,65E-6]	[3]
1 kHz	lb/√Hz [N/√Hz]	5.22E-7 [2,33E-6]	[3]
Polarity	compression	Positive	[3]

MECHANICAL

Stiffness	lb/μin [kN/μm]	6 [1,05]	[3]
Dimensions	in [mm]	0.625 x 0.625 [15,88 x 15,88]	
Weight	oz [gm]	0.80 [22.7]	
Housing/Sealing	material/type	Stainless Steel/Hermetic	
Connector/Connector Orientation	type/location	10-32 Coaxial Jack/Side	
Mounting Thread	type	10-32 UNF-2B	
Recommended Mounting Torque	in-lb [N-cm]	16 to 20 [181 to 226]	

CE [6]

PCB PIEZOTRONICS 3425 Walden Avenue, Depew, NY 14043 800-828-8840 Fax (716) 684-0987 E-Mail: sales@pcb.com

Drawn:	Date:	Engineer:	Date:	Sales:	Date:	Approved:	Date:	Spec Number: 8625

8561

APPLICATION				REVISIONS			
NEXT ASS'Y	USED ON	VAR	REV	DESCRIPTION	ECN	DATE	APP'
			B	UPDATE CONNECTOR LOCATION	12700	12/4/00	

Ø.50(Ø12.7)

.10(2.5)

MODEL 084M02
IMPACT CAP
MATERIAL: TOOL STEEL Rc 58
(NOT SUPPLIED)

MODEL 084A03
IMPACT CAP
MATERIAL: 17-4 PH(H900)
(SUPPLIED)

⑥
.625(15.88)
HEX

15.74

10-32 UNF-2B
X .17(4.3)▼ PERF THD
⊔ Ø.210(Ø5.33)
X .020(.51)▼
TYP EACH END

Ø.312(Ø7.92)

.59(15.0)

KAPTON TAPE

.10(2.5)

Ø.500(Ø12.7) TYP

③ 16/(0.4)/

.625±.001
(15.88±0.03)

③ 16/(0.4)/

ELECTRICAL CONNECTOR
COAXIAL 10-32 UNF-2A

.31(7.9)

.28(7.1)

MOUNTING HOLE PREPARATION:
DRILL Ø.159(Ø4.04) ④
X .23(5.8)▼ MIN.
TAP 10-32 UNF-2B
X .15(3.8)▼ MIN.

②

MODEL 081B05
MOUNTING STUD
10-32 UNF-2A
TYPICAL EACH END
(2 SUPPLIED)

⑥ MOUNTING TORQUE ON .625(15.88) HEX, 16-20 INCH POUNDS
(181-226 NEWTON CENTIMETERS).

5.) COMPRESSIVE FORCE ON CELL YIELDS POSITIVE OUTPUT VOLTAGE.

④ DRILL PERPENDICULAR TO MOUNTING SURFACE TO WITHIN ±1°.

③ THESE SURFACES GROUND FLAT AND PARALLEL TO WITHIN .001(0.03) TIR.

② MOUNTING SURFACE TO BE FLAT TO WITHIN .001(0.03) TIR WITH A MIN 125/(3.2/).

1.) CASE MATERIAL-STAINLESS STEEL.

UNLESS SPECIFIED TOLERANCES		DRAWN			MFG	DAS		PCB PIEZOTRONICS
DIMENSIONS IN INCHES	DIMENSIONS IN MILLIMETERS (IN PARENTHESIS)	CHK'D			ENGR			3425 WALDEN AVE. DEPEW, NY 14043 (716) 684-0001 EMAIL: SALES@PCB.COM
DECIMALS XX ±.01	DECIMALS XX ±0.3	APP'D						
XXX ±.005	XXX ±0.13	TITLE	INSTALLATION DRAWING MODEL 208C01 LOAD CELL			CODE IDENT. NO. 52681	DWG. NO. 8561	
ANGLES ±2 DEGREES	ANGLES ±2 DEGREES							
FILLETS AND RADII .003 - .005	FILLETS AND RADII (0.07 - 0.13)					SCALE: 2X	SHEET 1 OF 1	
00011 REV. B 03/13/98								

Appendix D-Technical Specifications of the 5 Phase stepper motor

m4com

5 Phase Stepper Motor (** CE approved)

- Five leads for easy wiring configurations
- Wide selection range to suit various applications
- 0.3~63 Kgcm Max. Holding Torque
- Compact size for high Torque performance
- Highly cost effective
- conformed to CE standard

5 Phase Stepper Motor

Type	Motor Size (mm)	Motor Model	Max. Holding Torque (kgcm)	Rotor Inertia (gcm^2)	Basic Step Angle***	Phase Current (Amps)	Motor Weight (kg)
HI-TORQUE	28	PEE 533 A (B)	0.33	9	0.72°	0.75	0.1
		PEE 535 A (B)	0.6	18	0.72°	0.75	0.17
	42	PF 543 AC (BC)	1.3	35	0.72°	0.75	0.25
		PF 544 AC (BC)	1.8	54	0.72°	0.75	0.3
		PF 545 AC (BC)	2.4	68	0.72°	0.75	0.4
	60	PCE 5641 AC (BC)	4.2	175	0.72°	1.4	0.6
		PCE 5661 AC (BC)	8.3	280	0.72°	1.4	0.8
		PCE 5691 AC (BC)	16.6	560	0.72°	1.4	1.3
	85	PCE 5961 AC (BC)	20.9	1400	0.72°	1.4	1.7
		PCE 5991 AC (BC)	40.9	2700	0.72°	1.4	2.8
		PCE 59131 AC (BC)	62.9	4000	0.72°	1.4	3.8
HI-TORQUE HI-SPEED	60	PCE 5692 AC (BC)	16.6	560	0.72°	2.8	1.3
	85	PCE 5962 AC (BC)	20.9	1400	0.72°	2.8	1.7
		PCE 5992 AC (BC)	40.9	2700	0.72°	2.8	2.8
		PCE 59132 AC (BC)	62.9	4000	0.72°	2.8	3.8

** Brake Type Stepper Motor **

Type	Motor Size (mm)	Motor Model	Max. Holding Torque (kgcm)	Rotor Inertia (gcm^2)	Basic Step Angle***	Phase Current (Amps)	Motor Weight (kg)
HI-TORQUE *Brake Type	60	PCE 5641 ACM	4.2	320	0.72°	1.4	0.9
		PCE 5661 ACM	8.3	425	0.72°	1.4	1.1
		PCE 5691 ACM	16.6	705	0.72°	1.4	1.6
	85	PCE 5961 ACM	20.9	2200	0.72°	1.4	2.4
		PCE 5991 ACM	40.9	3500	0.72°	1.4	3.5
		PCE 59131 ACM	62.9	4800	0.72°	1.4	4.5
HI-TORQUE HI-SPEED *Brake Type	60	PCE 5692 ACM	16.6	705	0.72°	2.8	1.6
		PCE 5962 ACM	20.9	2200	0.72°	2.8	2.4
	85	PCE 5992 ACM	40.9	3500	0.72°	2.8	3.5
		PCE 59132 ACM	62.9	4800	0.72°	2.8	4.5

(AC) after the unit # denotes single shaft configuration. (BC) after the unit # denotes thru-shaft configuration.

Other Specifications

Motor Electrical Specifications

Dielectric Strength	No abnormality detected after the application of 0.5KV at 50 Hz between motor windings and frame for duration of one minute		
Insulation Resistance	100 Mohms or better with 500V potential applied between motor windings and frame at normal ambient temperature and humidity		
Insulation Class	Class B	Operating Environment Temperature	0ºC ~ + 50ºC

Motor Mechanical Specifications

Shaft Radial Play	0.025 mm (max) at load 0.5 Kg
Shaft Axial Play	0.075mm (max) at load 1 Kg
Step Angle Accuracy	± 3 min

Applicable Driver Range

The above motors can be used on the following MYCOM stepping drivers. Selection is generally based on applicable speed range and supply input as indicated below :-

Low Speed Range (24Vdc supply input)

UPS503 series
IMS500 series
INS500 series (NanoDrive)
INS501 series (NanoDrive)

Standard Speed Range (110Vac supply input)

PSU50 series
UPS52 series
UPS53 series
IMS50-x1x series
INS50-x1x series (NanoDrive)

Standard Speed Range (220Vac supply input)

IMS50-x2x series
INS50-x2x series (NanoDrive)

** kindly refer to our sales staff for other series of drivers

5 Phase Motor Connection Diagram
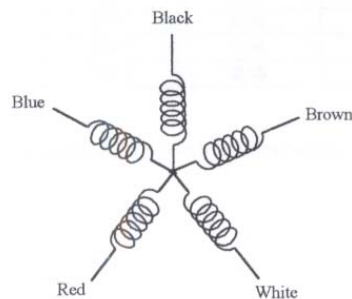
Model No. A - Single Shaft B - Thru' Shaft	A (mm)	B (mm)
PEE 533-A(B)	31±1	42±2
PEE 535-A(B)	50.5±1	42±2

PEE 53X-A(B)

5 Leads 600 mm
UL Style 3265 AWG 28

4 - M2.5P0.45
Depth 2.5

PEE 533-A(B) MGXX

5 Leads 600 mm
UL Style 3265 AWG 28

4 - M2.5P0.45
Depth 3.5

Motor	L1	L2
PF543AC	33 ± 1	53 ± 1
PF543BC		68 ± 1
PF544AC	39 ± 1	59 ± 1
PF544BC		74 ± 1
PF545AC	47 ± 1	67 ± 1
PF545BC		82 ± 1

Cable with
Connector Ø5.4

5 Leads AWG26
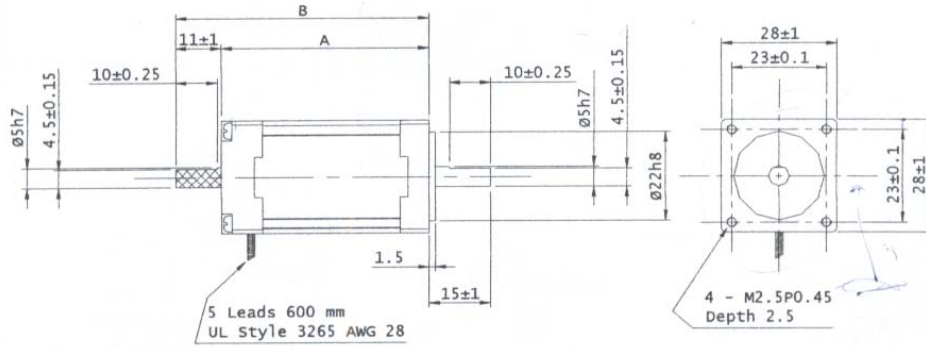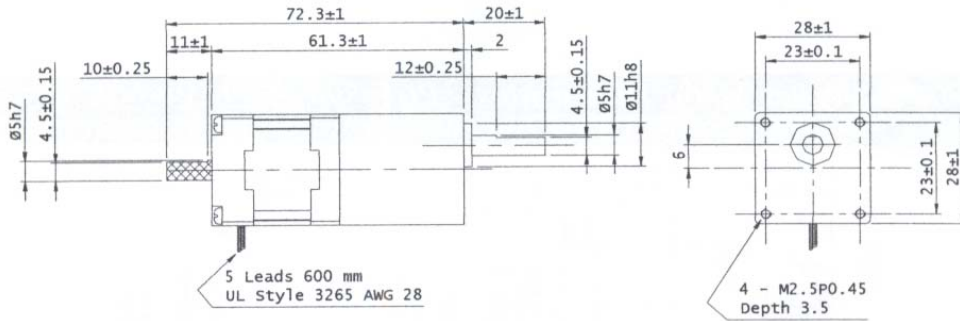
4-M3 P0.5
By Depth 4.5
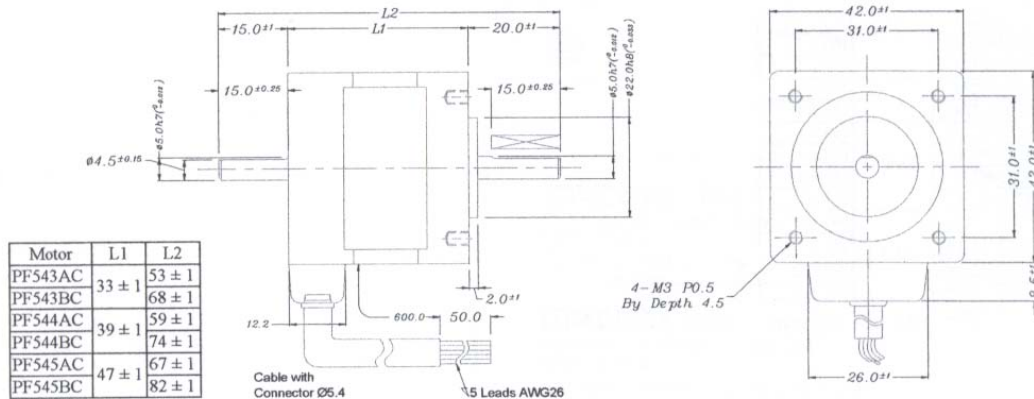
Appendix E- Technical Specifications of Controller

MYCOM

SNC 11   Stepper Motion Controller

- Single Axis stand-alone controller
- RS232 communication port
- Daisy chain up to 8 controller
- On-line mode control
- Simple programming using 'Terminal Software'
- 5 inputs and 4 outputs

Specifications

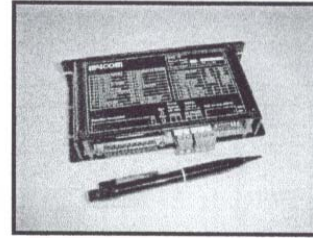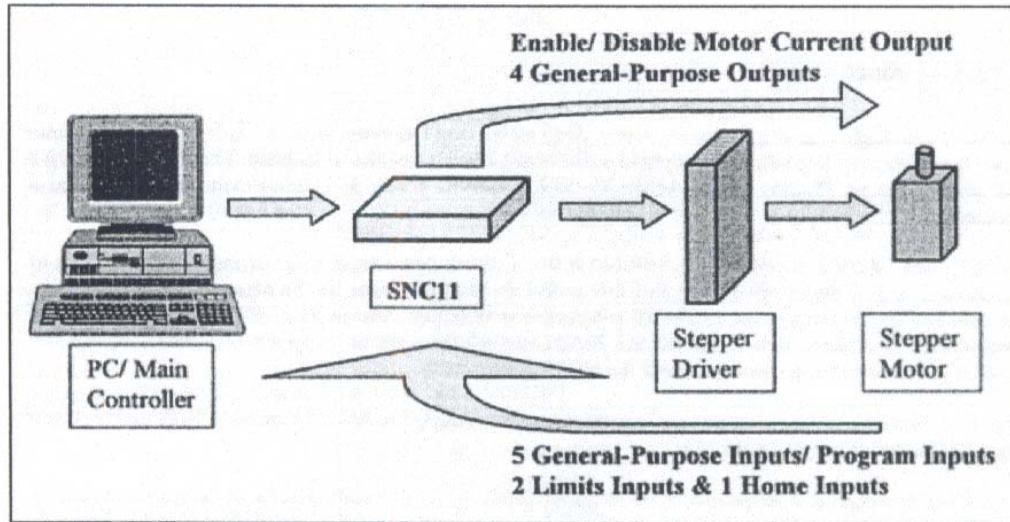| Items	Contents
Number of Axis	One
Compatible Motor type	Stepper or digital servo motor
Memory Retention	2Kbtyes EEPROM (approx. 2,000 characters) 100,000 write/erase cycles
Programming Language	ASCII characters
Programming Functions	- motor control parameter setup - absolute or relative move - jog commands - return to home - general purpose I/O select - program select (hardware trg : max of 32 prgms) (software trg : max of 128 prgms) - conditional jump - dwell timer - external stop - feedback message
Commands accepted from	Host computer via RS232/RS485 serial port
Move distance commands	Absolute or incremental (nos. of pulses)
Range of move	Absolute : -131,072 ∿ +131,071 pps Relative : -262,143 ∿ +262,143 pps
Range of homing freq	X 1:2 ∿ 16,382 pps
Range of Start/Stop freq	X 2:4 ∿ 32,764 pps
Range of Max Slew freq	X 4:8 ∿ 65,528 pps
Range of Jog freq	X 8:16 ∿ 131,056 pps
Acceleration/Deceleration	X 1:7,820 ∿ 4 Mpps^2 X 2:15,640 ∿ 8 Mpps^2 X 4:31,280 ∿ 16 Mpps^2 X 8:62,560 ∿ 32 Mpps^2
General purpose/program inputs	5 NPN opto-isolated input voltage = +5Vdc ; 1.5mA input voltage = +12Vdc ; 5.0mA input voltage = +24Vdc ; 10mA
Machine sensor interface inputs (opto-isolated)	Reverse limit } input voltage = +5Vdc ; 1.5mA Forward limit } input voltage = +12Vdc ; 5.0mA Home } input voltage = +24Vdc ; 10mA
General purpose outputs	4 opto-isolated open collector (50Vdc ; 250mA max)
Driver interface outputs Gate control (opto-isolated)	Pulse & Direction (15mA max) Motor current off output (16mA max)
Indicators	Power LED, Error LED
Power Requirement	5 Vdc ±5% ; 150mA typ, 230mA max
Serial port	RS232/RS485 – 9600 baud, 8 bit, 1 stop, no parity
Operating temp range	0°C ∿ 70°C
Size	133 x 76 x 29 mm

Mycom Technology (S) Pte Ltd   1

System Overview

Enable/ Disable Motor Current Output
4 General-Purpose Outputs

SNC11

PC/ Main Controller

Stepper Driver

Stepper Motor

5 General-Purpose Inputs/ Program Inputs
2 Limits Inputs & 1 Home Inputs

Dimension

160mm

32mm

Figure 2A : Front View (Overall Dimension)

160 mm

24mm

80 mm

25mm

Input Supply

Interface Connector
25 Way Male

ERR   5V 0V   TX RX   SW 1 (Default)   OFF

1

14   POW   1 2 3 4 5 6 7 8 ON

21mm

Mounting Hole : 5mm

Appendix F- Program for Stepper Motor

XU1 OT1XXX VL100 MR-250 GO OT0XXX	XU2 OTX1XX VL100 MR250 GO OTX0XX	XU4 OTXX10 AC1000 VL100 MR-500 GO WT100 OTXX01 MR500 GO WT100	XU127 SE1 OE4 MX1 VB50 VL100 AC1000 RL0 ES7 EP2 SN50	**Resolution = 1/100** **Movement = 500 pps** $= \dfrac{500}{500 \times 100} \times 360 = 3.6°$ $= \dfrac{500}{500 \times 100} \times \pi \times 34mm$ **= 1.06 mm** **59 mm * 1.8% = 1.06 mm**

According to the above programs written and stored in the controller, the following actions were enabled:

Switch 1; Turn the spool (1.8˚ in reverse direction) within 2.5 second and LED-1 will ON.

Switch 2: Turn the spool (1.8˚ in forward direction) within 2.5 second and LED-2 will ON.

Switch 3: Turn the spool (3.6˚ in reverse direction) within 5 seconds and LED 3 will ON then turn the spool back(3.6˚ in forward direction) within 5 seconds and LED 4 will ON.

Switch 4: emergency stop

Switch 1 and switch 2 are used to adjust the tension of scaffold before start stimulation. Switch 3 is used for continuous stimulation.

Appendix G - Alamar Blue Assay Protocol

ALAMAR BLUE ASSAY PROCEDURES:

1)   Prepare 5% Alamar Blue in culture medium(5% FBS), Submerge every test sample in   15 ml of dilute mixture . Wrap the container with aluminum foil and shake for a few second (10-15 s)

2)   Set up for control, put 3-5 ml of 5% Alamar Blue medium in round Petri dish and covered with aluminum foil .

3)   Incubate both setups at 37°C for 3 hours inside the incubator.

4)   Transfer mixtures from both setups into 96-well assay plate (5 wells per sample at 100μL to each well).

5)   Shake plate for 10 seconds and record absorbance at 570nm and 600nm.

ALAMAR BLUE ASSAY CALCULATIONS:
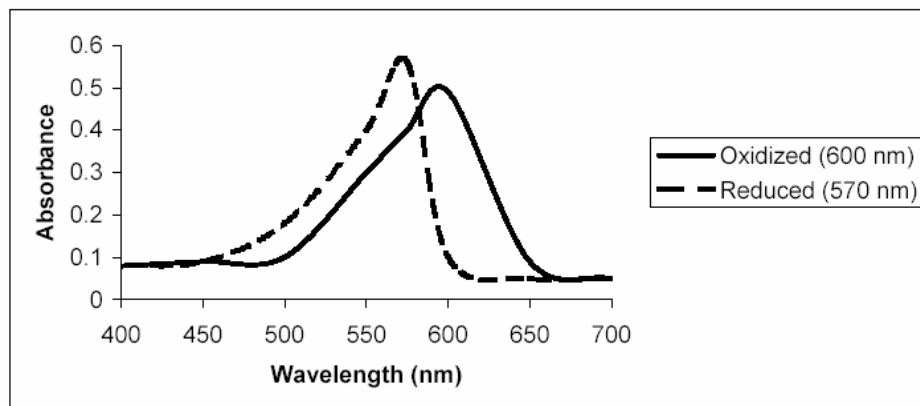
Figure G-1. Absorbance spectra of alamar blue at 600nm and 570nm

Figure G-1.above show that there is concesiderable overlap in the absorption spectra of the oxidized and reduced forms of Alamar blue . When there is no region in which just one component absorbs, it is still possible to determine the two substances by making two wavelengths. The two component must have different powers of light absorption at some points in the spectrum. Since absorbance is directly proportional the product of the molar

extinction coefficient and concentration, a pair of simultaneous equations may obtained from which two unknown concentration may be determined. [www.sereotec.co.uk]

$$C_{RED}(\varepsilon_{RED})\lambda_1 + C_{OX}(\varepsilon_{OX})\,\lambda_1 = A\,\lambda_1 \tag{1}$$

$$C_{RED}(\varepsilon_{RED})\lambda_2 + C_{OX}(\varepsilon_{OX})\,\lambda_2 = A\,\lambda_2 \tag{2}$$

To solve for the concentration of each component:

$$C_{RED} = \frac{(\varepsilon_{OX})\lambda_2 A\lambda_1 - (\varepsilon_{OX})A\lambda_1 A\lambda_2}{(\varepsilon_{RED})\lambda_1(\varepsilon_{OX})\lambda_2 - (\varepsilon_{OX})\lambda_1(\varepsilon_{RED})\lambda_2} \tag{3}$$

$$C_{OX} = \frac{(\varepsilon_{RED})\lambda_1 A\lambda_2 - (\varepsilon_{RED})\lambda_2 A\lambda_1}{(\varepsilon_{RED})\lambda_1(\varepsilon_{OX})\lambda_2 - (\varepsilon_{OX})\lambda_1(\varepsilon_{RED})\lambda_2} \tag{4}$$

To determine the percent reduction of alamar blue:

$$\% \text{ Reduction} = \frac{C_{RED}\,TestWell}{C_{OX}\,NegativeControlWell} \tag{5}$$

Since the samples are read at
$\lambda_1 = 570nm$
$\lambda_2 = 600nm$

$$\% \mathrm{Re}duction = \frac{(\varepsilon_{ox}\lambda_2)(A\lambda_1) - (\varepsilon_{ox}\lambda_1)(A\lambda_2)}{(\varepsilon_{red}\lambda_2)(A'\lambda_2) - (\varepsilon_{red}\lambda_2)(A'\lambda_1)} \times 100 \tag{6}$$

where

$(\varepsilon_{redx}\lambda_1)$ = 155,677 (Molar extinction coefficient of reduced Alamar Blue at 570nm)
$(\varepsilon_{red}\lambda_2)$ = 14,652 ((Molar extinction coefficient of reduced Alamar Blue at 600nm)
$(\varepsilon_{ox}\lambda_1)$ = 80,586 (Molar extinction coefficient of oxidized Alamar Blue at 570nm)
$(\varepsilon_{ox}\lambda_2)$ = 117, 216 ((Molar extinction coefficient of oxidized Alamar Blue at 600nm)
$(A\lambda_1)$ = Absorbance of tests wells at 570nm
$(A\lambda_2)$ = Absorbance of tests wells at 600nm
$(A'\lambda_1)$ = Absorbance of negative control wells which contain medium plus Alamar Blue but to which no cells have been added at 570nm.
$(A'\lambda_2)$ = Absorbance of negative control wells which contain medium plus Alamar Blue but to which no cells have been added at 600nm.

Table G-1: Alamar Blue reading and % reduction calculation for Day 3

Samples	Absorbance Wavelength	Average Absorbance Reading	Percentage Reduction (%)	Average % reduction ± SD (%)for each group
Control	570nm	0.3898	-	-
	600nm	0.3174		
Strained Sample-1	570nm	0.3682	62.29	63.0 ± 1.62
	600nm	0.1978		
Strained Sample-2	570nm	0.3896	64.85	
	600nm	0.215		
Strained Sample-3	570nm	0.3716	61.87	
	600nm	0.205		
Unstrained Sample-1	570nm	0.4392	70.82	69.57 ± 3.58
	600nm	0.2548		
Unstrained Sample-2	570nm	0.41	65.53	
	600nm	0.241		
Unstrained Sample-3	570nm	0.443	72.35	
	600nm	0.252		

Table G – 2 Alamar Blue reading and % reduction calculation for Day 17

Samples	Absorbance Wavelength	Average Absorbance Reading	Percentage Reduction (%)	Average % reduction ± SD (%)for each group
Control	570nm	0.3817	-	-
	600nm	0.306		
Strained Sample-1	570nm	0.4245	77.47	78.67 ± 1.06
	600nm	0.2133		
Strained Sample-2	570nm	0.427	79.50	
	600nm	0.2063		
Strained Sample-3	570nm	0.4325	79.02	
	600nm	0.2168		
Unstrained Sample-1	570nm	0.4056	72.90	76.46 ± 3.59
	600nm	0.2096		
Unstrained Sample-2	570nm	0.4156	76.38	
	600nm	0.206		
Unstrained Sample-3	570nm	0.4322	80.09	
	600nm	0.2108		

Appendix H- Data Analysis for mechanical testing

The peak load and stiffness of the scaffolds in elastic region need to be obtain from the data points recorded from the instron machine. The peak load was found by plotting the graph of load (N) versus extension (mm) of the scaffold.

The stiffness in the elastic region wass found by the following method:

1. The data for the load and extension up to the first peak (load) were extracted.

2. The gradients betwwen successive points were calculated i.e. g_1 and g_2 in Figure H-1

3. The difference in gradients calculated as a persentage of the first gradient.

   i.e.$(g_2 - g_1)/ g_1 \times 100$ %.

4. The graph of x_2 versus the difference in successive gradients was plotted . Figure H-2

5.From the graph x_2 versus the difference in successive gradients , the region of best linerity was signed out.

6. If more than one region of linerity were found, the regions were compared using the correlation method to single out the more linear region.

7. The region selected was tested with the correlation formula to ensure a square of correlation factor of more than 0.99(1.0 being a perfectly fitting straight line)

8. With the best linear region, a straight line was fitted using linear regression (least square method) and the gradient of the line would be the stiffness of the elastic region.
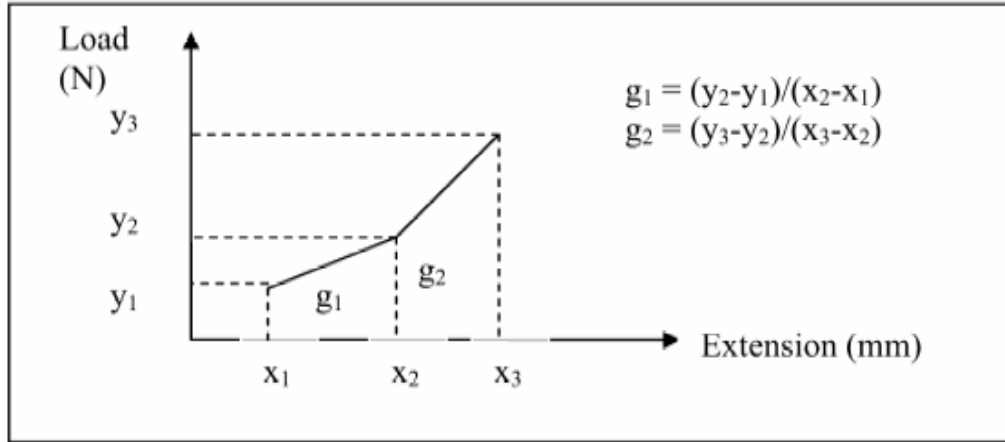
(Figure H-3)

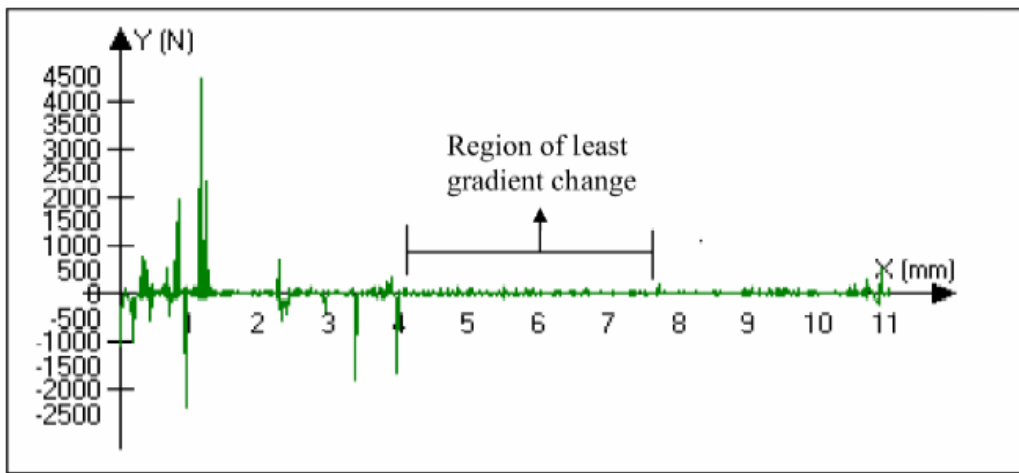Figure H-1: Calculation of gradient betwween two successive points

Figure H-2: Graph of percentage gradient changeversus extension. Region of least change in gradient can be deduced to be between X=4.0mm and X= 7.5 mm
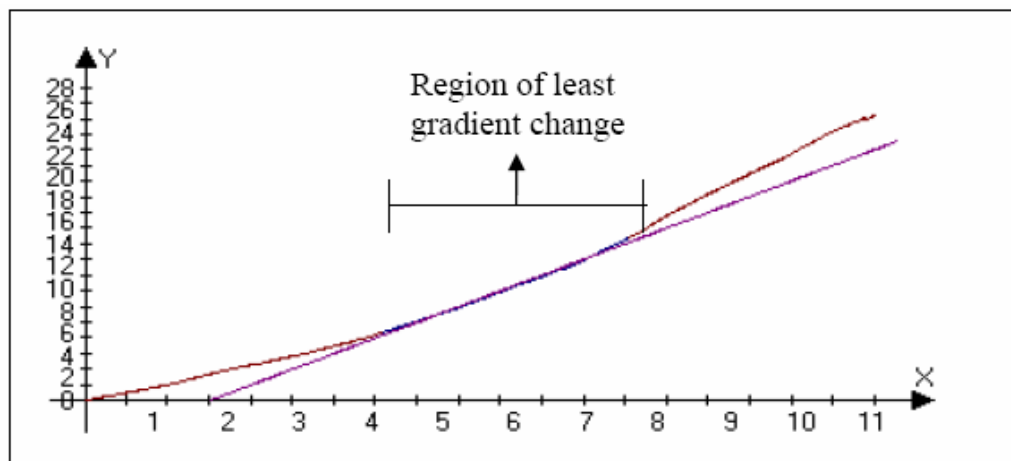

Figure H-3 :The blue colour line is the best fitted straight between X= 4mm and X= 7.5mm. Gradient of this blue line yields the elastic stiffness of the scaffold.